ANL-7450

ANL-7450

Argonne National Laboratory

CHEMICAL ENGINEERING DIVISION RESEARCH HIGHLIGHTS

May 1967-April 1968

The facilities of Argonne National Laboratory are owned by the United States Government. Under the terms of a contract (W-31-109-Eng-38) between the U. S. Atomic Energy Commission, Argonne Universities Association and The University of Chicago, the University employs the staff and operates the Laboratory in accordance with policies and programs formulated, approved and reviewed by the Association.

MEMBERS OF ARGONNE UNIVERSITIES ASSOCIATION

The University of Arizona
Carnegie Institute of Technology
Case Institute of Technology
The University of Chicago
University of Cincinnati
Illinois Institute of Technology
University of Illinois
Indiana University
Iowa State University
The University of Iowa
Kansas State University
The University of Kansas
Loyola University
Marquette University
Michigan State University
The University of Michigan
University of Minnesota
University of Missouri
Northwestern University
University of Notre Dame
The Ohio State University
Purdue University
Saint Louis University
Washington University
Wayne State University
The University of Wisconsin

LEGAL NOTICE

This report was prepared as an account of Government sponsored work. Neither the United States, nor the Commission, nor any person acting on behalf of the Commission:

A. Makes any warranty or representation, expressed or implied, with respect to the accuracy, completeness, or usefulness of the information contained in this report, or that the use of any information, apparatus, method, or process disclosed in this report may not infringe privately owned rights; or

B. Assumes any liabilities with respect to the use of, or for damages resulting from the use of any information, apparatus, method, or process disclosed in this report.

As used in the above, "person acting on behalf of the Commission" includes any employee or contractor of the Commission, or employee of such contractor, to the extent that such employee or contractor of the Commission, or employee of such contractor prepares, disseminates, or provides access to, any information pursuant to his employment or contract with the Commission, or his employment with such contractor.

Printed in the United States of America
Available from
Clearinghouse for Federal Scientific and Technical Information
National Bureau of Standards, U. S. Department of Commerce
Springfield, Virginia 22151
Price: Printed Copy $3.00; Microfiche $0.65

ANL-7450
General, Miscellaneous,
and Progress Reports
(TID-4500)
AEC Research and
Development Report

ARGONNE NATIONAL LABORATORY
9700 South Cass Avenue
Argonne, Illinois 60439

CHEMICAL ENGINEERING DIVISION RESEARCH HIGHLIGHTS

May 1967-April 1968

R. C. Vogel, Division Director
E. R. Proud, Assistant Division Director
J. Royal

TABLE OF CONTENTS

	Page
I. COMPACT PYROCHEMICAL PROCESSES	7
A. Continuous Salt Transport Process Flowsheet	7
B. Supporting Laboratory Studies	8
1. Reduction of Uranium Oxide	9
2. Distribution between Molten Salts and Liquid Alloys	9
C. Supporting Engineering Studies	11
D. Experimental Flowsheet Investigations	15
II. VOLATILITY AND FLUIDIZATION PROCESSES	21
A. Recovery of Uranium and Plutonium from Spent Nuclear Fuels	22
1. Engineering Development of Fluorination of Uranium Oxide with BrF_5	22
2. Engineering-Scale Alpha Facility Operations	25
3. Bench-Scale Fluid-Bed Studies with Irradiated Fuels	30
B. Supporting Investigations	35
1. Ruthenium Fluoride Separation Chemistry	35
III. MATERIALS CHEMISTRY AND THERMODYNAMICS	39
A. High Temperature Materials Development	39
1. Plutonium-Bearing Fuel Materials	39
2. Oxygen and Uranium Activities in Oxygen-Saturated Liquid Uranium	43
3. Mass Spectrometric Effusion Study of the Uranium-Uranium Phosphide System	46
B. Chemistry of Irradiated Fast Reactor Fuels	49
1. Electron Microprobe Studies	49
2. Laser-Beam Microsampling	53
C. Preparation of Reactor Materials - Ceramic Fuels	55
1. Synthesis of Carbides by Metal-Methane Reaction	55
2. Synthesis of Carbides by Conversion from Oxides	60

TABLE OF CONTENTS

Page

D. Calorimetry 61

1. Standard Enthalpies of Formation 62

2. Correlation and Estimation of Enthalpies of Formation for the Rare Earth Trifluorides. 64

3. Extended Hückel Molecular Orbital Calculations for the Chalcogen Hexafluorides 66

E. Chemistry of Liquid Metals. 67

1. Ultrasonic Measurements in Liquid Metallic Solutions. . 67

2. Carbon Transport Experiments in Liquid Sodium Systems 70

3. The Nature of Nitrogen in Sodium 71

IV. REACTOR SAFETY 75

A. Thermal Reactor Safety Studies 75

1. Analysis of Loss-of-Coolant Accidents 75

2. Pressure Generation due to Particle Coolant Energy Transfer 76

B. Fast Reactor Safety Studies. 82

1. High Temperature Physical Properties. 82

2. Pressure Generation due to Particle Coolant Energy Transfer 84

3. Reaction of Violently Sprayed Sodium with Air 84

4. Migration of Fuel Components under a Thermal Gradient 86

V. ENERGY CONVERSION 90

A. Research on High Specific Energy, High Specific Power Secondary Cells 90

1. Emf Studies of the Lithium-Tellurium System 90

2. Secondary Cell Experiments 92

B. Spectroscopic Investigations of Intermetallic Systems 100

C. Thermodynamics of the Sodium-Lead System by Vapor-Liquid Equilibrium Techniques 102

TABLE OF CONTENTS

Page

VI. NUCLEAR CONSTANTS 105

A. Neutron Reaction Cross Sections. 105

B. Low-Mass Fission Yield Studies 106

VII. DETERMINATION OF BURNUP IN FAST REACTOR FUELS . . 108

A. Methods for the Determination of Fission Products 108

1. Spectrophotometric Titration of Total Rare Earths . . . 108

2. X-Ray Spectrometric Determination of Rare Earth Fission Products 109

B. Evaluation of Burnup Monitors for Oxide Fuels 110

C. Irradiation in EBR-II 111

ADDENDUM 112

I. COMPACT PYROCHEMICAL PROCESSES

A. Continuous Salt Transport Process Flowsheet

Research and development work has continued on compact pyrochemical processes for the recovery and purification of ceramic (oxide or carbide) fast breeder reactor fuels. The studies have been concentrated on the development of a process employing salt transport separations. Salt transport separations are based on the selective transfer of a solute (plutonium or uranium) from one liquid metal solution (donor alloy) to another metal solution (acceptor alloy) by cycling a molten chloride salt between the two metal solutions.

Although the development work on pyrochemical processes has generally been oriented toward batch-processing methods, continuous or semi-continuous processes employing high temperature countercurrent contacting equipment are also being investigated. Continuous operations offer the possibility of higher capacities and more efficient separations which may be advantageous in future processes. A conceptual flowsheet (Fig. I-1) incorporating countercurrent extraction columns has been prepared as an alternative to the previous batch-processing flowsheet (see Research Highlights Report ANL-7350, May 1967, p. 6). The chemical separations in this flowsheet (Fig. I-1) are similar to those used in the batch version of the process. The stream quantities shown on the flowsheet are illustrative only and do not necessarily represent optimum conditions.

The following is a summary of the steps in the new flowsheet. The stainless steel cladding is removed from the oxide fuel by dissolution in molten zinc in the decladding step (1). The fuel is reduced by liquid Cu-33 w/o Mg alloy with the aid of a molten halide flux at 800°C in the reduction step (2). In this step, the volatile fission products are released, the alkali and alkaline earth fission products distribute to the salt phase, and the reduced uranium metal precipitates from the Cu-Mg alloy. The uranium is subsequently charged to a salt transport separation step (3) to remove residual fission products. A Zn-14 w/o Mg acceptor alloy is specified, but if the plutonium content of the uranium is high, a magnesium-rich acceptor alloy with low uranium solubility and high plutonium solubility would be used for further plutonium recovery. The purified uranium metal is recovered by vacuum retorting (4). The decanted Cu-Mg-Pu metal phase from the reduction step is processed at 600°C in a multistage, rare earth extraction column (5), where the rare earth fission products are extracted into a salt containing ~15 m/o $MgCl_2$. The salt is reused after the rare earths are removed through contact with a Bi-Mg alloy in a mixer-settler (6). The Cu-Mg-Pu alloy leaves the rare earth extraction column (7), where the plutonium is extracted into a

salt phase containing 50 or 60 m/o $MgCl_2$ at 600°C. A single-stage mixer-settler (8) is used to remove any copper that may be entrained in the plutonium-bearing salt. The plutonium is then extracted into a Cd-Mg metal phase at 600°C in a small extraction column (9). The solvent Cd-Mg alloy is separated from the metallic plutonium product by vacuum distillation (10).

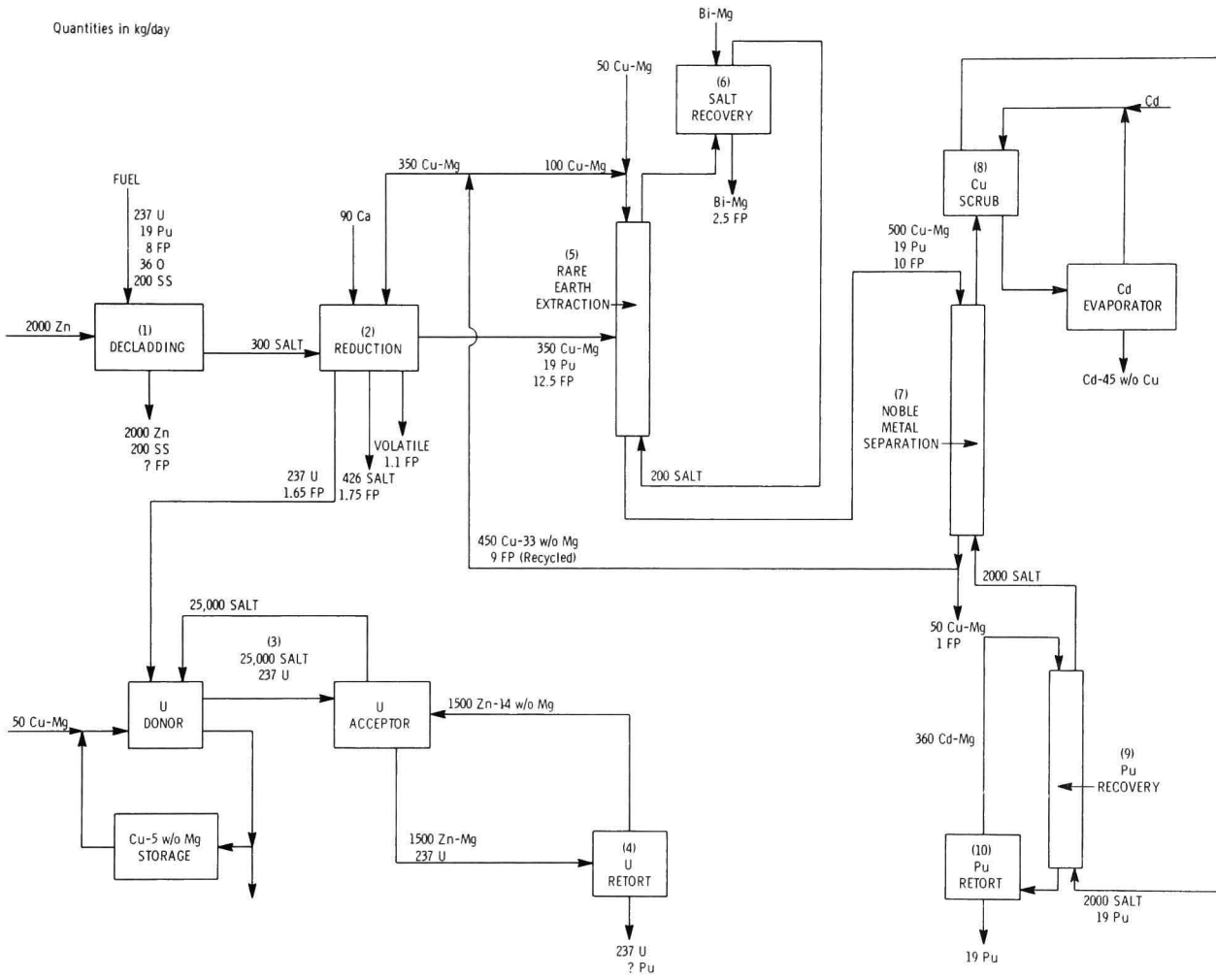

Fig. I-1. Conceptual Pyrochemical Flowsheet.

Further tests of the various steps in this flowsheet are being carried out in batch operations employing the equipment used for the plutonium salt transport experiment (see ANL-7350, p. 19, and Section I-D of this report).

B. Supporting Laboratory Studies

Most of the laboratory studies during the past year have centered around the oxide reduction and rare earth removal steps of the proposed pyrochemical process for fast breeder reactor fuels. These steps

(see Fig. I-1, ANL-7350, p. 6) involve a reduction of the uranium-plutonium oxide fuel to metallic uranium and plutonium and extraction of the alkali, alkaline earth, and rare earth fission products into salts which are discarded as waste. The reduction step consists of suspending the oxide mixture in a molten salt which is contacted with a liquid alloy. The alkali, alkaline earth, and rare earth fission products partition preferentially into the salt mixture while the metallic uranium and plutonium partition into the liquid metal phase.

In the earliest version of the process flowsheet, the same salt mixture was employed for the reduction and partition steps. This required that the compositions of the salt mixture and the alloy be chosen for the maximum fission product separation consistent with a high (99.5%) plutonium (and uranium) recovery in the partition step. Studies of the distribution behavior of plutonium, uranium, and selected fission product elements indicated that a Cu-33 w/o Mg alloy and a salt containing about 15 m/o $MgCl_2$ would provide the maximum fission product removal consistent with the desired plutonium recovery.

1. Reduction of Uranium Oxide

The system that was selected initially for the reduction and partition steps consisted of a Cu-33 w/o Mg liquid metal phase and a 15 m/o $MgCl_2$-37.5 m/o $CaCl_2$-42.5 m/o NaCl-5.0 m/o CaF_2 salt mixture. However, laboratory studies indicated that UO_2 reductions of only 90% could be achieved with this metal-salt system. Modifications of the salt composition, such as increasing the $MgCl_2$ concentration to 50 m/o, increased the reduction yield to only about 95%. The unsatisfactory reduction yields were attributed to the formation of a protective layer of MgO (a product of the reaction) on the UO_2 particles. On the basis of this hypothesis, UO_2 reduction studies were conducted with a salt composed of 80 m/o $CaCl_2$-20 m/o CaF_2 and an alloy consisting of 5 w/o Ca-31 w/o Mg-64 w/o Cu. In this system the reaction product is CaO which is soluble (~20 w/o) in the molten salt and would, therefore, not be expected to form a protective coating on the UO_2 particles. Essentially complete reductions of high-fired UO_2 pellets were achieved readily with this salt-metal system. The reduction of UO_2 was 99% complete in 60 min, compared with only 85% reduction of the UO_2 in the same period by Cu-Mg alloy and a salt containing $MgCl_2$.

2. Distribution between Molten Salts and Liquid Alloys

The decision to use the $CaCl_2$-CaF_2 salt and the Ca-Mg-Cu alloy for the reduction step required the redetermination of distribution coefficients (K_d = w/o in salt/w/o in metal) for plutonium and the alkali, alkaline earth, and rare earth fission product elements in this system.

The distribution coefficient for plutonium was needed to determine whether the reduction salt would require a treatment for additional plutonium recovery before it was discarded.

The distribution coefficients of plutonium for the 80 m/o $CaCl_2$-20 m/o CaF_2 salt mixture and liquid Cu-33 w/o Mg alloy containing varying amounts of calcium were determined at 700 and 800°C. Calcium metal was added incrementally to the alloy to produce calcium concentrations of 0.1, 0.2, and 3.4 w/o. Salt and metal samples were taken at 700 and 800°C at each calcium concentration. The resulting distribution coefficients of plutonium are presented in Table I-1. The results indicate that at 800°C about 0.01% of the plutonium would be lost with the salt if it were discarded after the reduction step (assuming that equal weights of salt and metal alloy are used in the reduction).

TABLE I-1. Distribution of Plutonium between 80 m/o $CaCl_2$-20 m/o CaF_2 and Cu-33 w/o Mg Alloy Containing Calcium

(Nominal Concentration of Pu in Alloy ~3 w/o)

	K_d[a]	
w/o Ca in Alloy	700°C	800°C
0.1	2.4×10^{-4}	7.6×10^{-5}
0.2	8.1×10^{-5}	3.6×10^{-5}
3.4	2.6×10^{-5}	2.9×10^{-5}

[a](w/o Pu in salt)/(w/o Pu in alloy).

The distribution coefficients of rubidium, barium, and cerium between a molten 80 m/o $CaCl_2$-20 m/o CaF_2 salt and a liquid 5 w/o Ca-31 w/o Mg-64 w/o Cu alloy at 800°C are ~500, 700, and 1×10^{-2}, respectively. These values indicate that about 98.8% of the rubidium and barium (probably also cesium and strontium) would be extracted into the reduction salt and would, therefore, be removed from the plutonium and uranium in the reduction step. Nearly all of the cerium (and presumably the other rare earth fission products) would remain with the plutonium and uranium. The rare earth fission products are extracted from the alloy by a salt containing $MgCl_2$ in a subsequent partition step.

The effectiveness of the separation of rare earth fission products from plutonium by preferential extraction into a salt phase depends upon the separation factor, i.e., the ratio of distribution coefficients for the rare earth element and plutonium. The separation factor was evaluated for a Cu-33 w/o Mg metal phase and a 50 m/o $MgCl_2$-30 m/o NaCl-20 m/o KCl salt phase by determining the distribution coefficients of plutonium

and cerium, a typical rare earth fission product. No difficulty was encountered in measuring the distribution coefficient of plutonium. Because the distribution coefficient of cerium has a high value (about 10^2-10^3), slight contamination of the metal alloy samples by the salt during the sampling operation causes a large error in the measured distribution coefficient. Therefore, a new sampling method was used in the cerium measurements. A small standpipe was inserted through the salt into the liquid metal. After an equilibration period, the thin layer of salt was removed from the liquid metal surface in the standpipe by means of a Fiberfrax[1] wick, and the liquid metal samples could thus be withdrawn without exposure to the salt. The results of these studies are summarized in Table I-2. The data show that the cerium-plutonium separation factor varied from 1150 at 600°C to 610 at 800°C. These values indicate that high decontamination of plutonium from rare earth fission products is possible in this system.

TABLE I-2. Cerium-Plutonium Separation Factor.
Salt: 50 m/o $MgCl_2$-30 m/o NaCl-20 m/o KCl;
Alloy: 33 w/o Mg-Cu

Temp. (°C)	K_d(Ce)	K_d(Pu)	Separation Factor
600	577	0.50	1150
700	476	0.44	1080
800	249	0.41	610

C. Supporting Engineering Studies

A small program was maintained during the past year to develop high capacity equipment components for semi-continuous or continuous pyrochemical processes. The principal effort was applied to the development of a mixer-settler and a packed column for liquid metal-molten salt contacting.

A system has been constructed that can provide a continuous flow of molten salt for testing liquid metal-molten salt contacting equipment. Fig. I-2 shows the system as it appeared during recent modifications. The tank at the lower right serves as a surge tank and as the pump sump. The pump is normally mounted on the leftmost flange of the tank, but it was raised out of the tank to facilitate the modifications to the sytem. The uppermost vessel is a constant-head tank that is kept full of molten salt by the pump. Excess salt returns from the constant-head tank to the pump sump through an overflow line. Salt from the constant-head tank is fed through a control valve to the metal-salt contactors to be tested (two mixer-settlers in this case), into a weigh tank, and back to the pump sump.

[1] Trade name for a fibrous form of aluminum silicate.

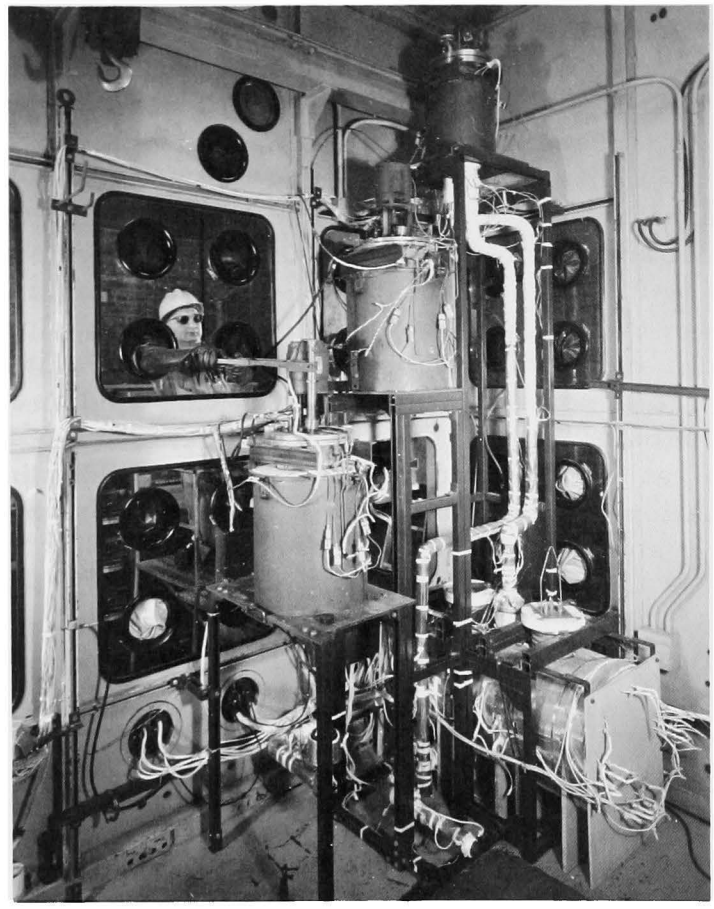

Fig. I-2. Test Facility for Metal-Salt Contacting Equipment.

Shakedown runs were made in which molten salt was circulated through the equipment with liquid metal present in the mixer-settlers. These runs suggested minor equipment modifications which have now been completed. The next experiments will evaluate phase separation and reaction characteristics for a $MgCl_2$-30 m/o NaCl-20 m/o KCl/cadmium alloy system. The performance of the mixer-settlers in salt transporting uranium from one cadmium alloy to another will be determined.

A few experiments have been performed to study the phase disengagement properties of various agitated metal-salt systems. The initial objective of this study is to provide an index of the relative ease of phase disengagement for the various metal-salt systems of current process interest.

In the procedure used, the metal alloy and salt mixture are stirred together to attain a steady-state dispersion of metal droplets in the salt phase. The melt is then allowed to settle for a fixed period of time (about one minute) and the bulk of the salt phase (~70%) is quickly poured into a receiver. The amount of metal remaining in the salt phase is then determined and compared with the amounts left in the salts in other tests with

different salt compositions and alloys. The vessel geometry, mixing conditions, and salt-to-metal volume ratio (2 to 1) are the same in all tests. The salt and alloy compositions and the temperature are the variables.

A few results of these experiments are presented in Table I-3. The entrainment levels are not those which would be expected in pyrochemical processes, since the experimental procedure was deliberately designed to produce measurable entrainment levels in the poured salt phases. The values given indicate the relative ease of achieving phase disengagement for the systems tested.

TABLE I-3. Partial Results of Phase Disengagement Experiments

System	Application	Entrainment Level (w/o)
Wood's metal/water, 85°C	for reference only	0.0003
Cu-33 w/o Mg/ternary salt[a] + 5 w/o MgF_2, 600°C	candidate Pu transport donor system	0.01
Cd-18 w/o Mg/ternary salt[a], 600°C	candidate Pu transport acceptor system	0.032
Zn-4 w/o Mg/ternary salt[a], 600°C	candidate Pu transport acceptor system	0.11
Cu-33 w/o Mg/$CaCl_2$-15 m/o CaF_2 (CaO level of 12 w/o after a UO_2 reduction), 800°C	current reference flowsheet reduction system	0.37
Cu-33 w/o Mg/ternary salt[a], 600°C	candidate Pu transport donor system without 5 w/o MgF_2 (see second system above)	0.87

[a]Ternary salt = 50 m/o $MgCl_2$-30 m/o NaCl-20 m/o KCl.

A high-temperature extraction facility has been designed and constructed to study mass-transfer rates between liquid metal and molten salt solvents in packed, countercurrent extraction columns. In addition, information on the design and operation of such equipment will be derived, limiting flow rates for columns of this type will be determined, and the entrainment of metal in the effluent salt stream will be studied.

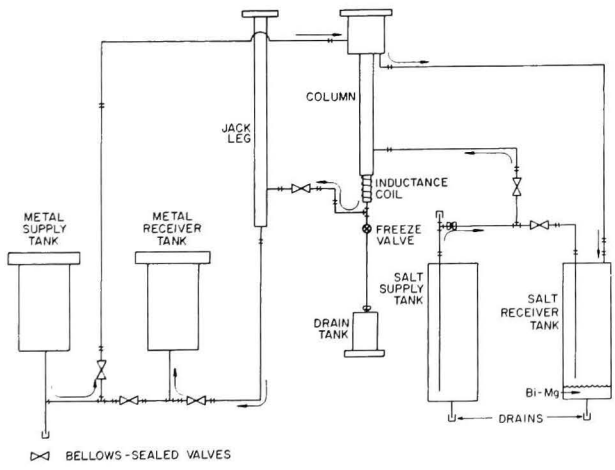

Fig. I-3. Schematic Diagram of High-Temperature Extraction Facility.

A schematic diagram of the equipment is presented in Fig. I-3. The equipment consists of a column, a jack leg to control the position of the metal-salt interface in the column, supply and receiver tanks for the metal

and salt solvents, a column drain tank, and bellows-sealed valves to control the flow of the fluids. The entire facility is constructed of type 304 stainless steel. Fig. I-4 is a photograph of the equipment.

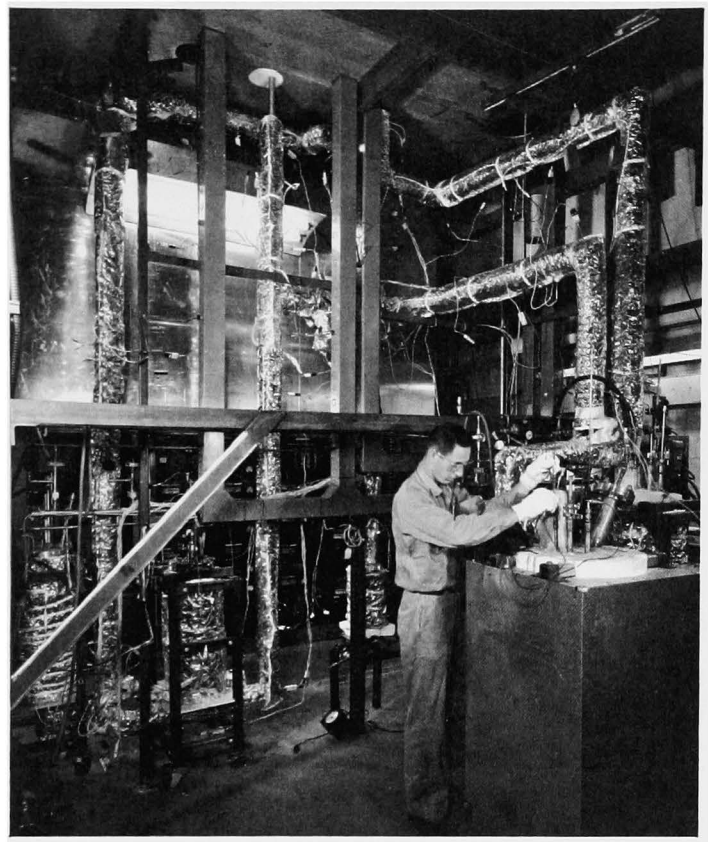

Fig. I-4. High-Temperature Extraction Facility.

The present column is a 1-in. pipe, 3 ft long, packed with 1/4-in. Raschig rings. Liquid metal (the discontinuous phase) is sprayed into the top of the column through several small holes in a horizontal tube in the top disengaging section (see Fig. I-5). The disengaging section is a 3-in. pipe containing a system of weirs to maintain the salt level in the column and to separate the metal feed from the salt effluent. Liquid salt (the continuous phase) enters the bottom of the column beneath the packed section. The position of the metal-salt interface below the packed section is determined by a mutual-inductance probe which surrounds the 1/2-in. tube where the interface is maintained.

The salt and metal supply and receiver tanks are equipped with agitators, thermocouple wells, sample ports, and movable resistance probes for liquid-level detection. In addition, the metal tanks have mutual-inductance probes and the salt tanks have time-delay reflectometry probes for liquid-level determination. Each tank has connections to the pressure-vacuum manifold to provide for movement of the solvents by pressure siphoning from tank to tank and to and from the column.

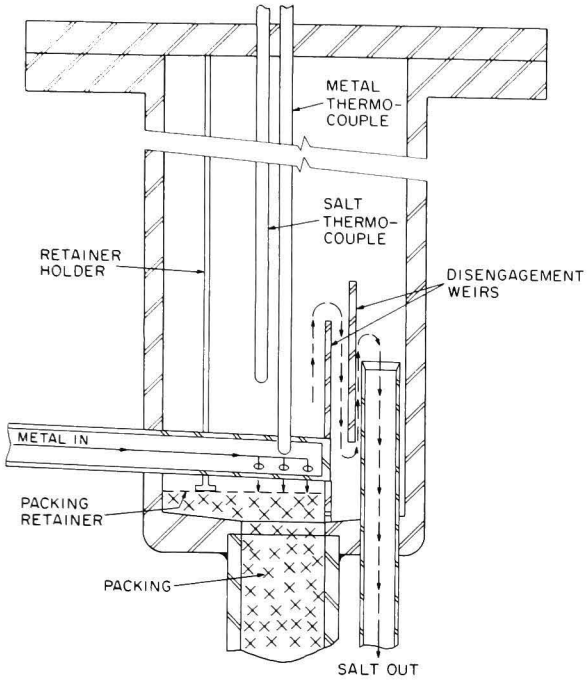

Fig. I-5. Top Disengagement Section of Metal-Salt Extraction Column.

A single extraction experiment lasts from 20 to 120 min, depending on the flow rates, and is terminated when the supply of metal or salt is exhausted. Prior to a subsequent experiment, the solute which was extracted from the metal into the salt is removed from the salt by contacting it with a Bi-6 w/o Mg alloy in the salt-receiver tank. Additional solute is then dissolved in the alloy in the metal-receiver tank for the next run. The entire apparatus is kept at operating temperature between experiments, and is only shut down completely at the end of a series of experiments.

In an experiment to study the extraction of cerium from a Cd-6.9 w/o Mg-2.2 w/o Zn-0.65 w/o Ce alloy into a 52.4 m/o $MgCl_2$-28.6 m/o NaCl-19 m/o KCl salt mixture at 600°C, 40 kg of metal was contacted with about 7 kg of salt over a 32-min period. The 33 in. of packed column length provided about 2.4 theoretical extraction stages, which is in good agreement with the value predicted from preliminary studies (see ANL-7175, p. 35). An extraction rate of 1.2 g Ce/min was realized with a metal flow rate of 1080 g/min and a salt flow rate of 181 to 276 g/min. During this run only 0.1 g of cadmium from the alloy was carried into the effluent salt. In future runs the effects of flow rates, flow ratios, temperature, and packing size will be studied.

D. Experimental Flowsheet Investigations

An experiment was conducted in which the steps of the batch flowsheet (Fig. I-6) for the plutonium salt transport process were carried out in sequence in bench-scale engineering equipment. The purpose of the experiment was to verify the chemistry of the proposed process and to identify potential engineering problems. All of the process steps except plutonium and uranium retorting were performed in equipment that was located in a walk-in-hood. Therefore, it was necessary to restrict the work to a narrower range of operations than those that are permissible in a normal alpha-glovebox facility.

Alumina crucibles (5 1/2-in. dia.) equipped with tantalum baffles and Mo-30 w/o W agitators were used in the experiment. Phase separations were accomplished either by pressure-siphoning one liquid phase

through a heated transfer line or by allowing a salt-metal system to freeze, breaking away the crucible, and physically separating the solidified salt and metal ingots.

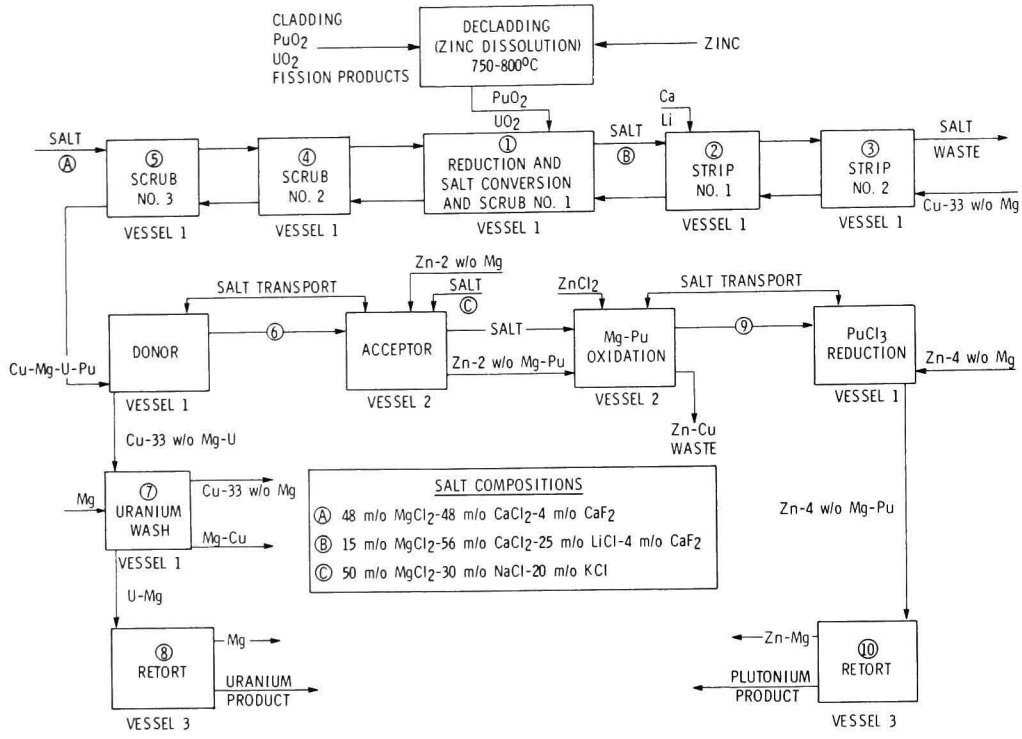

Fig. I-6. Flowsheet for Plutonium Salt Transport Experiment.

The starting material for the experiment was simulated fast breeder reactor core fuel consisting of 199 g of plutonium as PuO_2, 400 g of uranium as UO_2, and oxides of 24 inactive fission product elements. The fission product elements were present in amounts corresponding to a burnup of 10%, a specific power of 150 kW/kg(U + Pu), and a cooling period of 15 days.[2] About half of the plutonium that was charged to the experiment represented in-process inventory.

Oxide Reduction (Step 1). The simulated oxide fuel was introduced to the reduction step in which plutonium, uranium, and most of the fission product elements were reduced to the metallic state by a liquid Cu-33 w/o Mg alloy in the presence of a 47.5 m/o $MgCl_2$-47.5 m/o $CaCl_2$-5.0 m/o CaF_2 salt phase. The reduction was carried out at 800°C for 4 hr at a mixing speed of 600 rpm. At the completion of the reduction step, the uranium was present as precipitated metal in the bottom of the vessel, while the plutonium and most of the fission products were distributed between the liquid metal and molten salt phases. The reduction yields were ~99% and ~99.9%, respectively, for uranium and plutonium. The loading of

[2] L. Burris and I. G. Dillon, "Estimation of Fission Product Spectra in Discharged Fuel from Fast Reactors," ANL-5742 (July 1957).

MgO by-product in the salt was about 12 w/o. A plutonium material balance of ~100% was obtained for this step and the plutonium distribution coefficient was 0.33, which is consistent with previously determined values.

Scrub (Steps 4 and 5). The rare earths and the other more electropositive fission product metals were separated from the plutonium and uranium by a five-stage, countercurrent, batch extraction (1-5, the reduction step providing one stage) in which the fission products were extracted into a waste salt stream (3) and the plutonium was collected in the liquid Cu-Mg alloy (5). Two of the five extraction stages were scrub steps (4, 5) in which the Cu-Mg alloy from the reduction step was contacted with fresh reduction salt to provide additional fission product removal from the plutonium. Each of these two steps was conducted at 800°C for 2.5 hr with a mixing speed of ~450 rpm. In the scrub steps, the plutonium distributed as expected, with a distribution coefficient of 0.37. Although 97-99% of the major rare earth elements (Pr, La, Nd and Ce) were removed, removals exceeding 99.9% should be attainable by this process. The rare earth removal may have been limited by carry-over of small amounts of salt from the reduction and scrub steps to the succeeding steps of the process. It is believed that this phenomenon can be minimized in future experiments through changes in operating procedures.

Strip (Steps 2 and 3). Two plutonium strip steps were employed to recover residual plutonium from the waste reduction salt. Prior to the first step, calcium and lithium metal were added to the salt to change its composition and thereby enhance the recovery of plutonium by decreasing its distribution coefficient (0.04 vs. ~0.35). In each step the salt was then contacted with fresh Cu-Mg alloy at 700°C for 5 hr with a mixing speed of 250 rpm. Plutonium distribution coefficients of 0.045 and 0.036 were observed for the first and second strips, respectively, based on analysis of filtered samples of the salt and metal. However, chemical analysis of the salt phases from both steps showed that the plutonium content was much higher than that indicated by the filtered samples. Apparently, an insoluble plutonium phase was present which resulted in a loss of 0.75% of the plutonium to the waste salt stream in addition to the 0.02% which was soluble in the salt phase. The nature of this insoluble phase and the reason for its formation are being investigated.

Salt Transport (Step 6). In the salt transport step, plutonium was transported at 600°C from the Cu-33 w/o Mg donor alloy to a Zn-2 w/o Mg acceptor alloy using a 50 m/o $MgCl_2$-30 m/o NaCl-20 m/o KCl salt mixture as the transport salt. The donor and acceptor alloys were located in adjacent vessels connected by a heated transfer line. The bulk of the refractory and noble metals remained in the Cu-Mg alloy. The process operation consisted of (a) extraction of plutonium into the salt phase in the donor vessel, (b) transfer of plutonium-bearing salt to the acceptor vessel, (c) stripping of the plutonium into the acceptor alloy, (d) transfer

of the salt back to the donor vessel, and (e) repetition of the above steps until a satisfactory plutonium recovery was attained. In this experiment 14 cycles were conducted and 99.3% of the plutonium was transported. The rate of the plutonium transport is shown in Fig. I-7. The transport rate was limited by the size of the Al_2O_3 vessels. In an optimized plant operation, it is expected that over 99.9% of the plutonium could be transported in about six cycles. About one gram of copper (or 0.05% of the copper in the donor alloy) was found in the acceptor alloy. Operation of the salt transport step proved to be highly satisfactory.

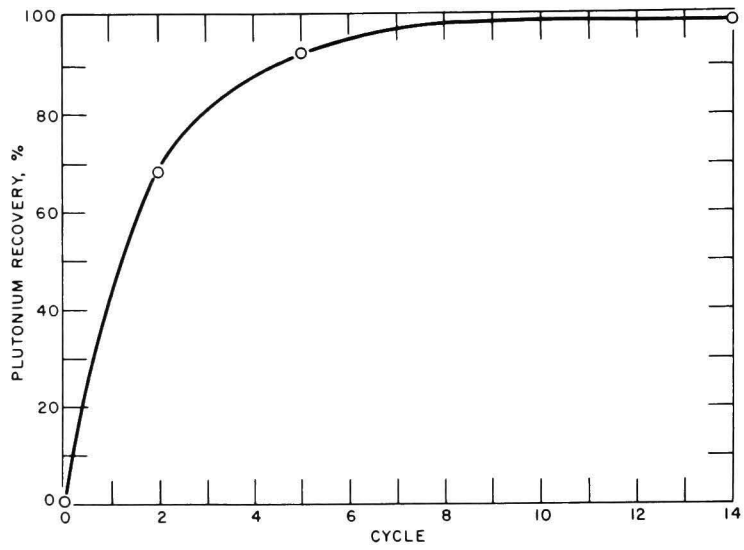

Fig I-7. Rate of Plutonium Transport. (Donor Alloy, Cu-33 w/o Mg; Acceptor Alloy, Zn-2 w/o Mg; Salt, $MgCl_2$-30 m/o NaCl-20 m/o KCl.)

Copper Removal (Step 9). In the plutonium-copper separation step, $ZnCl_2$ was added to the transport salt (in contact with the Zn-Mg-Pu acceptor alloy) to oxidize the magnesium and plutonium in the alloy to $MgCl_2$ and $PuCl_3$ which distribute to the salt phase. This oxidation was carried out at 600°C for a period of 1.5 hr at a mixing speed of 570 rpm. Analytical results indicated that the removal of plutonium and magnesium from the metal alloy was essentially complete. After the oxidation procedure, six salt-transfer cycles were performed, using a new transfer line and a Zn-4 w/o Mg acceptor alloy. (Only about two cycles would be required in plant-scale equipment.) At the completion of the process step, the waste zinc stream contained only ~0.003 g of plutonium. Spark-source mass-spectrometric analyses showed the copper level in the product solution to be about 0.01 g, which corresponds to the level of copper impurity in the zinc and magnesium reagents used in the Zn-Mg acceptor alloy. This process step appears to be highly satisfactory.

Uranium Wash (Step 7). The supernatant Cu-Mg solution in the donor vessel of the salt transport step was poured away from the precipitated uranium, which contained residual copper and magnesium. The precipitate was then given a series of three washes at 700-750°C with liquid magnesium to remove copper and the soluble fission products. A filtered sample of the Cu-Mg alloy prior to the washes indicated the presence of 0.67 g of plutonium. However, analysis of the combined Mg-Cu wash solutions showed that 2.2 g of Pu was present in this waste stream. Possible explanations for this loss include (1) slight coprecipitation of plutonium with uranium during the reduction step, (2) entrapment of some of the Cu-Mg-Pu solution in either the precipitated uranium matrix or in metal-salt agglomerates formed on the baffles during the reduction, and (3) entrapment of unreduced PuO_2 in the precipitated uranium or in the agglomerates. Any unreduced PuO_2 would be reduced to soluble plutonium metal upon exposure to the magnesium in the wash step. This phenomenon is being investigated in additional experiments.

Plutonium and Uranium Recovery (Steps 8 and 10). The plutonium and uranium product solutions were retorted to remove the solvent metals. Samples of the products from the retorting step were submitted for spark-source mass-spectrometric analysis.

Process and Equipment Performance

The results of the first plutonium salt-transport experiment are summarized in Table I-4. In general, the separation of fission product

TABLE I-4. Summary of Results of Plutonium Salt Transport Experiment

Plutonium Recovery[a]: (199.3 g Charged)	51% (of Pu charged) in product solution 47% (of Pu charged) in process inventory 2% (of Pu charged) in waste streams 100% material balance
Plutonium Purity:	>99% removal for noble and refractory metal fission products 97-99% removals for rare earth fission products <0.1% uranium in product ~50 ppm copper expected in retorted product

[a]Since there was no plutonium present in reagents recycled from a previous run, the level of plutonium recycle (in-process inventory) was estimated and compensated for by having sufficient original charge to provide a reasonable throughput of plutonium.

elements from plutonium was satisfactory, but the recovery of plutonium was slightly lower than expected. Alumina crucibles were used for convenience in the experiment, and recent evidence suggests that a portion of the plutonium loss resulted from interactions with these crucibles. All equipment components such as agitators, furnaces, and transfer tubes performed satisfactorily. A total of 28 salt transfers were made in the salt transport step and 12 salt transfers were made in the copper separation step. The trouble-free operation of the transfer tubes in this experiment further demonstrates the reliability of the present transfer tube designs. Careful techniques and radiation monitoring during charging, unloading, and sampling for all steps of the process limited the alpha activity almost entirely to the interior of the furnace vessels.

Future experiments of this type will be directed primarily to evaluations of chemical flowsheets that incorporate semicontinuous or continuous extraction steps, although the experiments themselves will be conducted on a batch basis. Meanwhile, an inert-atmosphere glovebox facility is being installed for larger-scale engineering demonstrations of the plutonium salt transport process.

II. VOLATILITY AND FLUIDIZATION PROCESSES

The reaction of fluorinating agents with nuclear reactor fuel materials in fluid-bed systems to produce volatile UF_6 and PuF_6 is the basis of fluid-bed fluoride volatility processing of spent nuclear fuels. Major attention in the development program has been directed toward development and demonstration of a flowsheet for light water reactor fuels. After the fuel is declad, this flowsheet provides for the pulverization of $(U,Pu)O_2$ fuel to fines by reaction with oxygen at 450°C, followed by volatilization of uranium (as UF_6) by reaction with BrF_5 at 300°C, and then volatilization of plutonium (as PuF_6) by reaction with fluorine at 300 to 550°C. The volatile fluorides of certain fission product elements accompany the hexafluorides of uranium and plutonium, necessitating additional separation procedures to produce purified products.

A major effort during the past reporting period consisted of engineering-scale runs to determine for scale-up purposes the effects of process variables during the BrF_5 step on UF_6 production rate and BrF_5 utilization efficiency. UO_2 charges in these runs ranged up to 4.4 kg. In other work, a series of experiments was performed to provide information on the rate of fluorination of PuF_4 in an alumina fluid bed and to demonstrate the feasibility of producing and transporting PuF_6 in engineering-scale equipment and collecting it quantitatively. In nine experiments, a total of ~2 kg of plutonium (as PuF_4) was successfully fluorinated and transferred in a gas stream to cold traps.

To determine the effects of a radiation field and a fission product content representative of high-burnup reactor fuels, five bench-scale experiments were completed with declad fuel that had been irradiated to ~40,000 MWd/metric ton and cooled 1 to 1 1/2 yr.

In other backup work, the purification problem of separation of PuF_6 from volatile fluorides of the fission product elements was investigated. Ruthenium fluoride (which is considered the most difficult to separate of the fission product fluorides) was mixed with plutonium hexafluoride, and a variety of separation procedures were tested.

At the request of the AEC, the program is being reoriented toward an evaluation of the potential of the process for fast breeder reactor fuel application. Since most of the work reported was done prior to reorientation of the program, the work was directed toward developing reprocessing methods for light water reactor fuels. Nevertheless, much of it is applicable to recovery processes for fast breeder reactor fuels as well.

A. Recovery of Uranium and Plutonium from Spent Nuclear Fuels

1. Engineering Development of Fluorination of Uranium Oxide with BrF_5

A fractional factorial experiment has been completed in which the effects of process variables on the fluorination of U_3O_8 with BrF_5 were studied in an engineering-scale 3-in. dia. fluid-bed facility. BrF_5 can be used for separating uranium, as volatile UF_6, from plutonium since plutonium is not fluorinated to a volatile compound by BrF_5.

The objectives were (1) to determine the effects of process variables on the oxidation of UO_2 to U_3O_8, the UF_6 fluorination rate, BrF_5 utilization efficiency, and operating characteristics of the system and (2) to demonstrate the feasibility and reliability of fluorinating large quantities of U_3O_8 fines with BrF_5. During fluorination, the effects of six independent variables were studied: bed temperature (300°C or 225°C), inlet partial pressure of BrF_5 (~0.16 or ~0.29 atm), fluidizing gas velocity (0.53 or 0.89 ft/sec), quantity of UO_2 charged (2.2 or 4.4 kg), particle size of alumina bed material (-100 or 48-100 mesh), and the presence or absence of inactive fission product compounds. This work complements the bench-scale study described elsewhere in this report on the separation of uranium from plutonium using BrF_5, followed by recovery of the plutonium by fluorination to volatile PuF_6 using elemental fluorine.

The major equipment items used in this study were (1) a preheater to heat the reagent gases to operating temperatures, (2) a reaction section of the fluid-bed reactor to contain the fluidized bed and fuel charge, (3) a filter section of the fluid-bed reactor to prevent entrained solids from entering the off-gas pipes, (4) sodium fluoride traps to sorb UF_6 from the off-gases, and (5) a scrubbing system to remove interhalogens and residual UF_6 from the off-gases that pass through the sodium fluoride traps. A schematic of this equipment is shown in Fig. II-1.

At the start of each run, the alumina bed was prefluorinated with fluorine to simulate the effect of a plutonium fluorination conducted in the bed in a prior run. Crushed UO_2 pellets (and in some cases a mixture of fission product compounds) were then added to the bed and oxidized in an oxygen-nitrogen gas stream at 450°C to form U_3O_8 fines. The amount of UO_2 charged in the oxidation step was such that the bed contained 40 w/o U_3O_8 at the end of the step. In the next step, U_3O_8 was fluorinated with BrF_5, using one of the specified sets of process conditions.

a. Results and Discussion

In general, operation of the reactor was very smooth. In all cases the beds were well fluidized and free-flowing at the end of the processing cycle.

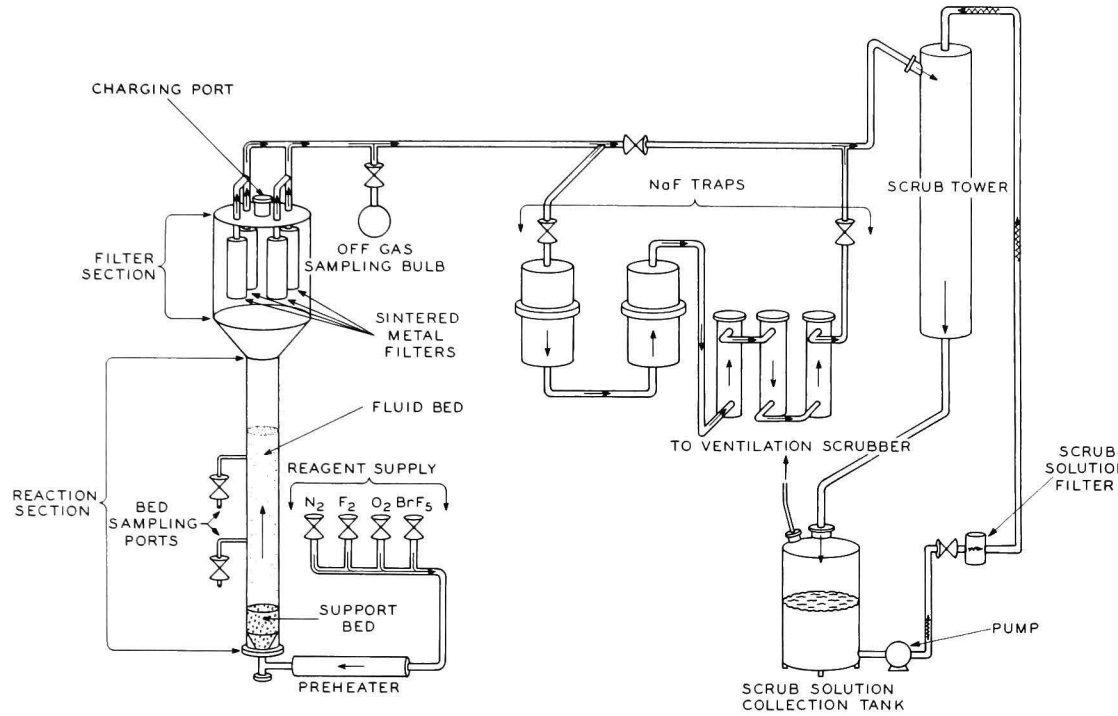

Fig. II-1. Engineering-Scale Equipment Used To Study the BrF_5 Fluorination of Uranium Oxide.

Oxidation Step. The rate of oxidation of UO_2 to U_3O_8 varied from about 3 to 9 lb/hr over the period when the first half of the UO_2 charge was being reacted. The utilization of oxygen was as high as 10% over the same period. The larger UO_2 charge (4.4 kg) and smaller fluidized particle size (-100 mesh) gave higher reaction rates and oxygen utilizations. The particle size of U_3O_8 fines produced by the oxidation of UO_2 in four runs was analyzed employing a Coulter counter. The results showed that a majority of the U_3O_8 particles were in the range 0.3 to 5 microns diameter and that the average particle diameter was about 3 microns.

BrF_5 Fluorination of U_3O_8. In some of the runs in which the charge contained fission products, small (3/8 in.) agglomerates were found in the alumina beds. Their formation was related to the presence of barium, cesium, molybdenum, and rubidium. The agglomerates did not appear to affect operation during the runs or to hinder the removal of the beds at the end of a run.

Data were obtained for the average UF_6 production rate and the average BrF_5 utilization efficiency from the time of startup to the times when the fraction of uranium reacted, F, reached 0.50, 0.667, and 0.75. The average UF_6 production rate ranged from 3.0 lb/hr [58 lb/(hr)(ft^2)] to 9.0 lb/hr [176 lb/(hr)(ft^2)]. The average BrF_5 utilization efficiency ranged from 31 to 78%.

The UF_6 production rates at the two levels of each variable given earlier were compared, and the following levels were found to give the higher production rates: a temperature of 300°C, a BrF_5 inlet partial pressure of 0.29 atm, a fluidization gas velocity of 0.89 ft/sec, and a UO_2 charge of 4.4 kg. Similarly, a temperature of 300°C, a BrF_5 inlet partial pressure of 0.29 atm, and a fluidization gas velocity of 0.89 ft/sec gave the higher diminishing-sphere rate constants; and a temperature of 300°C and a UO_2 charge of 4.4 kg gave the higher BrF_5 utilization efficiencies. Quantitative data on these results and on other results (UO_2 oxidation rates, corrosion data, and the use of on-line gas analyzers, etc.) are reported in a topical report, ANL-7370 (in press).

Within the ranges studied, the conditions that would give the best UF_6 production rate and BrF_5 utilization efficiency are those shown in Table II-1. No runs were performed using the "best" conditions, but it has been estimated that they would give the UF_6 production rates and BrF_5 utilization efficiencies shown in Table II-1. These production rates and utilization efficiencies are considered highly acceptable for process application.

TABLE II-1. Average UF_6 Production Rate and BrF_5 Utilization Efficiency Predicted at "Best" Levels of Independent Variables

	Oxidation Step	BrF_5 Fluorination Step		
Temperature, °C	450[a]	300		
Concentration	19.2 v/o[a] (O_2 in N_2)	0.29 atm (BrF_5 in N_2)		
Superficial velocity, ft/sec	1.4[a]	0.89		
UO_2 charge, kg	4.4	4.4		
Alumina particle size, mesh	-100	-100 or 48-100		
Fission products	Present[b] or Absent	Present[b] or Absent		
		F, Fraction of Uranium Reacted		
		0.50	0.667	0.75
Estimated Average UF_6 Production Rate, lb/hr		9.5	9.1	8.4
lb/(hr)(ft^2)		185	177	164
Estimated Average BrF_5 Utilization Efficiency, %		75	67	60

[a]Not varied in this work.

[b]The relative quantities of fission product compounds added represent the amounts which would be present in five batches of spent UO_2 of typical burnups. The fission products were SeO_2, SrF_2, RbF, Y_2O_3, ZrO_2, MoO_3, RuO_2, RhO, PdO, Ag_2O, CdO, In_2O, SnO_2, Sb_2O_5, I, CsF, BaO, La_2O_3, CeO_2, PrO_2, Nd_2O_3, Sm_2O_3, Eu_2O_3, and Gd_2O_3.

2. Engineering-Scale Alpha Facility Operations

Development work on the fluid-bed fluoride volatility process for the recovery of uranium and plutonium from spent uranium dioxide fuels is being carried out in the engineering-scale alpha facility. The major objectives of this work are to demonstrate PuF_6 handling in engineering-scale equipment and to determine the feasibility of fluoride volatility flowsheets.

The facility comprises two large alpha boxes, one containing process equipment and the other containing equipment for scrubbing and filtering process exhaust gases and ventilation air. Housed in the process equipment alpha box are two fluid-bed reactors, primary and backup filters, and two in-series cold traps. One of the fluid-bed reactors is a fluorinator for carrying out head-end steps on synthetic fuel materials, and the other is a converter that was used in a successful exploratory fluid-bed study on separating plutonium as PuF_4 from uranium-plutonium hexafluoride mixtures by thermal decomposition (see ANL-7350, p. 27, 1967). The converter may be used in the future for studies of the conversion of uranium and plutonium hexafluorides to oxides. A recent addition, to provide flexibility in flowsheet development work, was equipment for handling BrF_5. A shakedown test of the BrF_5 feed and off-gas treatment system was successfully completed during the current report period.

a. Plutonium Fluorination Campaigns

Three campaigns were performed to provide information on the rates of fluorination of PuF_4 from an alumina fluid bed for scale-up purposes and to demonstrate the feasibility of producing and transporting PuF_6 in engineering-scale equipment and collecting it quantitatively.

A campaign consisted of three successive experiments in which PuF_4 was fluorinated to PuF_6 with fluorine, followed by a cleanup-fluorination experiment, which included fluorination of the primary filter region and a separate cleanup of the lines and other equipment (secondary filter section and cold traps) to recover PuF_4 deposited as a result of alpha decomposition of PuF_6 (or other interaction mechanisms). A single bed consisting of about 6500 g of 48-100 mesh prefluorinated alumina was used in each campaign.

The effect of the starting temperature of the fluorination on plutonium behavior, i.e., retention by alumina and overall recovery, was investigated. Starting temperatures were 300, 375, and 450°C in the three successive campaigns. This series of experiments may be considered (1) a demonstration of the plutonium recovery step of the interhalogen flowsheet for light water reactor fuels (see ANL-7350, p. 21) or

(2) representative of a step that may be required in a plutonium purification scheme for fast breeder fuels. The results of this work are, thus, applicable to fuel for both thermal power reactors and fast breeder reactors.

Each individual fluorination experiment involved the fluorination of 200 g of plutonium (charged as -325 mesh PuF_4). Thus, almost 2 kg of plutonium was involved in the nine campaign-type experiments, compared with a total of about 600 g of plutonium used in some 15 experiments up to this time.

The bed was brought to the starting temperature while fluidized with nitrogen; the gas stream was then put on total recycle and fluorine flow was started at a rate equivalent to about 20% of the total gas flow rate while the gas mixture was bled off at the same rate. The ratio of fluorine flow rate to nitrogen (purge and filter blowback gas) flow rate was such that a steady-state fluorine concentration of about 85% was attained. In each experiment the temperature was increased incrementally, 25°C every 15 min, until the final temperature of 550°C was reached. The total time for fluorination was 5 hr for each experiment in Campaigns 1 and 2. The fluorination time was reduced to 3 hr in each experiment of Campaign 3.

The PuF_6 was collected in two in-series cold traps operated at about -65°C and was subsequently transferred with an inert-gas purge to NaF sorption traps. In two instances during high PuF_6 production periods, the PuF_6 was trapped directly on NaF to obtain information on fluorine utilization and to determine how close to equilibrium the system was operating.

Samples from these traps and from the alumina beds provided the basis for analysis of the experiments. Separate cleanup fluorinations (2 hr of fluorination with fluorine at 300°C) were conducted on the primary fluorinator filters and remaining process equipment (cold traps, lines, secondary filter), and the amount and location of plutonium deposits in the equipment was determined. This information was useful not only for material balance purposes but also for studying the basic question of plutonium holdup as a function of plutonium throughput. If the plutonium is recoverable, this interim holdup does not represent a process loss, but merely reflects the need for an additional operating period. As shown in the summary of results below, recovery of PuF_4 deposits is feasible.

Very encouraging results were obtained, as may be seen in the summary of data presented in Table II-2. The low residual concentrations of plutonium in the three final alumina beds, 0.010, 0.029, and 0.022 w/o, represent a total loss of only about 0.25% of the plutonium charged. The reduction in run time from 5 hr in Campaigns 1 and 2 to 3 hr in Campaign 3 had no adverse effect on plutonium retention by alumina.

TABLE II-2. Summary of Fluorination Campaign Experiments

Operating Conditions:
Campaign 1: 592 g Pu, 300-550°C, 5-hr experiments
Campaign 2: 587 g Pu, 375-550°C, 5-hr experiments
Campaign 3: 578 g Pu, 450-550°C, 3-hr experiments

Campaign	Residual Plutonium Concentration in Alumina (w/o)	PuF_6 Production Rate [lb/(hr)(ft^2)]	Average Fluorine Utilization Efficiency[a] (%)	Plutonium Material Balance (%)
1	0.010	2.4	22	97
2	0.029	2.4	17	101
3	0.022	4.1	28	99

[a]Calculated as the amount of PuF_6 produced during the total run time compared with the amount of PuF_6 that could be produced at equilibrium ($PuF_4 + F_2 \rightleftharpoons PuF_6$); the change in fluorine requirement with temperature was considered in this calculation.

Both the average PuF_6 production rate and the fluorine utilization efficiency[1] were higher in the third campaign than in the earlier campaigns. The improvement was directly related to the amount of plutonium in the fluidized bed at a given time as shown in Table II-3. For example, during the first half-hour of Run 1 of Campaign 3, the average quantity of plutonium in the bed was 204 g and a fluorine efficiency of 98% was achieved. During the next half-hour, the average plutonium content was only 154 g and the efficiency dropped to 51%. As the plutonium content diminished during the final two hours, a further significant drop in efficiency occurred. It is likely that similar characteristics prevailed during the final period of the earlier 5-hr runs and led to reduced fluorine efficiencies.

TABLE II-3. Fluorine Efficiencies and PuF_6 Production Rates during First and Second Runs of Campaign 3

Time Period	Operating Conditions in Period		Run 1			Run 2			Average PuF_6 Production Rate [lb PuF_6/(hr)(ft^2)]	
	Fluorine Conc. in Fluorinator (%)	Fluidized Bed Temp. (°C)	Amount of Plutonium in Fluorinator (g) Beginning of Period	Amount of Plutonium in Fluorinator (g) End of Period	Fluorine Efficiency (%)	Amount of Plutonium in Fluorinator (g) Beginning of Period	Amount of Plutonium in Fluorinator (g) End of Period	Fluorine Efficiency (%)	Run 1	Run 2
First half-hour	Increasing 6 → 91	Increasing 450 → 525	194.3	145.1	77	228.0	180.0	98	5.20	6.53
Second half-hour	91 → 95	525 → 550	145.1	108.1	42	180.0	129.4	51	4.70	6.41
Final two hours	95	550	108.3	33.7	17	129.4	35.7	20	2.25	2.97

Comparison of fluorine efficiencies and PuF_6 production rates for the first two runs of Campaign 3 revealed that fluorine efficiency and production rate were higher in the second run, reflecting the higher plutonium content of the bed in the second run. Only five-sixths of the

[1]Calculated as the amount of PuF_6 produced during the total run time compared with the amount of PuF_6 that could be produced at equilibrium ($PuF_4 + F_2 \rightleftharpoons PuF_6$); the change in fluorine requirement with temperature was considered in this calculation.

charged plutonium was fluorinated during the first run of Campaign 3, possibly as a result of the short fluorination period. This 1/6th heel plus the second charge then gave the improved results in the second run.

Fluorine efficiencies near 100% and production rates up to 6.5 lb $PuF_6/(hr)(ft^2)$ were obtained in the initial period of the second run. The high production rate is not limiting and further improvement in production rate could have been realized by starting with a high concentration of fluorine in the fluidizing gas; in the current procedure, the fluorine concentration is gradually increased from 0 to 95% in the course of gas recycle. Higher rates could also probably have been achieved by operating at a higher initial fluorination temperature, and by passing more fluorine through the bed by increasing the gas velocity and the fluorinator pressure.

The range of material balance values, 97-101% (Table II-2), lies within the range expected on the basis of a statistical sampling experiment conducted recently. Sample treatment includes milling (coarse grinding in a disk mill), sample splitting by riffling, and fine grinding steps, followed by chemical analysis. Gross sampling error proved to be about ±4%.

A complete plutonium material balance for one of the campaigns (Campaign 2) is presented in Table II-4. These data show

TABLE II-4. Plutonium Material Balance - Campaign 2

	Plutonium	
	(g)	% of Charge
Charge	587.1	100.0
Processed to PuF_6		
Recovered from cold trap 1	566.4	96.5
Recovered from cold trap 2	7.6	1.3
Recovered from cold traps and lines during cleanup fluorination	8.0	1.4
Loss through cold traps	4.0	0.7[a]
Subtotal		99.9
Recovered from Primary Sintered Metal Filters during Cleanup Fluorination	4.1	0.7
Unprocessed and Lost		
Grab samples and reactor cleanout	0.7	0.1
Final bed (loss)	1.9	0.3
Total Accounted for	592.7	101.0

[a]Assumed to be recoverable by using a lower cold trap temperature.

that about 99% of the PuF_4 charge was fluorinated to PuF_6 and collected in the two cold traps during the main fluorination period. The cold traps were quite efficient at the current operating temperature of about -65°C. Increased efficiency can probably be achieved by operating at lower temperatures since the small loss (0.7%) sustained is about equivalent to the quantity represented by vapor-pressure considerations alone.

The problem of holdup of plutonium on the primary filters appears to diminish with increased plutonium throughput. The fraction retained on the filters during Campaign 2, 0.7% of the charge, was rather insignificant in terms of the quantity of material processed. In earlier studies with plutonium charges ranging from 20 to 100 g, filter holdup represented as much as 15% of the charge. Holdup, of course, is a function of total available filter area and is responsive to the filter blowback system.

The recovery of material retained on filters is dependent on the ability to expose the filters to concentrated fluorine at 300°C (conditions required for cleanup). Examination of the filters after a total exposure at 300°C of about 30 hr disclosed no obvious deterioration. Much more testing will be needed, however, before conclusions about filter life can be made.

The only nonrecoverable loss is probably represented by the quantity of plutonium retained by the alumina bed, about 2 g or 0.3% of the charged plutonium. This value represents the loss sustained when the bed is used in only one campaign. Losses may be further reduced by using the same bed for several campaigns, if this technique is feasible in practice.

b. Experience with Neutron Counters as Plutonium Monitors

The use of neutron counting equipment was exploited rather widely in plutonium monitoring applications in the current program. Standard neutron survey instruments with either 2.5-in. long or 10-in. long BF_3 probes were mounted at strategic locations (cold traps and NaF traps) and coupled to scalers and recording instruments to record the movement of PuF_6 from the reactor to the cold traps during fluorination and from the cold traps to the NaF traps during PuF_6 transfer. Operating procedures, such as the time-temperature program used in the fluorination experiments, were selected on the basis of the response of the instruments to PuF_6 collection in the cold traps. Similarly, the decision to reduce the fluorination period from 5 hr to 3 hr was based on these data. Transfer of the PuF_6 from the cold traps to the NaF sorption traps was also followed closely with this monitoring technique.

Neutron response curves obtained during the first fluorination experiment of Campaign 3, which were typcial of the curves obtained in

all three campaigns, are shown in Fig. II-2. Figure II-2a shows PuF_6 sorption on NaF (trap 1) during the first 3 hr of this experiment. The observed change in activity level during the first hour was in response to the collection of 86 g of plutonium. During the second and third hours, the PuF_6 was fed directly to the cold traps. As seen by the plateauing in Fig. II-2b, fluorination was essentially complete after the second hour. The transfer of PuF_6 out of the cold trap and the corresponding sorption of this material onto NaF (trap 2) is shown in Fig. II-2c. Approximately 74 g of plutonium was transferred in about 1 hr. Curves similar to those in Fig. II-2b and II-2c were obtained in the other two campaigns.

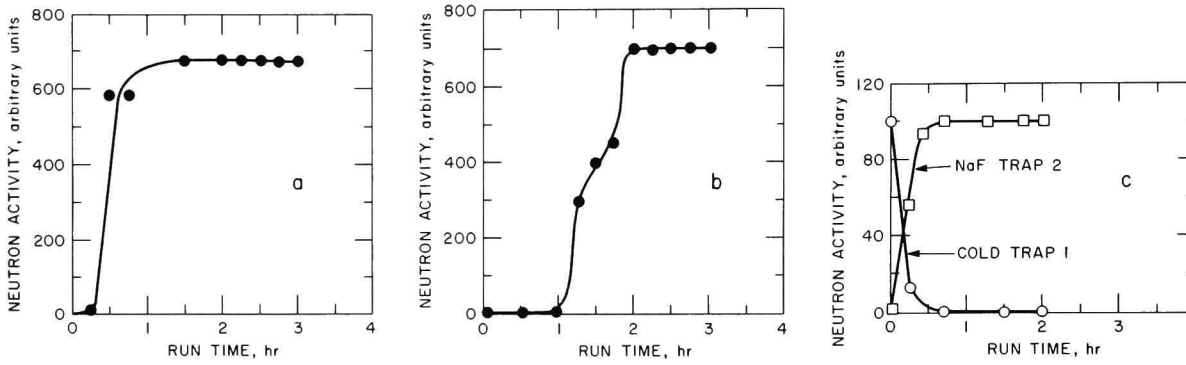

Fig. II-2. Neutron Activity in NaF Traps and Cold Trap during First Fluorination of Campaign 3. a. PuF_6 Sorption on NaF (Trap 1) during Fluorination; b. PuF_6 Collection in Cold Trap 1 during Fluorination; and c. PuF_6 Transfer from Cold Trap to NaF (Trap 2).

Use of these instruments for more quantitative measurements is limited, in large part, by equipment geometry, i.e., the capability of bringing the source close to the detector, because of the inverse square law. In addition, above about 40°C, these detectors are sensitive to temperature. Nevertheless, their value has been proved, and further efforts to extend their use to more quantitative applications appear to be warranted.

3. Bench-Scale Fluid-Bed Studies with Irradiated Fuels

A program demonstrating the fluid-bed volatility processing of irradiated fuel materials is in progress. Experiments are being conducted in a 1 1/2-in. dia. fluid-bed reactor installed in the senior cave facility of the Chemical Engineering Division. Present work is directed to determining the distribution of the actinides and fission products in each of the process streams for the interhalogen process and to test several simple schemes for plutonium decontamination. The fuel charge used was highly irradiated UO_2 pellets, and the bed material was alumina powder.

A series of five bench-scale experiments was completed in which the interhalogen reference flowsheet[2] was tested with declad UO_2

[2]Power Reactor Technology and Reactor Fuel Processing, 10(1), 73-75 (Winter 1966-1967).

irradiated to ~40,000 MWd/metric ton and cooled 1 to 1 1/2 yr. Results for the first two experiments are reported in ANL-7350, pp. 29-31, and the results of all five experiments are summarized here.

The process consists of the oxidation of UO_2 to U_3O_8, uranium volatilization with BrF_5, and plutonium volatilization with fluorine. The equipment, which was previously used for the processing of irradiated uranium alloy fuels, was modified by the installation of a sintered nickel filter (which replaced a packed-bed filter) and the addition of other traps. A schematic of the modified experimental unit is shown in Fig. II-3, and a photograph of the equipment is shown in Fig. II-4.

In each experiment, ~100 g of irradiated UO_2 (containing ~1 g plutonium) was added to a bed of 350 g refractory alumina (T-61, Alcoa) in the fluid-bed reactor. The UO_2 pellets were converted to U_3O_8-PuO_2 fines at 450°C by reaction with 20 v/o oxygen in nitrogen. The sintered nickel filter prevented elutriation of uranium oxides and bed material from the reactor. In this step, the process off-gas passed through two traps containing activated charcoal to remove any volatile products prior to discharge of the gas stream to the cave exhaust.

In the uranium volatilization step, the uranium was separated as UF_6 from plutonium and from most of the fission products by fluorinating with 10 v/o BrF_5 at 300 or 360°C. The process off-gas leaving the sintered nickel filter contained UF_6, Br_2, BrF_5, and volatile fission product fluorides in nitrogen diluent. It was passed through four traps containing various sorbents to remove these volatile species.

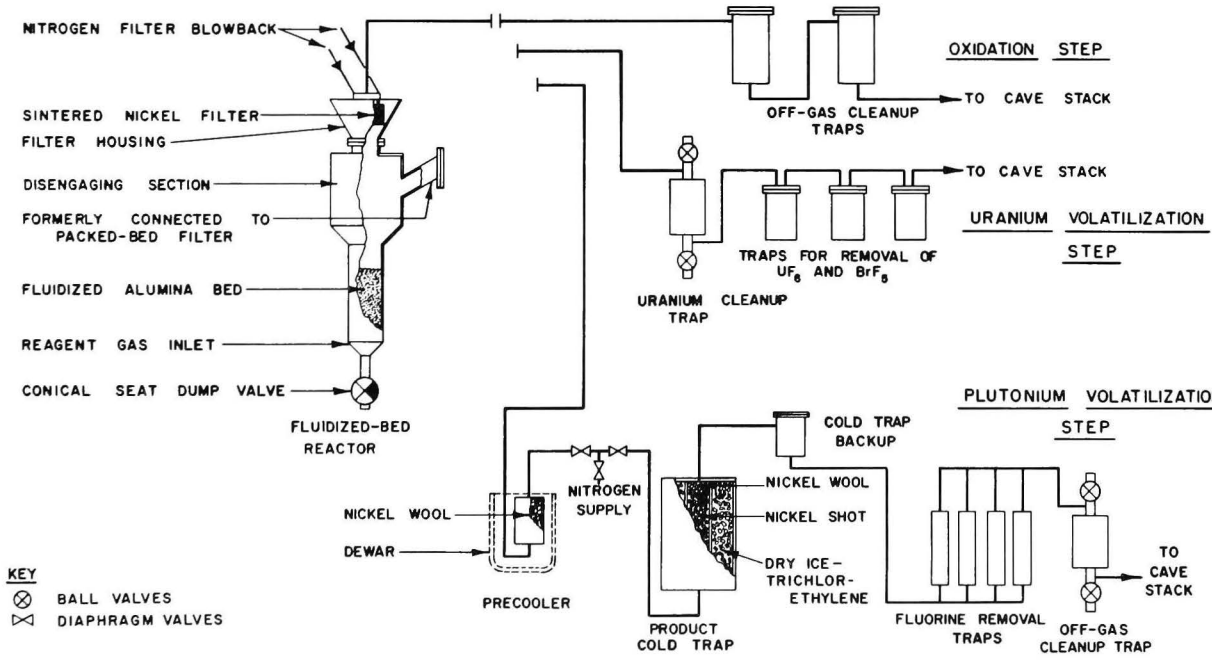

Fig. II-3. Fluidized-Bed Fluoride Volatility Processing Unit Used for Bench-Scale Studies with Irradiated UO_2.

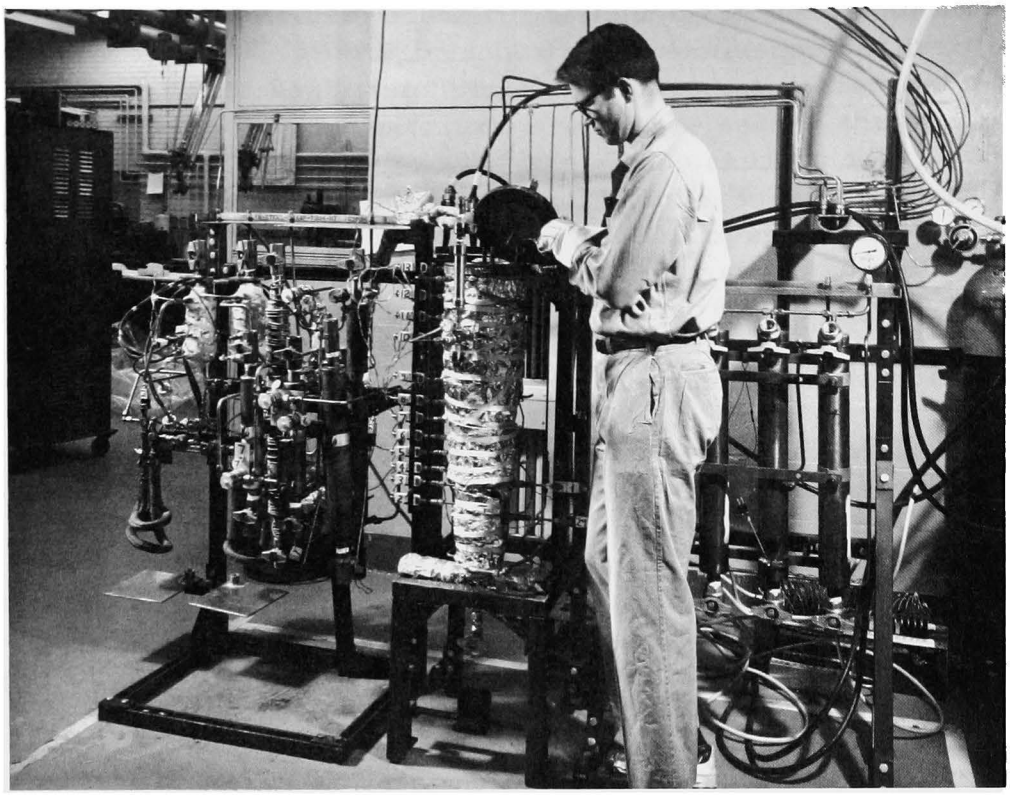

Fig. II-4. The Top Flange of a 1 1/2-in. Fluidized-Bed Reactor Being Removed in Preparation for Equipment Shakedown Testing.

In the plutonium removal step, plutonium was volatilized from the fluidized bed, using 10-90 v/o fluorine at 300-550°C. The off-gas from the fluid-bed reactor first passed through a precooler at 0°C where high-boiling fission product fluorides were collected, and then through the product cold trap where PuF_6 was collected along with some undesired fission products. A backup trap containing NaF pellets at 350°C removed trace quantities of PuF_6 passing through the cold trap. The fluorine in the off-gas was removed by four traps in parallel containing activated alumina. The off-gas cleanup trap downstream from the fluorine-removal traps was filled with NaF pellets at about 400°C for the removal of trace amounts of volatile fission products.

a. Distribution of Actinides and Fission Products in the Process Streams

The ranges of values for the volatile products collected in the traps during the five runs are shown in Table II-5. Examination of these results shows:

1. The principal activities that volatilized during the oxidation step (for fuel cooled 1 yr or more) were krypton (see following discussion) and ruthenium. Up to 3.3% of the ruthenium charged was volatilized.

2. Up to about 13% of the total beta and gamma activity was volatilized with the uranium during the BrF_5 step. The principal gamma activity that accompanied the uranium was ruthenium. In addition, up to 76% of the molybdenum, 2.7% of the antimony, 0.24% of the zirconium, and 1.9% of the niobium were also volatilized with the uranium. More than 99.5% of the uranium and up to 0.95% of the plutonium volatilized during the BrF_5 step.

3. During volatilization of plutonium with fluorine, up to about 2% of the gross beta-gamma activity was transported concurrently. The principal gamma activity transported was ruthenium (3-14%); up to 38% of the molybdenum and small amounts of zirconium (≤0.21%), niobium (≤5.8%), and antimony (≤1.2%) were also volatilized.

TABLE II-5. Volatile Products Collected in Traps during Processing of Irradiated UO_2 (All Five Runs)

	Percent of Charge		
Activity	Oxidation Step	U Volatilization Step	Pu Volatilization Step
U	NA[a]	71-112	0.05-0.33
Pu	NA[a]	0.025-0.95	31-63
β	<0.0001-0.05	7.7-13.7	0.7-0.84
γ	<0.0001-0.5	6.9-11.7	0.5-2.3
Zr	0	0-0.24	0-0.21
Nb	0-<0.0001	0-1.9	0-5.8
Ru	<0.0001-3.3	44-71	3.2-14
Sb	NA[a]	<0.001-<2.7	<0.12-1.2
Mo	NA[a]	<51-76	<6-38
Te	0-0.08	NA[a]	NA[a]

[a]NA = Not analyzed.

The off-gases that passed through the traps and entered the stack were sampled and analyzed for ruthenium, tellurium, and krypton. The krypton values are given as percent of the total krypton released during all processing steps. The amount of krypton, if any, released during decladding is unknown. During the oxidation step, <0.00004% of the ruthenium charged and <0.15% of the tellurium charged were found in the process off-gas discharged to the atmosphere. From 13 to 27% of the krypton was given off during this step, and its discharge to the atmosphere was safely accomplished by dilution with 2000 cfm of cell ventilation air.

Up to 87% of the krypton accounted for was released to the process off-gas during the BrF_5 step. Less than 0.001% of the ruthenium and tellurium charged was found in the stack gas.

Up to 9.6% of the krypton was found in the off-gas during the plutonium volatilization step of three of the five runs, suggesting that a small residue of uranium oxide remained in the reactor after the BrF_5 step. In addition to a small amount of ruthenium ($\leq$0.01%), up to 40% of the tellurium charged was found in the process off-gas that passed through the traps and into the stack. The concentration of volatile activities in the process off-gas discharged to the atmosphere was in all cases within the recommended limiting concentration as defined by AEC standards.

b. Uranium and Plutonium in Final Reactor Beds

The quantitative removal of uranium and plutonium from the fluid bed of the reactor is essential for economic operation of this process. An important part of the work with irradiated fuels is to determine whether or not the presence of fission products and a radiation field significantly affects removal of uranium and plutonium from the fluid-bed material. The results of the five experiments show uranium concentrations in the final alumina beds of 0.0007 to 0.0072 w/o; the mean uranium content was 0.0042 w/o.

Conversion of these data to percentages of the uranium charged show that greater than 99.9% of the uranium was removed from the reactor bed. This result indicates that the presence of fission products and a radiation field does not have an inhibiting effect upon uranium recovery.

The values for plutonium retention (0.003 to 0.036 w/o plutonium in the final alumina beds) were slightly higher than those obtained in three runs in a 2-in. dia. reactor with simulated reactor fuel. The latter three runs[3] were performed in a single alumina bed with non-irradiated UO_2-PuO_2 containing fission product elements equivalent to a burnup of about 10,000 MWd/metric ton U; the plutonium concentration in the final reactor bed was 0.009 w/o (equivalent to removal of 99% of the plutonium). The mean value (0.016 w/o plutonium) for the five runs with highly irradiated UO_2 was obtained by using a new bed for each run and a low charge-to-bed ratio. Extrapolating these results to conditions of larger charge-to-bed ratio and reuse of the alumina bed, greater than 98% plutonium removal from the reactor would be expected. It should be noted that the tests with the irradiated fuel were conducted in apparatus originally designed for alloy fuels and that this equipment is not optimized for work with oxides.

[3]Argonne National Laboratory, "Chemical Engineering Division Semiannual Report, July-December 1966," ANL-7325, pp. 55-56 (April, 1967).

While not conclusive, the experiments with irradiated fuel tend to support the view that fission products and a radiation field associated with irradiated fuels do not significantly affect the removal of plutonium from the fluidized bed.

c. Purification of Plutonium

Certain operations for the purification of plutonium, which might be easily incorporated into a process scheme, were examined in a preliminary fashion. In addition to the decontamination from nonvolatile fission products accomplished in the plutonium fluorination step, a step was added at the end of Experiments 3, 4, and 5 to further decontaminate the plutonium. Either PuF_6 was sublimed from a cold trap at 0°C using a nitrogen gas carrier and collected on NaF pellets at 350°C or the PuF_6 was sublimed at 0°C as above but was thermally decomposed to PuF_4 on a bed of refractory alumina at 300°C.

The primary separation of plutonium from the nonvolatile fission products, which occurs during the production of PuF_6, resulted in a decontamination factor[4] from gamma activities of about 120 for a fuel cooled about one year. When the PuF_6 was collected in a cold trap, sublimed at 0°C, and collected on NaF pellets at 350°C (Experiment 3), the decontamination factor from gamma activities was 1400. In Experiments 4 and 5, which combined sublimation at 0°C with product collection on an alumina bed at 300°C (where thermal decomposition of PuF_6 to PuF_4 occurred), the gamma decontamination achieved was 3200. In each purification process, ruthenium was the predominant gamma-active contaminant[5] accompanying the plutonium.

Experiments 4 and 5 provided an opportunity to examine the movement of ruthenium in terms of the vapor pressures of the compounds of ruthenium likely to be present. The results of this analysis[6] suggested that the ruthenium contaminant was a mixture of RuF_5 with one or more other compounds, possibly $RuOF_4$ and RuF_6.

B. Supporting Investigations

1. Ruthenium Fluoride Separation Chemistry

The fluorination of oxidized nuclear fuel produces the hexafluorides of uranium and plutonium. When these are volatilized from the

[4]Decontamination factor = $\frac{\text{activity per gram Pu in the charge}}{\text{activity per gram Pu in the product}}$.

[5]The antimony activity, which was present in a very small amount, appears to have been masked by the ruthenium activity. Analyses were not obtained for other possible contaminants such as tellurium, technetium, and neptunium.

[6]Argonne National Laboratory, "Chemical Engineering Division Semiannual Report, January-June 1967," ANL-7375.

fuel residue and nonvolatile fluorides of the fission elements, a partial purification of uranium and plutonium is achieved. Since the volatile fluorides of the fission product elements ruthenium, niobium, technetium, tellurium, antimony, and molybdenum accompany the hexafluorides of uranium and plutonium, additional separation procedures are needed to produce products of acceptable purity.

The decontamination factors required of these separation procedures will depend on fuel burnups and the particular demands of fuel refabrication techniques. Therefore, decontamination factors cannot be specified, but it is likely that decontamination factors of the order of 10^6 to 10^7 may be necessary. Decontamination factors of this magnitude need not be the result of a single operation, but may be achieved by successive applications of an operation.

Previous demonstrations have shown that an acceptable separation of UF_6 from fission product fluorides can be achieved by fractional distillation. Thus the remaining purification problem is the development of a procedure for separating PuF_6 from volatile fluorides of the fission product elements. The use of fractional distillation to separate PuF_6 from fission product fluorides has not been pursued because of the anticipated difficulty of operating a distillation column containing solid PuF_4 formed by partial decomposition of PuF_6.

Since previous experience has shown that the fission product element most difficult to control in a separations operation may be ruthenium, experimental testing of procedures for the purification of plutonium have been carried out with particular attention to the behavior of ruthenium. Experiments are reviewed here on several potential procedures for the separation of ruthenium from plutonium. The experiments were made on a laboratory scale except for one experiment (item 3 below), which was carried out in the engineering-scale alpha facility.

1) Selective Sorption with Alkaline Earth Fluorides. Gaseous mixtures of ruthenium fluoride and UF_6 (a substitute for PuF_6) were passed through beds containing BaF_2, CaF_2, or MgF_2 in granular form at 100-150°C. The results showed that ruthenium is preferentially retained by alkaline earth fluorides, yielding decontamination factors of 374, 55, and 9 for the use of BaF_2, CaF_2, and MgF_2, respectively.

2) Transpiration Sublimation. In these experiments, uranium was used as a substitute for plutonium since the vapor pressures of PuF_6 and UF_6 are similar. Mixtures of UF_4 and ruthenium metal spiked with ^{106}Ru tracer were fluorinated to produce mixtures of UF_6 and ruthenium fluoride, and a stream of dry nitrogen (carrier gas) was passed over the mixture contained in a vessel at 0°C. Analyses of the residue and the sublimate for uranium and ruthenium yielded decontamination factors

ranging from 146 to 388. These values, however, are smaller by a factor of about 10^5 than the theoretical values calculated from the vapor pressures of PuF_6 and RuF_5 indicating that other, undefined factors are important in the sublimation.

In experiments in which samples of irradiated fuels were fluorinated, transpiration sublimation was tested as a procedure for separating mixtures of PuF_6 and fission product fluorides. The bench-scale experiments were performed on UO_2 fuel pellets that had been irradiated in the Yankee reactor to burnups of 33,200 and 41,600 MWd/metric ton U and cooled for 1 to 1 1/2 yr. Transpiration sublimation at 0°C yielded decontamination factors in the range of 100-250.

3) Thermal Decomposition. Information on thermal decomposition as a means of separating PuF_6 from ruthenium fluoride was also obtained in experiments performed in the engineering-scale alpha facility. The fluorination of pellets containing PuO_2, UO_2, and fission element oxides produced a mixture of PuF_6, UF_6, and fission element fluorides that was passed through a fluidized bed of granular alumina at 300°C. The plutonium, deposited in the form of solid PuF_4 on the surface of the alumina granules, was retained by the alumina bed. Analyses showed that the initial mixture contained 31 g of plutonium and 5.2 ± 2.6 g of ruthenium, whereas the alumina bed contained all of the plutonium, but only 8×10^{-4} g of ruthenium. These results indicate a decontamination factor of 10^3 to 10^4.

4) Preferential Reduction of PuF_6 with BrF_3. The use of BrF_3 to selectively reduce PuF_6 to PuF_4 and thereby separate plutonium from uranium and fission elements was investigated. Mixtures containing PuF_6 (2-5 g) with UF_6, NpF_6, SbF_5, and RuF_5 were heated to 80-90°C with liquid BrF_3, and then all volatile materials were removed from the mixture by vacuum distillation. The nonvolatile residue was then treated with BrF_5 vapor at 300-400°C. Analyses were performed to determine the quantity of each constituent of the original mixture present in the final, nonvolatile residue. The results showed that PuF_6 was preferentially reduced by BrF_3, as expected, and that decontamination factors up to about 500 were obtained for separation of plutonium from ruthenium.

5) Gas-Phase Transport of RuO_4. The formation and gas-phase transport of the volatile oxide RuO_4 was tested as a means of removing ruthenium from PuF_4. A sample of PuF_4 spiked with ^{106}Ru was subjected to pyrohydrolysis by steam-air mixtures at 500°C for 1 hr followed by ignition in air at 900°C for 2 hr. A similar sample of PuF_4 spiked with ^{106}Ru and ruthenium carrier was subjected to pyrohydrolysis at 700°C for 2 hr. The decontamination factors obtained in these procedures ranged from 1.3 to 1.6.

6) Solvolysis. The solvolysis by anhydrous HF of the solid complexes formed in the reactions of plutonium and ruthenium fluoride with

NaF was tested as a basis for separating mixtures of PuF_6 and ruthenium fluoride. Pure PuF_6 reacts with NaF at 100°C to produce a solid complex, tentatively identified as $3NaF \cdot PuF_4$ by X-ray analysis and analogy of the diffraction pattern to the corresponding uranium compound. The solvolysis by anhydrous HF of the solid formed in the reaction of PuF_6-ruthenium fluoride mixtures with NaF produces a slurry that can be filtered to yield a solution of sodium and ruthenium fluoride in HF and a partially purified sample of solid PuF_4. In laboratory experiments, mixtures of PuF_4 (~250 mg) and ruthenium metal spiked with ^{106}Ru were fluorinated with fluorine at 350-450°C, and the resulting gaseous mixture of PuF_6, ruthenium fluoride, and excess fluorine was passed through a vessel containing a bed of NaF pellets. Following the fluorination step, anhydrous liquid HF was added at 25°C to the bed of NaF, and the resulting slurry was filtered on a sintered nickel filter built into the vessel. In some experiments the PuF_4 filter cake was washed with BrF_3 or BrF_5. The highest decontamination factor was obtained when the PuF_4 was washed with BrF_5. Determinations of the ^{106}Ru activity in the PuF_4 and in the filtrate yielded decontamination factors ranging from about 40 to about 200.

7) Selective Sorption with LiF. The reaction of solid LiF with gaseous PuF_6-ruthenium fluoride mixtures at 300°C resulted in preferential retention of the ruthenium by the solid phase. In each of a series of experiments, a gaseous mixture of PuF_6, ruthenium fluoride, and fluorine, generated by fluorination of mixtures of PuF_4 and ruthenium metal spiked with ^{106}Ru, was passed through a series of two beds of solids. The first bed contained granulated LiF at ~300°C to test the separation effect, and the second bed contained NaF pellets to collect the plutonium product and any ruthenium that penetrated the LiF bed. Each experiment was terminated after 7 or 10 hr and the entire LiF bed and the entire NaF bed were removed from their containers and analyzed for plutonium and ruthenium. Decontamination factors, based on the ratio of ruthenium to plutonium in the gas stream entering the LiF beds and the ratio of ruthenium to plutonium in the product collected in the NaF beds, varied from 100 to 2000.

Although a combination of various procedures may yield a high decontamination of plutonium, additonal experiments are needed to develop a simple and effective purification method; such work is in progress.

III. MATERIALS CHEMISTRY AND THERMODYNAMICS

A. High Temperature Materials Development

1. Plutonium-Bearing Fuel Materials

The objective of the high-temperature materials development program is to obtain phase-diagram and thermodynamic data that can be used to interpret and evaluate the performance of candidate fast-breeder reactor fuels. This information will aid in understanding and predicting (1) interactions among fuel, fission product, and cladding materials and (2) migration by diffusion or vapor transport of fissile atoms, anion atoms, and fission products. In addition, these data will help to identify phases formed in fuel under operating conditions and to choose cation additives for controlling the chemical potentials of the fuel anions.

Current investigations are concerned with two possible fuel systems, U-Pu-O and U-Pu-C, with the binary systems Pu-O and Pu-C being studied initially. The uranium-oxygen system has been thoroughly studied in this laboratory[1] and elsewhere. The U-C system has also been studied, and carbon activities have been obtained mass spectrometrically.[2] To check these results, as well as to gain experience with another technique before applying it to plutonium carbides, the vaporization behavior of the U-C system is being investigated by transpiration.

The experimental program consists of phase-diagram, mass spectrometic, effusion, and, as already indicated, transpiration studies. Together, these studies yield complementary data to meet the objectives of the program. The status of each is discussed below.

a. Phase-Diagram Studies

The initial objective of the phase-diagram studies on the U-Pu-O system is to define the phase boundaries of the fluorite phase, $(U,Pu)O_{2\pm x}$, up to incipient melting. Experimentation will be carried out in a recently acquired three-module, 1 1/2-tier glovebox. The glovebox is to be connected to a recirculating-helium system designed to maintain water vapor and air contamination levels below 5 ppm each.

The phase-diagram data will be obtained from metallographic and chemical analysis of quenched samples, from cooling curves and differential thermal analysis, dilatometric measurements, and high-temperature X-ray analysis. Equipment for the dilatometric and X-ray studies will be obtained in the coming year. The samples will be treated

[1] ANL-7175, pp. 119-126.

[2] E. K. Storms, in Thermodynamics, Vol. I, p. 309, IAEA, Vienna (1966).

in one of the three furnaces now being installed in the glovebox. The first furnace (see Figure III-1) is a front-opening, tungsten-mesh, resistance furnace equipped with a quenching attachment; it can be operated in vacuum or inert atmospheres up to 3000°C. The second is a small, 4-in.-dia.-hearth arc furnace designed by the ANL Metallurgy Division, in which fused samples will be prepared for further experimentation or for phase identification and composition analysis. The third is a platinum-resistance furnace for the preparation and equilibration of oxygen-rich samples; it also will be equipped with a quenching attachment. After the equipment has been installed and tested within the glovebox, the glovebox will be closed and experimentation on the U-Pu-O system will commence.

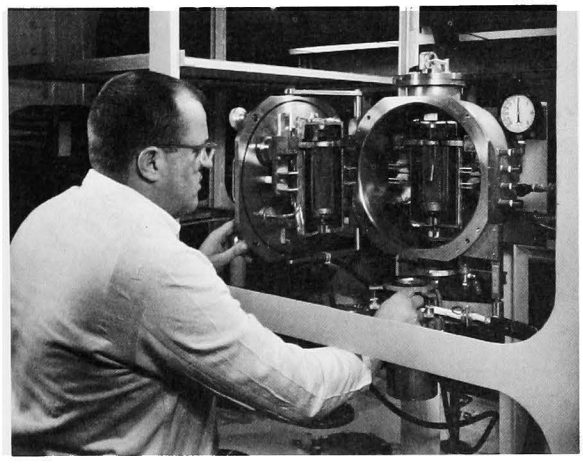

Fig. III-1

Front-Opening, Tungsten-Mesh, Resistance Furnace. The quenching chamber is being swung into position to receive the suspended tungsten crucible. The chamber can be heated, which enables molten metals (e.g., tin) to be used for quenching.

Many of the experimental procedures to be used for the U-Pu-O system have been tested with the U-O system. Recently completed tests have shown that UO_{2+x} must be quenched extremely rapidly to retain the high-temperature phase. New metallographic equipment for examining ternary U-Pu-O phases is being set up in an existing plutonium glovebox facility.

b. Mass Spectrometric Studies

One of the aims of the mass spectrometric studies is to establish thermodynamic values for the gaseous species PuO_2, PuO, and PuC_2. This will be accomplished by measuring vapor pressures as a function of temperature over well-defined two-phase regions such as Pu_2O_3-$PuO_{1.61}$ and Pu_2C_3-C or PuC_2-C.

The principal regions of interest in the ternary systems $(U,Pu)O_{2\pm x}$ and $(U,Pu)C_{1\pm x}$ will be investigated to determine partial vapor pressures and constituent activities. The oxygen-rich fluorite phase, $(U,Pu)O_{2+x}$, is expected to yield high UO_3 pressures. The mixed "monocarbide" phase should vaporize mostly as uranium and plutonium atoms, with plutonium the more abundant. In fact, the uranium pressures over

(U,Pu)C are expected to be so low relative to plutonium that mass spectrometry may be the only method for establishing the uranium activity. Complex vapor species in the ternary systems (e.g., $UPuO_2$), although unlikely, will also be sought.

The initial mass spectrometric studies on the Pu-O system were carried out to determine the compatibility of rhenium and tungsten Knudsen cells with PuO_{2-x}. Both cell materials were found to be reducing with respect to PuO_2, as indicated by high pressures of rhenium and tungsten oxide vapor. The oxygen content of the samples decreased to $PuO_{1.83\pm0.02}$ at 1900°C as a result of reaction with the cell and preferential loss of oxygen-rich gas.

The plutonium species detected over $PuO_{1.83\pm0.02}$ were Pu, PuO, and PuO_2. From its second-law slope and appearance potential, Pu was found to result from fragmentation of PuO. Partial molar heats of vaporization (1700 to 2000°C) of 124 and 136 kcal/mole, respectively, were calculated for PuO and PuO_2, in good agreement with the total-pressure data of Ackermann et al[3] and Mulford and Lamar.[4] Further work is required to determine the heats of formation of PuO(g) and PuO_2(g).

The evidence for reaction between PuO_2 and the tungsten and rhenium cells was the formation of a metallic coating on the inside of the cell lids. With the tungsten cells, the coating was shown to be tungsten metal. In one experiment at 1770°C, the lid was found to be ~15°C hotter than the bottom of the cell. Since large pressures of WO_3 and WO_2 are produced by reaction of the cell with oxygen-rich plutonia, it may be that a portion of the tungsten oxide vapor dissociated at the hotter lid to form tungsten metal and oxygen. Recycle of the oxygen, to form more tungsten oxide vapor, could have occurred until the oxygen disappeared through the cell orifice.

c. Effusion Studies

The objectives of the effusion studies are (1) the measurement of total pressures, which will enable us to calibrate mass-spectrometric ion-intensity data and to check total pressures found by transpiration, and (2) the determination of congruently vaporizing compositions in binary systems. The determination of congruently vaporizing compositions in the U-O system proved to be a powerful tool for checking the self-consistency of our vapor pressure data on urania.[5]

The effusion measurements will be carried out in a glovebox in the same ultrahigh-vacuum furnace system[6] previously used for

[3] R. J. Ackermann, R. L. Faircloth, M. H. Rand, J. Phys. Chem. 70, 3698 (1966).

[4] R. N. R. Mulford, L. E. Lamar, in Plutonium 1960, p. 411, E. Grison, W. G. H. Lord, R. D. Fowler (eds.), Cleaver-Hume Press, Ltd., London (1961).

[5] ANL-7350, pp. 38-42.

[6] ANL-7125, pp. 122-123.

congruency experiments with urania. The stainless steel vacuum chamber can be evacuated with sputter ion and sublimation pumps to pressures as low as 10^{-10} torr in the presence of samples heated to 2000°C. A residual gas analyzer measures background gases up to mass 250 at pressures as low as 10^{-10} torr. Extremely low background pressures are required to prevent contamination of condensates collected on targets; for example, oxygen background pressures exceeding 10^{-8} torr can produce significant changes in the oxygen content of condensates.

The effusion rate from a Knudsen cell can be determined from the weight change of the cell or from the weight change of a target. When targets are used, the vapor composition is determined by analysis of the condensate. In the congruency experiments, the congruently vaporizing composition is determined by analysis of the residue after enough sample has vaporized to bring the residue to the congruent composition.

d. Transpiration Studies

The objective of the transpiration studies is to measure total pressures and constituent activities of the U-Pu-C and U-Pu-O systems as functions of temperature and composition.

The initial study on carbides is being made with the U-C system in equipment (see Figure III-2) formerly used to study the

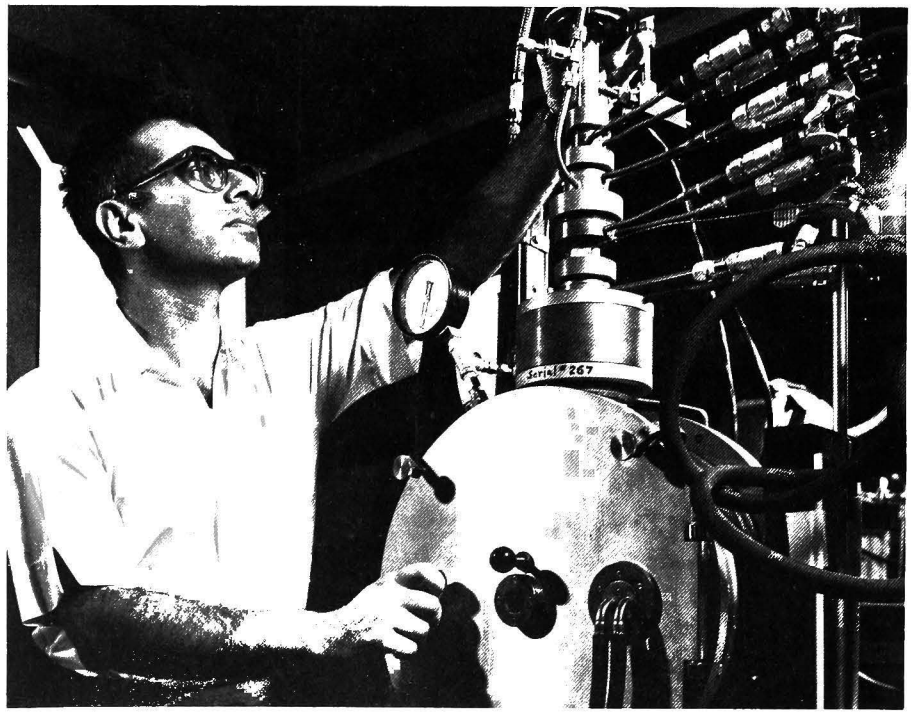

Fig. III-2. High Temperature Transpiration Apparatus. Previously used with H_2O-H_2 mixtures at temperatures up to 2600°C to study the vaporization behavior of urania, the equipment is now being used with CH_4-H_2 mixtures to study the vaporization behavior of uranium carbides.

U-O system.[7] The carrier gas, a mixture of methane in hydrogen, is passed over the sample on a once-through basis; a hydrocarbon analyzer (flame ionization) monitors the methane concentration in the exit gas.

The equipment has been modified to permit recycling of the carrier gas, although this feature is not being used in the current uranium carbide experiments. By recycling, the composition of the gas adjusts to that of the sample; in the once-through process, the composition of the sample changes until equilibrium with the gas is reached. The recycling procedure was found to be satisfactory in tests with the U-UO_2 system (see Part 2).

A second transpiration system with gas-recycling capability is being built within a glovebox to handle plutonium samples. The sample weight will be monitored continuously by a recording vacuum microbalance during transpiration. For study of the oxide systems, Pu-O and U-Pu-O, iridium transpiration tubes will be used to minimize sample reduction.

2. Oxygen and Uranium Activities in Oxygen-Saturated Liquid Uranium

Our previous investigations of the uranium-oxygen system included phase studies and measurements of oxygen partial pressure and total pressure over UO_{2-x}. Critical evaluation of these results and comparison with existing literature revealed the need for further investigation.

Disagreement exists concerning the thermodynamic activity of uranium in liquid uranium saturated with oxygen. Thorn and coworkers[8,9] have suggested that the activity of uranium decreases to ~0.1 when the liquid is saturated with oxygen at high temperatures. This decrease would then explain the much lower vapor pressures of uranium they observed for U-UO_2 mixtures as compared with those observed for pure uranium. Drowart and coworkers,[10-12] however, reported nearly equal uranium pressures for pure uranium and for U-UO_2 mixtures, the latter being about the same as those measured by Thorn and coworkers for U-UO_2. If the results of Drowart are correct, the uranium activity is near unity for oxygen-saturated urania.

The question was first tentatively answered by examination of the oxygen partial pressures measured by Tetenbaum and Hunt[7] for

[7] ANL-7225, pp. 137-139.

[8] E. G. Rauh, R. J. Thorn, J. Chem. Phys. 22, 1414 (1954).

[9] R. J. Ackermann, E. G. Rauh, R. J. Thorn, J. Chem. Phys. 37, 2693 (1962); 42, 2630 (1965).

[10] G. DeMaria, R. P. Burns, J. Drowart, M. G. Inghram, J. Chem. Phys. 32, 1373 (1960).

[11] J. Drowart, A. Pattoret, S. Smoes, J. Chem. Phys. 42, 2629 (1965).

[12] A. Pattoret, S. Smoes, J. Drowart, in Thermodynamics, Vol. I, p. 377, IAEA, Vienna (1966).

hypostoichiometric urania (UO_{2-x}). Extrapolation of their data to the hypostoichiometric boundary gave oxygen partial pressures over oxygen-saturated uranium that are consistent with a uranium activity of about unity. Although the extrapolations are relatively long and the shape of the curves uncertain, it is difficult to extrapolate to oxygen pressures much higher than those that would be in equilibrium with a phase having a uranium activity near unity. Indeed, some measurements well within the single-phase urania region indicate that the activity of uranium must be greater than 0.4. The purpose of the present research was to measure by more direct means oxygen and uranium activities in liquid uranium saturated with oxygen. To this end, the partial pressure of water in equilibrium with the condensed two-phase system and hydrogen was measured. Partial pressures of oxygen were calculated from H_2O/H_2 ratios with the aid of thermodynamic tables, and uranium activities were calculated from the partial pressures by the Duhem-Margules equation, as described below.

The partial pressure of oxygen ($p^\circ_{O_2}$) and activity of uranium (a°_U) for stoichiometric UO_2 may be related to the free energy of formation of UO_2 [$\Delta Gf^\circ(UO_2)$] by

$$\Delta Gf^\circ(UO_2) = RT \ln a^\circ_U + RT \ln p^\circ_{O_2} \tag{1}$$

From Tentenbaum and Hunt's measurements on hypostoichiometric urania, we may deduce that the partial pressure of oxygen over UO_{2-x} varies inversely as the square of the concentration of oxygen vacancies; the concentration of oxygen vacancies may be taken equal to x, except when x is very small. If pressures and activities for the single-phase urania field are denoted by p(x) and a(x), and the corresponding terms for uranium-saturated urania compositions by $p(x_s)$ and $a(x_s)$, then

$$\ln p_{O_2}(x) = \ln p_{O_2}(x_s) + 2 \ln (x_s/x) \tag{2}$$

By application of the Duhem-Margules equation in the form

$$\frac{d \ln p_{O_2}}{d \ln N_{O_2}} = \frac{d \ln a_U}{d \ln N_U} \tag{3}$$

to single-phase urania, one obtains

$$\ln a_U(x) = \ln a_U(x_s) - 2 \ln (x_s/x) + (x_s - x) \tag{4}$$

Substitution of Eqs. 2 and 4 in Eq. 1 and rearrangement yields the relation

$$\Delta\overline{G}_U(x_s) = -\Delta Gf^\circ(UO_2) - \Delta\overline{G}_{O_2}(x_s) + x_s RT \tag{5}$$

where $\Delta\bar{G}_U(x_s) = -RT \ln a_U(x_s)$ and $\Delta\bar{G}_{O_2}(x_s) = -RT \ln p_{O_2}(x_s)$. Thus, by measuring $p_{O_2}(x_s)$ and using known values of x_s, one hopes to calculate $a_U(x_s)$, the activity of uranium in urania saturated with liquid uranium, or conversely, in liquid uranium saturated with oxygen.

Experimental Procedure and Results. The transpiration apparatus used for these measurements has been described.[13] The leak tightness and degassing procedures were improved to allow water contents as low as 0.5 ppm to be measured. In addition, the gas-handling system was rebuilt for continuous recirculation of moist hydrogen.

The sample was a pressed and sintered pellet weighing 1.4 g and having an initial O/U ratio of 1.7. This composition was well within the U-UO_{2-x} two-phase field in the temperature range (1964-2261°K) of the experiments. The pellet was held in a tungsten crucible that rested on a tungsten plate at the bottom of a 5/8-in.-dia. tube of molybdenum-tungsten alloy. A 1/4-in.-dia. tungsten condenser tube was positioned 1/16 in. above the crucible. Moist hydrogen passed through the larger tube, out the condenser tube, and was then recirculated. The moisture content of the hydrogen was continuously monitored with a Beckman hygrometer.

Special techniques were adopted to improve the precision of the hygrometry. First, the water contents were measured at both 1 and 2 atm total pressure. The difference between the two measurements was taken as the measured value for a total pressure of 1 atm; this procedure was intended to minimize systematic errors due to water desorption from equipment surfaces, minute air leaks, and drifts in the hygrometer zero. Secondly, the output of the hygrometer was read with a potentiometer to eliminate the mechanical hysteresis of the meter provided with the instrument.

The results are presented in Table III-1 in the order of increasing temperature although they were obtained in the order indicated.

TABLE III-1. Partial Molar Free Energies of Oxygen and Liquid Uranium in the U-UO_{2-x} System

Temp. (°K)	Order Obtained	H_2O (ppm)	x_s	x_sRT (kcal/mole)	$\Delta\bar{G}_{O_2}(x_s)$ (kcal/mole)	$-\Delta G_f°(UO_2)$ (kcal/mole)	$\Delta\bar{G}_U(x_s)$ (kcal/mole)
1964	7	0.33	0.060	0.2	182.3	178.1	-4.0
1969	5	0.65	0.061	0.2	177.1	177.9	+1.0
1974	1	0.50	0.062	0.2	179.3	177.7	-1.4
2051	8	1.2	0.080	0.3	174.5	174.4	+0.2
2052	6	0.66	0.080	0.3	179.4	174.4	-4.7
2053	2	1.6	0.080	0.3	172.2	174.3	+2.4
2156	9	3.8	0.108	0.5	167.4	170.0	+3.1
2163	3	4.7	0.110	0.5	165.7	169.7	+4.5
2261	4	4.4	0.143	0.6	168.4	165.6	-2.2
2261	10	9.8	0.143	0.6	161.2	165.6	+5.0
2261	11	7.0	0.143	0.6	164.2	165.6	+2.0

Mean $\Delta\bar{G}_U(x_s) = +0.5 \pm 3.3$ (std. dev.) kcal/mole

[13] ANL-6900, p. 214.

The water concentrations, given in parts per million, were converted to the corresponding partial molar free energies of oxygen with the aid of the JANAF tables. The partial molar free energy of uranium, $\Delta\overline{G}_U(x_s)$, was calculated from Eq. 5 with the data of Schick et al[14] for $\Delta Gf^\circ(UO_2)$ and our previously determined values[15] for x_s. $\Delta\overline{G}_U(x_s)$ exhibits no significant trend with temperature and is nearly as often negative (implying an activity greater than one, which has no physical significance) as positive. Since the variations from run to run are larger than can reasonably be expected to arise from small changes in liquid phase composition over the temperature range or from systematic errors in the literature values for $\Delta Gf^\circ(UO_2)$, we have chosen to ascribe the scatter in the results to experimental variability and have calculated an average value of $\Delta\overline{G}_U(x_s)$. This value, $+0.5 \pm 3.3$ kcal/mole, corresponds to a physically realizable uranium activity of $0.9^{+0.1}_{-0.4}$ at ~2110°K.[16] The corresponding pressure of U(g) over oxygen-saturated liquid uranium should be not less than one-half of the pressure over the pure metal, consonant with the observations by Drowart and coworkers.[11] The difference between the heats of vaporization of uranium obtained by Rauh and Thorn,[8] ΔH_{298} = 117 kcal/mole, and by Drowart and coworkers,[11] ΔH_{298} = 126 kcal/mole, must arise from some cause other than a low activity of uranium in the oxygen-saturated metal.

3. Mass Spectrometric Effusion Study of the Uranium-Uranium Phosphide System

A mass spectrometric, Knudsen effusion investigation of uranium monophosphide, UP, has been carried out in the range 2073-2425°K. An earlier mass spectrometric study by Gingerich and Lee[19] yielded data that disagreed in two respects with the literature: (1) The heat of the dissociation $P_2 \rightleftarrows 2P$ from these data was about 15 kcal/mole higher than that calculated from spectroscopic data, which suggests an error of about 10% in the heats of vaporization. The relative phosphorus pressures were also at variance with the spectroscopic data. (2) UP was found to vaporize congruently, whereas Baskin[20] and Allbutt et al[21] have since found that uranium phosphide moves into the two-phase region U(l) + UP(c) during vaporization.

The objective of this study was to measure the equilibrium partial pressures of uranium and phosphorus species over UP and to derive

---

[14] H. L. Schick et al, "Thermodynamics of Certain Refractory Compounds, Fourth Quarterly Progress Report," AVCO RAD-SR-63-105, p. 193 (June 15, 1963).

[15] ANL-7125, p. 119.

[16] Such a high value of uranium activity in oxygen-saturated uranium is entirely compatible with reported values of its oxygen content, which vary from 0.6 a/o[15,17] to 26 a/o[18] at 2000°C.

[17] H. E. Cleaves, M. M. Cron, J. T. Sterling, Natl. Bur. Std. report CT-2618 (February 1945).

[18] P. Guinet, H. Vaugoyeau, P. L. Blum, Compt. Rend. 263, 17 (1966); CEA-R-3060 (1966).

[19] K. A. Gingerich, P. K. Lee, J. Chem. Phys. 40, 3520 (1964).

[20] Y. Baskin, J. Amer. Ceram. Soc. 49, 541 (1966).

[21] M. Allbutt, A. R. Junkison, R. G. Carney, UK Atomic Energy Authority report AERE-R-4903 (1965).

their partial molar heats of vaporization. The experimental technique involved vaporization of UP within a tungsten effusion cell and analysis of the effusing species with a Bendix time-of-flight mass spectrometer. In addition, the residues left after vaporization were examined metallographically. Both types of analysis showed that UP loses phosphorus preferentially and converts to the two-phase system $U(l)\text{-}UP_{1-x}(c)$. Further confirmation of this shift was obtained by heating a mixture of U and UP and finding that the partial pressures of U(g), P(g), and $P_2(g)$ over the mixture were the same as those over UP that had been evaporated to a constant pressure.

The partial molar enthalpies of vaporization for U(g), P(g), and $P_2(g)$ over the two-phase system were obtained by combining the results of four series of measurements on the temperature dependence of the U^+, P^+, and P_2^+ ion currents. The partial pressures were evaluated[22] by combining measurements at constant temperature of the effusion rate of samples with the ion intensity of each species integrated as a function of time. Corrections for the relative ionization cross sections were made with literature values.[23] Multiplier efficiencies were estimated on the assumption[24] that ions of equal velocity have equal multiplier efficiencies, i.e., $\gamma_1/\gamma_2 = (M_2/M_1)^{1/2}$, where M is the molecular weight.

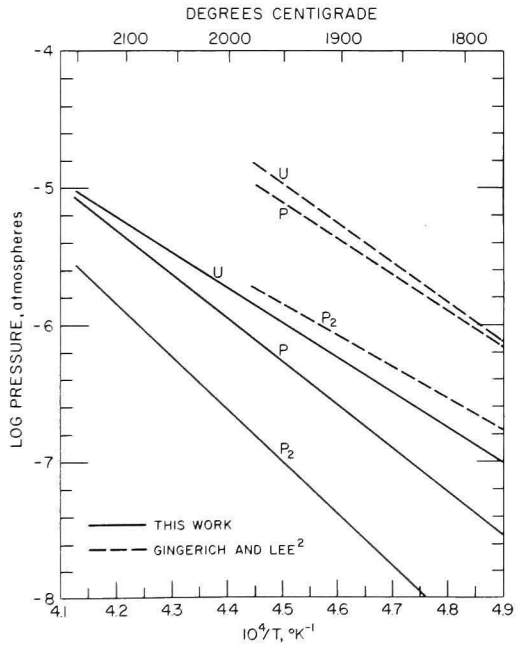

Fig. III-3. Partial Pressures of U, P, and P_2 over the U-UP System.

The partial-pressure equations derived for the two-phase U(l)-UP(c) system between 2073 and 2425°K are:

$$\log P_U = (5.677 \pm 0.273) - (25{,}898 \pm 192)/T \quad (6)$$

$$\log P_P = (8.062 \pm 0.240) - (31{,}831 \pm 340)/T \quad (7)$$

$$\log P_{P_2} = (10.319 \pm 1.203) - (38{,}454 \pm 1480)/T \quad (8)$$

Figure III-3 shows a plot of these equations as well as the partial pressures reported by Gingerich and Lee.[19] There is considerable disagreement between the two sets of data. Their partial pressures are approximately an order of magnitude greater than ours. Also, the partial molar enthalpies of vaporization (in kcal/mole) they reported,

[22] J. L. Margrave, in Physico-Chemical Measurements at High Temperature, Chap. 10, J. O'M. Bockris, J. L. White, J. D. MacKenzie (eds.) Butterworth Scientific Publications, Ltd., London (1959).

[23] J. W. Otvos, D. P. Stevenson, J. Amer. Chem. Soc. 78, 546 (1956).

[24] W. Ploch, W. Walcher, Rev. Sci. Instrum. 22, 1028 (1951).

$\Delta H(U) = 131.2$, $\Delta H(P) = 120.0$, and $\Delta H(P_2) = 105.5$, differ considerably from the values derived from Eqs. 6, 7, and 8, namely, $\Delta H(U) = 118.5$, $\Delta H(P) = 145.7$, and $\Delta H(P_2) = 176.0$. The internal consistency of our results, as judged by the equilibrium $P_2 \rightleftarrows 2P$, is very satisfactory: the heat calculated for this dissociation is 115.4 kcal/mole, as compared with the spectroscopic value[25] of 119.2 kcal/mole.

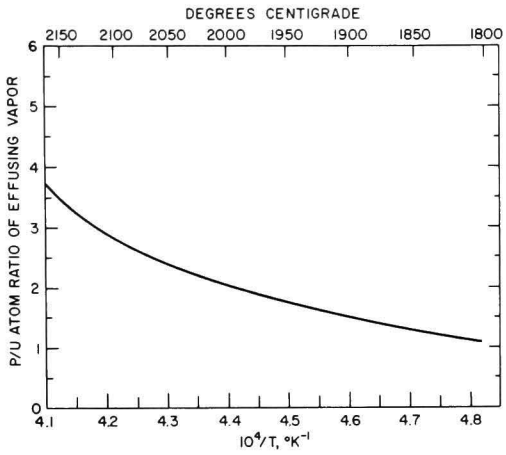

Fig. III-4. P/U Ratio of Effusing Vapor over U-UP System vs. Temperature.

The compositional changes that are observed during effusion of stoichiometric UP, namely, the transition to liquid uranium and hypostoichiometric UP and the relative growth of uranium in the two-phase system, require that the effusing vapor be phosphorus-rich. The partial pressures expressed by Eqs. 6, 7, and 8 are consistent with these observations as shown by Fig. III-4, in which the P/U atom ratio of the vapor effusing from the two-phase system is plotted as a function of temperature.

A value for the enthalpy of formation of uranium monophosphide [$\Delta Hf°(UP,c)$] can be estimated from the results of this investigation. From Eqs. 6 and 7 and enthalpy-of-formation data[25] for U(g) and P(g), the enthalpy $\Delta Hf_{2250} = -264.2 \pm 2.5$ kcal/mole was derived for the reaction

$$U(g) + P(g) = UP(c)$$

By extrapolation of the recently reported mean heat capacity for uranium monophosphide, 13.8 cal/(deg)(mole)[26] in the range 1073-1473°K, the value $\Delta Hf^{\circ}_{298}(UP,c) = -76.1 \pm 4.8$ kcal/mole was obtained for the reaction

$$U(\alpha) + P(\alpha\text{-white}) = UP(c)$$

This enthalpy of formation agrees with the recent calorimetric data of O'Hare et al[27] on the combustion of uranium monophosphide in fluorine, which indicated that $\Delta Hf^{\circ}_{298}(UP,c) = -75.5 \pm 0.7$ kcal/mole.

---

[25] D. R. Stull, G. C. Sinke, Advan. Chem. Ser. 18 (1956).

[26] ANL-7175, p. 142.

[27] P. A. G. O'Hare et al, "The Thermochemistry of Some Uranium Compounds," presented at IAEA Symposium on Thermodynamics of Nuclear Materials with Emphasis on Solution Systems, Vienna, Austria (September 4-8, 1967).

B. Chemistry of Irradiated Fast Reactor Fuels

An understanding of the chemical behavior of fast reactor fuels during irradiation is necessary for the development of new fuels with increased integrity and burnup capability. The analysis of fuel microstructure is expected to contribute significantly to this understanding. For this reason, considerable emphasis is being placed on techniques of microsampling and on direct microanalysis.

1. Electron Microprobe Studies

The electron probe microanalyzer (Fig. III-5) accomplishes microsampling and analysis directly. The electron beam can be focused on an area as small as 1 μ in dia. The energy and intensity of the characteristic X-rays emitted provide both qualitative and quantitative analysis of the composition of the area.

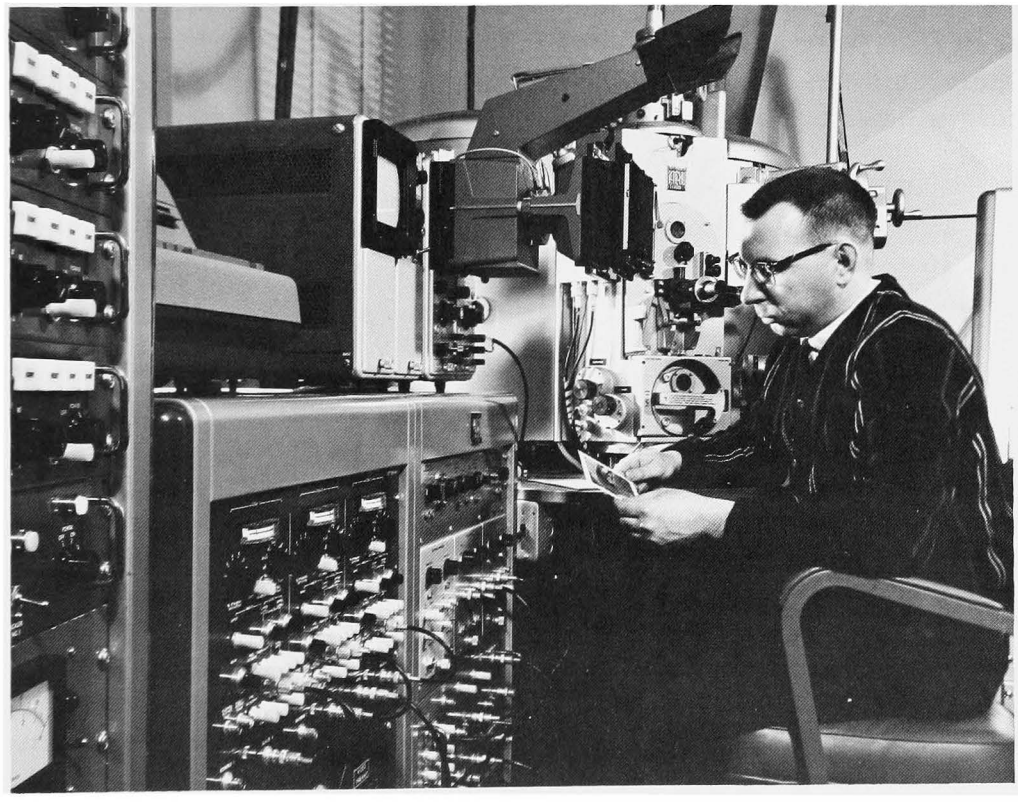

Fig. III-5. Electron Probe Microanalyzer.

Cross sections of a group of irradiated UO_2 fuel pins have been analyzed with an unshielded microprobe to determine the behavior of fission products during irradiation. The fuel pins, which were 13% enriched UO_2(O/U, 2.019) clad with type 304 stainless steel, were irradiated in a thermal flux in the Materials Test Reactor (MTR) to burnups ranging from about 1 to 7 a/o.

Electron probe analyses of cross sections of these fuel pins revealed several different types of metallic inclusions dispersed throughout the oxide matrix. Inclusions in the peripheral areas of the fuel were either stainless steel[1] or stainless steel containing the transition metal fission products, molybdenum, technetium, ruthenium, rhodium and palladium. The stainless steel-containing inclusions had apparently migrated to the outer (cooler) edges of the fuel during irradiation; none were found in the columnar grain-growth regions.

Inclusions (<1 to ~2 μ in dia.) in the columnar grain-growth regions contained the transition metal fission products molybdenum, technetium, ruthenium, and rhodium in ratios that varied as a function of radial position. These inclusions were free of uranium, indicating that no intermetallics or solid solutions of uranium-transition metal fission products were formed by reduction of the UO_2 matrix.

In this group of fuel pins, a portion of the molybdenum (approximately half) was also found in the fuel matrix (oxide phase). This behavior is attributed to the fact that the UO_2 fuel material was hyperstoichiometric (O/U, 2.019). The presence of molybdenum in the fuel matrix has not been observed in stoichiometric oxide fuels.

The discovery of the mobility of the transition metal fission products suggests that they should not be used indiscriminately as burnup monitors in oxide fuels. (For a further discussion of the suitability of burnup monitors, see Section VIIB.)

The fission product elements strontium, yttrium, zirconium, cesium, barium, lanthanum, cerium, praseodymium, neodymium, promethium, samarium, europium, and gadolinium were found in the oxide phase. Although most of these elements were evenly distributed throughout the fuel oxide matrix, large amounts of the fission products cesium and barium had migrated during irradiation to the relatively cool fuel-cladding interface.

A cross section of a vibratorily compacted UO_2-20 w/o PuO_2 fuel pin, clad with type 304 stainless steel, was also examined. This pin was irradiated in EBR-II to a burnup of 2.9 a/o. The oxygen-to-metal ratio of the mixed oxide was 2.00. The distribution of fission products was, in general, similar to that in the UO_2 fuel pins, but some differences were observed.

Inclusions containing the transition metal fission products, similar to those in the UO_2 fuel, were found in the mixed-oxide fuel. However, molybdenum was found only in the inclusions and not in the

[1]Micron-size particles of stainless steel were introduced into the UO_2 from blending equipment during preparation of the fuel.

oxide matrix. This finding is consistent with the hypothesis, discussed above, that the behavior of molybdenum is related to the stoichiometry of the fuel (the mixed-oxide fuel was stoichiometric).

Stainless steel was not present in the UO_2-PuO_2 fuel because a different method of fuel preparation had been used. Instead, the mixed-oxide fuel contained an aluminum oxide impurity that was introduced during ball milling. The aluminum oxide was found to associate selectively with fission product barium, forming inclusions of a barium oxide-aluminum oxide compound that approximates the composition $BaO \cdot 6Al_2O_3$.

In both the UO_2 and UO_2-PuO_2 fuels, cesium had migrated to the fuel-cladding interface. However, in the mixed-oxide fuel, cesium was involved in a mechanism which caused intergranular attack of the cladding. Sixteen different areas of the fuel-cladding interface were analyzed with the electron probe microanalyzer. All the analyses showed a depletion of iron and chromium, and an enhancement of nickel in the cladding grain boundaries. Cesium was found in the grain boundaries, associated with chromium on the fuel side of the fuel-cladding interface and unassociated with uranium, plutonium, or fission products in voids and fissures near the cladding.

Electron microprobe scanning images of one of these areas is shown in Fig. III-6. The brightness in the specimen current image (Fig. III-6a) is inversely proportional to the mean atomic number of the elements present, i.e., UO_2 appears black. The iron, nickel and chromium X-ray images are biased to show the enhancement of nickel and the depletion of chromium and iron at the grain boundaries. The depletion of iron and chromium in the grain boundaries can be seen in Figs. III-6b and c. The enhanced concentration of chromium at the fuel side of the cladding was found in each of the areas analyzed and was always associated with cesium (Fig. III-6d).

Samples of the fuel-cladding interface of the UO_2 fuels showed no such interaction between cesium and the stainless steel cladding. It is believed that this difference may have resulted from temperature differences during irradiation. The inner cladding temperature of the UO_2-PuO_2 fuel irradiated in EBR-II was about 600°C, whereas that of the UO_2 fuel irradiated in MTR was only about 180°C.

The first complete radial distribution of uranium and plutonium on a micron scale has been obtained in the studies of mixed oxide fuels. The distribution of plutonium as a function of radial position is shown in Fig. III-7. The most significant finding was that the concentration of plutonium dioxide, which was originally 20 w/o, was found to be higher (~27 w/o) in the center (hottest) portion of the fuel after irradiation. (A corresponding decrease in uranium dioxide concentration was measured in this area.) The center of the fuel attained a temperature

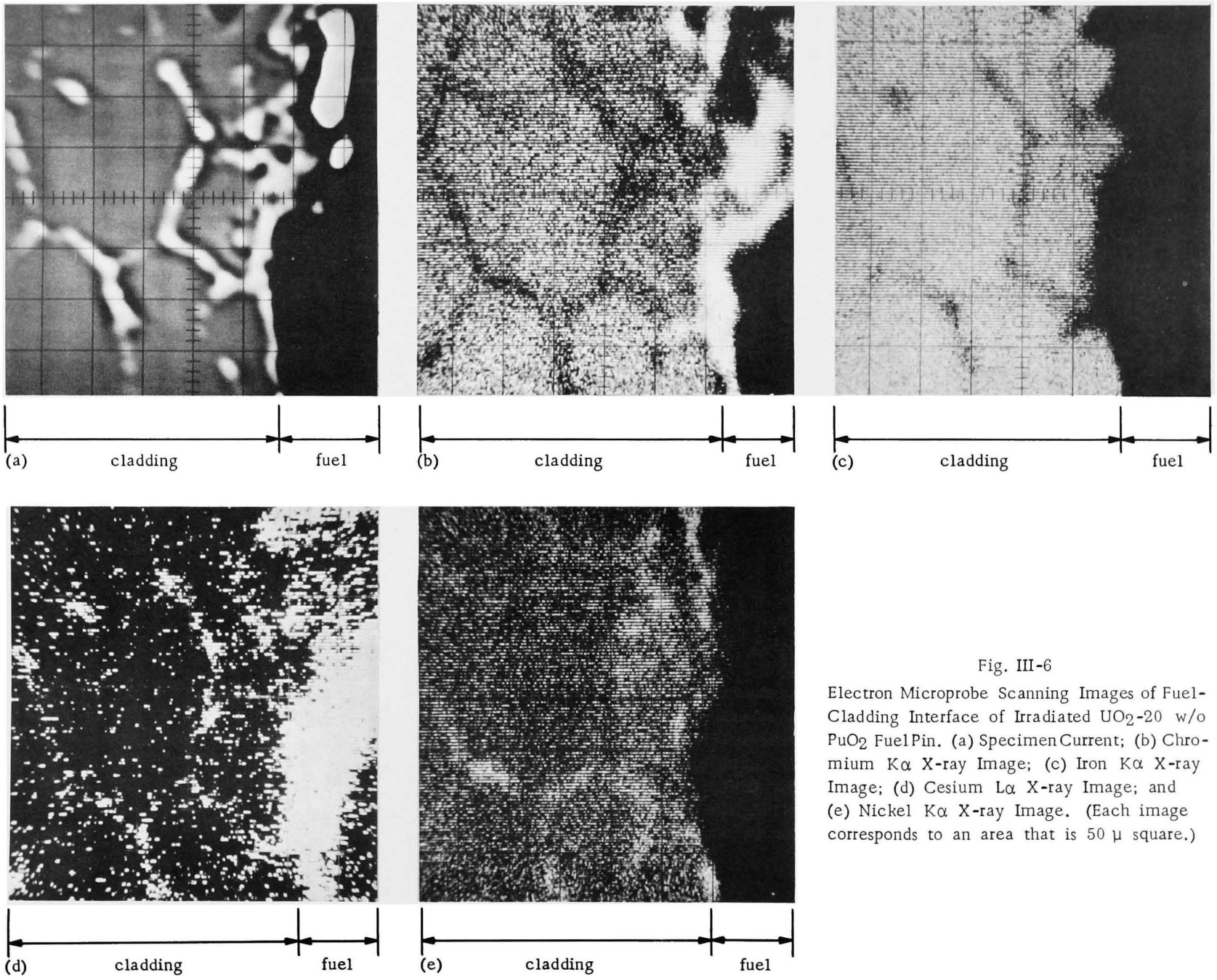

Fig. III-6

Electron Microprobe Scanning Images of Fuel-Cladding Interface of Irradiated UO_2-20 w/o PuO_2 Fuel Pin. (a) Specimen Current; (b) Chromium Kα X-ray Image; (c) Iron Kα X-ray Image; (d) Cesium Lα X-ray Image; and (e) Nickel Kα X-ray Image. (Each image corresponds to an area that is 50 μ square.)

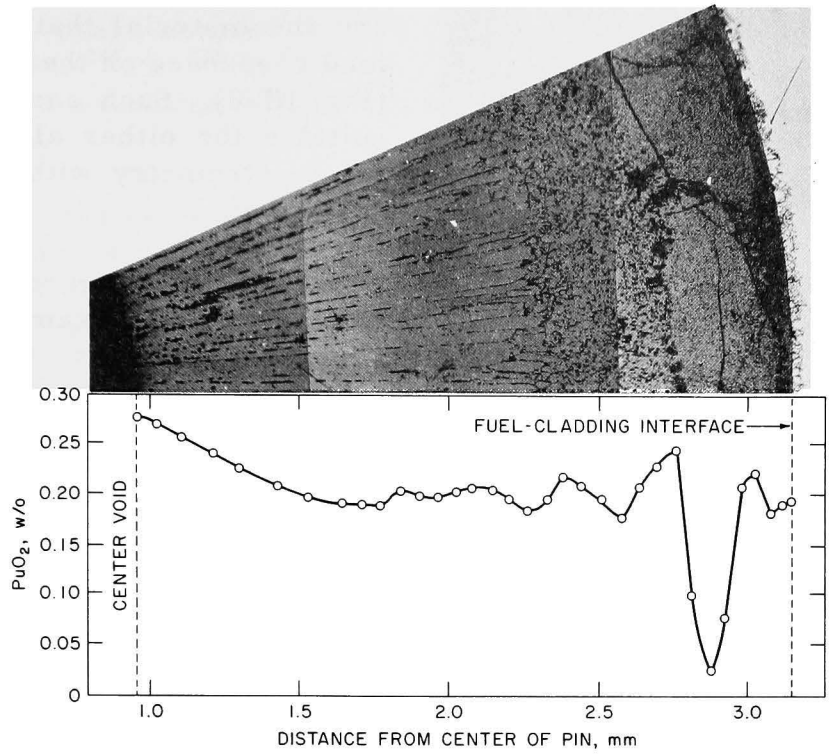

Fig. III-7. Complete Radial Distribution of Plutonium in UO_2-20 w/o PuO_2. (2.9 a/o burnup.)

hot enough to form a solid solution of the separate particles of UO_2 and PuO_2 in the original fuel material. However, near the periphery of the fuel pin, which was at a lower temperature, discrete particles of PuO_2 and UO_2 remained after irradiation. The extreme variations in plutonium concentration in this area are the result of analyses of these particles (either UO_2 or PuO_2). Such information on the distribution of fuel constituents during irradiation will be of value in predicting the operating characteristics of a reactor.

Future plans include the study of the microstructure of carbide fuels. In addition, the acquisition of a shielded electron probe will decrease the restrictions on sample activity levels imposed by the use of an unshielded instrument.

2. Laser-Beam Microsampling

Laser-beam vaporization is being used as a technique for microsampling of irradiated fuels. A small ruby laser that is fired through the optical system of a microscope vaporizes a specimen of the fuel (see ANL-7350, p. 47). Depending on the selection of optical components and the input power to the laser, samples 10 to 100 μ in dia. can be vaporized in uranium dioxide. A microscope cover glass is mounted about 0.2 mm

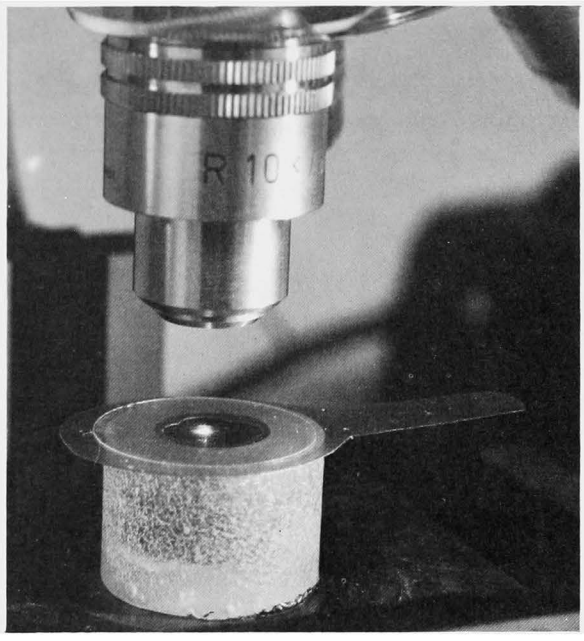

Fig. III-8. Laser-Beam Sampling System.

above the surface of the specimen, and the material that is vaporized condenses on the cover glass (Fig. III-8). Such samples are suitable for either alpha or gamma spectrometry without further treatment.

Laser-beam vaporization has been used to examine the behavior of radioactive fission products and fuel constituents in a uranium dioxide fuel pin. The pin examined had a burnup of about 7 a/o and was one of a group of 13% enriched UO_2 fuel pins (see preceding subsection) that were irradiated in MTR.

Twenty-five samples were taken across the radius of a cross section of the pin. Craters approximately 50 μ in dia. (Fig. III-9) were formed at each location, a size that corresponds to a sample weight of ~0.5 μg.

Information on the distribution of radioactive fission products was obtained by gamma spectrometry. The isotopes that were identified from the scans were ^{144}Ce, ^{144}Pr, ^{106}Ru, ^{95}Zr, ^{95}Nb, ^{134}Cs, ^{137}Cs, and ^{125}Sb. Although equipment is not yet set up for precise quantitative analysis, relative concentrations of these isotopes across the radius of the pin were established. Few major differences in fission product ratios were noted; however, the concentrations of cesium and, in some places, antimony, were higher at the fuel-cladding interface than in the body of the fuel pin. The increased concentration of antimony in this region was not expected, nor was it found by electron microprobe analysis of the same fuel pin. The reason for this difference in results is not known at this time. In the examination of future fuel samples, an effort will be made to gain an understanding of the behavior of antimony.

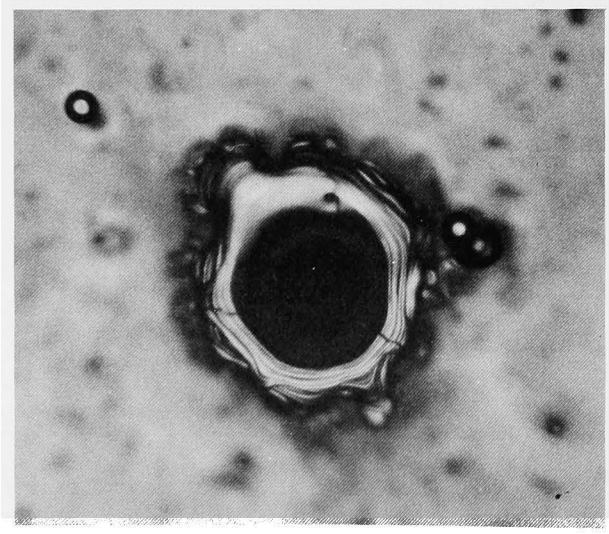

Fig. III-9. Crater Produced in UO_2 by Laser-Beam Vaporization. (Diameter, 50 μ.)

Some of the specimens were also examined by alpha spectrometry. Energy peaks obtained at 5.14, 5.48 and 6.1 MeV corresponded to the peaks for ^{239}Pu-^{240}Pu, ^{238}Pu-^{241}Am, and ^{242}Cm, respectively; relative concentrations as a function of radial position were established for the three energy peaks.

Other potential methods of analysis in which laser-vaporized samples might be utilized include mass spectrometry and neutron activation. Although these techniques are only in the preliminary stages of development, results thus far have been encouraging.

C. Preparation of Reactor Materials - Ceramic Fuels

The preparation of ceramic fuels for nuclear reactors is being studied to develop processes that economically fit into appropriate fuel cycles, and to make well-defined fuels for further experimental studies, particularly irradiation studies. Processes for the preparation of uranium carbide and uranium-plutonium carbide fuels are under current investigation.

The fluidized-bed technique is especially attractive for preparation of carbide fuels; it affords efficient gas-solids contacting and the product is a powder which can be fabricated into fuel pellets or densified into particles suitable for vibratory compaction. Two fluidized-bed processes are being used in this program for preparing the carbide fuels: (1) carburization of hydrided metal or alloy at 750 to 850°C with methane-hydrogen gas mixtures; and (2) conversion of oxides to carbides at 1600 to 1800°C, either by reaction with admixed carbon or with a fluidizing gas containing methane.

The first of the above processes, the metal-methane reaction, has been successfully demonstrated. This process is now being used to prepare high purity powder of controlled stoichiometry. The powder is pressed and sintered into pellets for use in irradiation testing by the Metallurgy Division. The second process, the conversion of oxides to carbides, is still in the equipment preparation stage. However, tests have begun on the preparation and fluidization of the feed materials.

1. Synthesis of Carbides by Metal-Methane Reaction

a. Preparation of Powder

The fluidized-bed process for the preparation of carbide fuel powders from a metallic starting material consists of hydriding and dehydriding uranium or uranium-plutonium alloy rods, and then carbiding the product by reaction with a methane-hydrogen fluidizing-gas mixture. This process, including thermodynamic considerations and scale-up potential, was discussed in detail in previous reports in this series

(ANL-7175, p. 126 and ANL-7350, p. 47). Carbide fuel for irradiation testing is now being routinely prepared by this technique.

Fuel for irradiation testing is required with carbon contents in two ranges: 4.80 to 4.90 w/o and 5.00 to 5.20 w/o. Since carbide fuel with a low oxygen content is expected to be more stable under irradiation than fuel with a high oxygen content, and to avoid extraneous variables in the testing, a specification for the oxygen content of the test fuel has been set at <500 ppm.

In recent runs to prepare (U, 15 w/o Pu)C for use in preparing pellets for the above testing program, 400-g batches of U-Pu alloy (3/8-in. dia. rods) were hydrided at 250°C and dehydrided by heating at about 500°C. This procedure was repeated once to produce a fine powder which was then reacted at 800°C with methane-hydrogen fluidizing gas at 2 atm pressure to produce the carbide. These runs were carried out using once-through gas flow in a 1 5/8-in. ID reactor. This reactor is operated in a high purity helium-atmosphere glovebox and can be manipulated by hand (e.g., for product removal).

In these experiments, the rate of methane consumption (and hence the rate of reaction) was determined from the gas flow rate and the inlet and outlet methane concentrations as determined by an infrared analyzer. The carbon content of the product leveled off at slightly above the stoichiometric value as illustrated in Figure III-10. The virtual cessation of reaction at this level despite a methane concentration high enough to cause formation of the sesquicarbide at equilibrium is probably due to the formation of a thin layer of $(U,Pu)_2C_3$ around the powder particles; this restricts further diffusion of carbon to the interior of the particle. The thin $(U,Pu)_2C_3$ layer can be removed by reacting the powder with pure hydrogen at 800°C after carbiding has been completed. This results in reduction of the carbon content from about 5.0 w/o to the stoichiometric monocarbide level of 4.8 w/o.

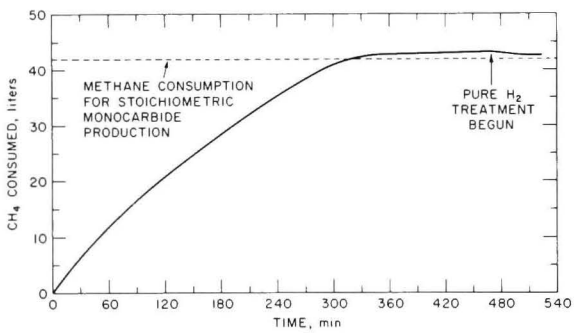

Fig. III-10. Preparation of (U, 15 w/o Pu)C in a Fluidized Bed (Run 23). (Conditions: temperature, 800°C; pressure, 2 atm; gas velocity, 12 cm/sec; gas composition, 6.2 v/o CH_4-93.8 v/o H_2.)

It has been established that the excess carbon is not present as adsorbed methane. This was done by contacting a batch of newly prepared carbide powder, first with helium at 800°C and then with hydrogen at the same temperature, while noting the presence of methane in the off-gas.

No methane was released by the helium treatment, whereas during the hydrogen treatment a significant amount of methane was released, indicating removal of the excess carbon that must have been present as sesquicarbide.

Both the carbon and oxygen contents of the products of recent runs have been controlled to within acceptable tolerances (Table III-2). The nitrogen analyses for these runs indicate a higher nitrogen content than the 200 ppm that has normally been obtained in the past. Temporary operating or analytical difficulties are believed to be responsible for this increase.

TABLE III-2. Preparation of (U, 15 w/o Pu)C by the Metal-Methane Fluidized-Bed Process

Process conditions: Temperature: 800°C
Pressure: 2 atm
Gas Composition: H_2-6.2 v/o CH_4

Experiment Number[a]	Charge Weight (g)	Product Composition			
		Carbon (w/o)	Oxygen (ppm)	Nitrogen (ppm)	Hydrogen (ppm)
20	300	4.92	340	1700	-
21	300	5.00	260	800	55
22	400	4.93[b]	190	500	180
23	400	4.76[b]	320	300	>250
24	400	4.75[b]	270	900	>200

[a]The starting alloy for experiments 20 and 21 contained normal uranium, whereas that for experiments 22, 23, and 24 contained fully enriched uranium. The impurity content of the enriched starting alloy was as follows: oxygen, 100 ppm; nitrogen, 600 ppm; hydrogen, 3 ppm.

[b]The products of experiments 22 to 24 were treated with hydrogen at 800°C to reduce the carbon content. The products of the other runs were not so treated.

Similar experiments have been carried out on the preparation of UC with comparable results, except that the oxygen content of the product is 1000 to 3000 ppm, which is considerably higher than that of (U,Pu)C. However, this is thought to be the result of more rapid oxidation by the glovebox atmosphere subsequent to removal of the product from the reactor (see below).

The volume median particle diameter for the (U,Pu)C obtained in these recent runs is about 30 to 40 microns, as determined by sieve analysis. The carbon content was determined for five size fractions of (U,Pu)C that had a composite analysis of 5.00 w/o carbon. The analysis for the fractions varied between 4.97 and 5.05 w/o with no significant correlation with the size fraction. This uniformity of carbon content with size distribution is another indication that the extent of carbiding in the fluidized-bed is self-limiting at a carbon content slightly above the stoichiometric value of 4.80 w/o.

The surface area was determined for several batches of carbide by nitrogen adsorption method (Perkin-Elmer-Shell Sorptometer). For several (U, 15 w/o Pu)C samples, the surface area varied from 0.2 to 0.3 m^2/g, whereas a sample of UC powder had a surface area of 0.5 m^2/g.

The bulk density of several batches of (U,Pu)C powder varied between 3.6 and 4.2 g/cc. The tap density varied from 4.4 to 5.0 g/cc.

In recent experiments, the reactivities of UC and (U, 15 w/o Pu)C powder samples with impurities present in a helium glovebox atmosphere (~100 ppm O_2, 2-4 ppm H_2O) were compared over a long time period. The carbon and oxygen contents of both carbides were essentially the same. The results of these tests are summarized in Figure III-11. The curves show a rapid increase in weight during the first two days. After fourteen days, the UC sample had increased in weight by 0.73 w/o, whereas the (U,Pu)C had increased by only 0.13 w/o. This greater reactivity of the UC powder can be partly accounted for by the twofold greater specific surface area of the UC powder noted earlier.

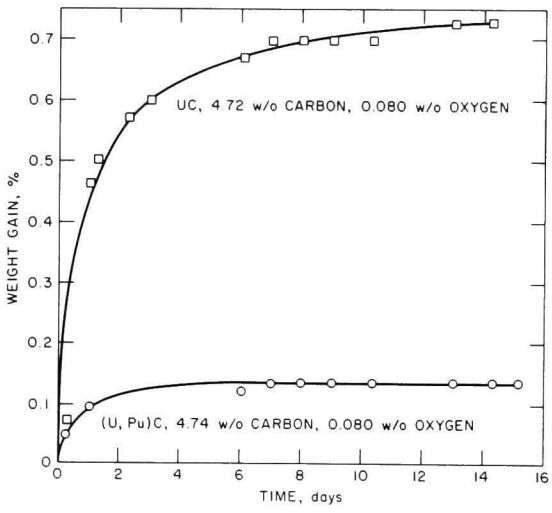

Fig. III-11. Weight Gain of Fluidized-Bed UC and (U, 15 w/o Pu)C Powder in Ambient Helium Atmosphere (~100 ppm, O_2 2 to 4 ppm H_2O).

Short-term tests were also made in which the (U,Pu)C powders were exposed to a more typical helium atmosphere (2 ppm H_2O, 10 ppm O_2) attainable with the glovebox purification system. In 6 1/2 hr, the UC sample gained 0.073 w/o, whereas the (U,Pu)C sample gained 0.049 w/o.

Tests comparing the rate of reaction of (U,Pu)C powder with the helium glovebox atmosphere with that of (U,Pu)C green pellets described below indicated that the powder and green pellets

react at about the same rate, and that the percentage weight gains level off at the same value. However, sintered pellets react much more slowly than the powder, and the percentage weight gain for pellets levels out at about one-fifth the value for powder under equivalent conditions.

b. Pressing and Sintering of Pellets

High purity UC and (U, 15 w/o Pu)C powder prepared by the metal-methane reaction process is being pressed and sintered into pellets suitable for irradiation testing. To minimize the possibility of contamination, the pellets are being pressed directly from the fluidized-bed products without milling or addition of binders. Several batches of 5 to 10 pellets each have been pressed and sintered to determine the proper procedures to be used in preparing the specimens for irradiation testing. Typical requirements for these pellets are: diameter, 0.255 ± 0.001 in.; length, 0.325 in.; density, 85 ± 3% of theoretical.

Pellet pressing is carried out with a double-acting hydraulic press. The pressing and ejection cycle of 23 sec is automatically controlled. The pressing portion of the cycle is 9 sec, including a dwell-time of 2.6 sec. Although no binder is used, the die is lubricated by pressing a stearic acid pellet after each carbide pellet pressing. The powder is manually fed into the die cavity with a volumetric measuring scoop, and the pellets are pressed at 75,000 psi. With this technique, the pellet weight has been found to vary by ±5%. At the present pressing rate, a maximum of 20 pellets may be produced each hour. Green pellets of satisfactory strength are produced which may easily be measured and weighed without damage. Green densities of these UC and (U,Pu)C pellets are about 7.4 ± 0.1 and 8.1 ± 0.1 g/cc, respectively.

Pellets are sintered in a high temperature, high vacuum furnace (Centorr Corp.) heated with a graphite resistance element. It has been necessary to sinter the (U,Pu)C pellets at a temperature of 2100°C to achieve the required density of 85 ± 3% of theoretical. In the present sintering procedure, the pellets are heated to 2100°C in one hour, held at temperature for 40 min, and cooled to room temperature in one hour. During the heating cycle, a vacuum of 10^{-5} torr is maintained until 1000°C is reached. At that time, high purity argon is added to adjust the pressure to 10 to 45 torr for the rest of the run.

The high sintering temperature of 2100°C is required because of certain characteristics of the feed material, such as its coarseness and, perhaps, its high purity. However, the high sintering temperature is not considered a disadvantage because the weight losses by the above sintering procedure have been only 0.1 to 0.2 w/o. It is hoped that the high sintering temperature may yield pellets that are dimensionally stable at high irradiation temperatures.

The short sintering cycle and the 10 to 45 torr argon pressure are important factors in reducing the weight loss; longer cycles and lower pressures have resulted in weight losses of several percent, probably as a result of plutonium evaporation. Containment of the pellets during sintering in a tantalum enclosure is also believed to have contributed to the reduction of weight losses by restricting the escape of effused gases and vapors. A tighter enclosure will be used in future runs in an attempt to reduce weight losses even further.

Uranium carbide pellets with satisfactory densities are achieved by sintering at a temperature of 1710°C for 2 to 3 hr. The achievement of satisfactory densification at a lower temperature than is required for (U,Pu)C pellets may be due to a higher oxygen content.

Little data have been obtained during these initial experiments on the purity of the pellets, because in many cases the powder has been known to be contaminated with oxygen during handling. In the most recent run, however, in which high purity (U,Pu)C feed material was used and the procedure was exactly as described above, the pellets had the following analysis:

Carbon:	4.99 w/o
Oxygen:	150 ppm
Nitrogen:	300 ppm

The number of pellets pressed has been insufficient to gain statistically significant data on the percentage of pellets meeting the exacting diameter specification of 0.255 ± 0.001 in. In the most recent batch, five out of eight (U,Pu)C pellets met this specification. When the pressing is done on a larger scale, however, the percentage meeting the specification as-pressed is not expected to be satisfactorily high. Therefore, plans are being made to grind the pellets to the final diameter.

2. Synthesis of Carbides by Conversion from Oxides

A fluidized-bed process is being developed to convert UO_2 to UC. This process is also expected to be applicable to the preparation of (U,Pu)C. The preparation of UC and (U,Pu)C from oxide feed materials is attractive because oxides are less expensive than the metallic feed material required for the metal-methane fluidized-bed process described above.

In the process under development, UO_2 and carbon are blended and UO_2-carbon particles are formed that are suitable for fluidizing. Particles so prepared have had a volume median diameter of 640 μ. In fluidization tests at room temperature, a bed of these particles began to fluidize at a superficial gas velocity of 2 ft/sec, and expanded to 350% of the initial bed height at the maximum practical fluidizing velocity of 5 ft/sec.

A fluidized-bed reactor for conversion of UO_2 to UC was constructed for operation at temperatures up to 2000°C and pressures of full vacuum to 10 atm. This reactor, shown in Figure III-12, has been installed and tested while empty at the maximum operating temperature of 2000°C. Conversion of 0.5- to 1.0-kg batches of UO_2 to UC in this equipment should begin in the near future.

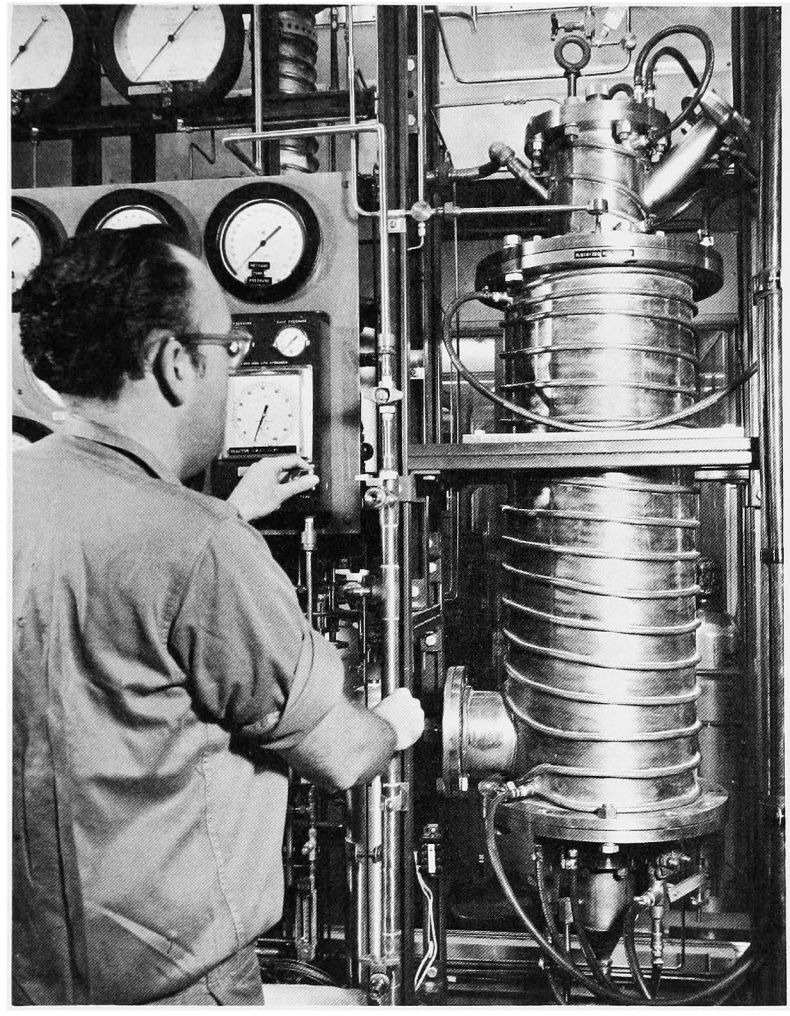

Fig. III-12. Fluidized-Bed Reactor for Conversion of UO_2 to UC. The 2-in. dia. reactor is enclosed within a graphite resistance furnace. Fluidized particles of UO_2 and carbon will be reacted at temperatures up to 2000°C, with the CO reaction product being carried off by the argon fluidizing gas.

D. Calorimetry

The determination of standard enthalpies of formation at 25°C (ΔHf°_{298}) of various compounds important in high-temperature chemistry and nuclear technology is of interest. Data have been obtained by reactions with oxygen in a bomb calorimeter, by reactions with fluorine in both bomb

and flow calorimeters, and by heat-of-solution measurements. Because of the refractory nature of many of the materials investigated, most of the data have been generated by the relatively new and powerful technique of fluorine bomb calorimetry.

1. Standard Enthalpies of Formation

Standard enthalpies of formation that have been determined and/or reported during this period are summarized in Table III-3. All unpublished values are to be considered tentative.

TABLE III-3. Standard Enthalpies of Formation

Compound	ΔHf°_{298} [a] (kcal mol^{-1})	Method	Publication or Status
$NbB_{1.875\pm0.006}(c)$	-58.6 ± 1.6	F_2-bomb	J. Chem. Eng. Data (1967)
$TaB_{1.919\pm0.004}(c)$	-43.9 ± 1.2	F_2-bomb	J. Chem. Eng. Data (1967)
$AlF_3(c)$	-360.7 ± 0.3	F_2-bomb	Inorg. Chem. 6, 1716 (1967)
$CF_4(g)$	-223.04 ± 0.18	F_2-bomb	J. Phys. Chem. 72, 222 (1968)
$UN_{0.965}(c)$	-71.5 ± 1.1	F_2-bomb	"The Thermochemistry of Some Uranium Compounds," IAEA Symposium on Thermodynamics of Nuclear Materials with Emphasis on Solution Systems, Vienna, Austria, Sept. 4-8, 1967 (in press).
$UN_{1.510}(c)$	-90.1 ± 1.7	F_2-bomb	
$UN_{1.690}(c)$	-94.1 ± 1.7	F_2-bomb	
$UP_{0.992}(c)$	-75.2 ± 1.3	F_2-bomb	
$US_{1.011\pm0.004}(c)$	-73.2 ± 3.5	F_2-flow	
$US_{1.011\pm0.004}(c)$	-74.6[b]	F_2-bomb	
$ThF_4(c)$	-504.6 ± 1.8	F_2-bomb	Recalculation
$ScF_3(c)$	-389.3 ± 3.0	F_2-bomb	New determination
$LaF_3(c)$	-419.3 ± 1.4	F_2-bomb	Redetermination
$NdF_3(c)$	-395.8 ± 1.4	F_2-bomb	New determination
$GdF_3(c)$	-406.5 ± 0.5	F_2-bomb	Recalculation
$HoF_3(c)$	-407.7 ± 0.6	F_2-bomb	Redetermination
$ErF_3(c)$	-409.3 ± 1.2	F_2-bomb	New determination
$IF_5(l)$	-211.3 ± 0.8	F_2-bomb	New determination
$ZrI_4(c)$	-119 ± 4	F_2-bomb	New determination
$PuO_2(c)$	-252.2 ± 0.3	O_2-bomb	New determination
$B_2O_3(c)$	-304.01 ± 0.42	ΔH_{soln}	New determination
$B_2O_3(gl)$	-299.62 ± 0.42	ΔH_{soln}	New determination

[a] 2σ uncertainties.
[b] Average of two experiments.

Various other values have been derived or estimated from the new results. The datum for AlF_3, when combined with earlier results[1,2] for the reaction of PbF_2 with Al to give AlF_3 and Pb, yields $\Delta Hf^\circ_{298}(PbF_2,c)$ = -161.7 ± 0.3 kcal mol^{-1}.

The datum for CF_4, when combined with the results for the combustion of Teflon in oxygen[3] and for the combustion of Teflon in fluorine,[4,5] yields $\Delta Hf^\circ[HF \cdot 10\ H_2O(l)]$ = -77.02 or -76.75 kcal mol^{-1}, depending on which of refs. 4 and 5 is accepted. Both values are in general accord with many other lines of evidence that indicate that the currently tabulated values for $\Delta Hf^\circ(HF,aq)$ are in error.

The values for the uranium compounds given in Table III-3 have been used to estimate the following values (in kcal mol^{-1} at 298°K) for compounds that have not yet been examined: $\Delta Hf^\circ(UN_2,c)$ = -107 ± 3 and $\Delta Hf^\circ(U_3P_4,c)$ = -266 ± 14. The enthalpy-of-formation values for some of the uranium compounds have been combined with data from recent high-temperature vaporization studies to estimate a value for the heat of sublimation of uranium and to help shed light on the discrepant literature values for the latter quantity. The results obtained, while not definitive, do tend to support the higher of the two literature values.

The data on rare earth trifluorides given in Table III-3 have been used to estimate enthalpies of formation for the remainder of the rare earth trifluorides. These estimates are discussed more fully in Part 2.

The calorimetric combustion of metallic plutonium in oxygen was carried out in a new glovebox facility (Fig. III-13), which appears to be functioning very well for this purpose.

The values given for crystalline and glassy B_2O_3 were obtained with an LKB Instrument Co. solution calorimeter, which had been placed in this laboratory for evaluation. The accuracy of the instrument was checked by measurements of the heat of solution of THAM (tris-hydroxymethyl-aminomethane), and the value obtained, -7,111 cal mol^{-1}, was in good accord with accepted values.

In various calorimetric reactions with fluorine it is helpful to be able to separate the resulting mixtures of fluorinated gaseous

---

1 P. Gross, C. Hayman, D. L. Levi, in Physical Chemistry of Process Metallurgy, Part 2, p. 903, G. R. St. Pierre (ed.), Interscience Publishers, Inc., New York, N. Y. (1961).

2 V. P. Kolesov, A. M. Martynov, S. M. Skuratov, Russ. J. Inorg. Chem. 6, 1376 (1961).

3 W. D. Good, D. W. Scott, G. Waddington, J. Phys. Chem. 60, 1080 (1956).

4 J. L. Wood, R. J. Lagow, J. L. Margrave, J. Chem. Eng. Data 12, 255 (1967).

5 E. S. Domalski, G. T. Armstrong, J. Res. Natl. Bur. Std. 71A, 105 (1967).

products and to determine the detection limits of the components. The description of a method developed in this laboratory for this purpose has been published;[6] the method combines transpiration and gas chromatographic techniques to yield results of excellent sensitivity.

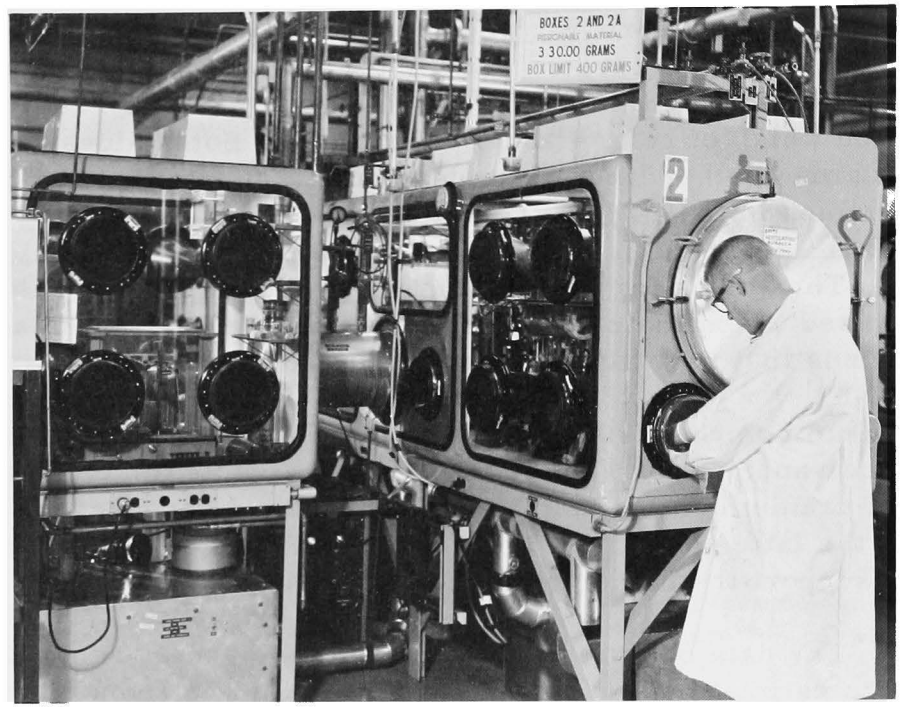

Fig. III-13. Glovebox Facility Houses a Bomb Calorimeter Being Used for the Combustion of Plutonium and Plutonium Compounds in Oxygen, Fluorine, or Chlorine.

The description of a special two-chambered vessel for the determination of the enthalpy of formation of $CF_4(g)$ was also published[7] during this period.

2. Correlation and Estimation of Enthalpies of Formation for the Rare Earth Trifluorides

The purpose of this work was to estimate enthalpies of formation for all the rare earth trifluorides from the data already obtained on ScF_3, YF_3, LaF_3, NdF_3, GdF_3, HoF_3, and ErF_3 and existing data on the trichlorides and sesquioxides of the rare earths. These estimates are given in Table III-4. Except for $TbF_3(c)$ and $DyF_3(c)$, which were obtained by simple interpolation by analogy with the corresponding trichlorides and sesquioxides, the estimates were obtained by means of the Born-Haber cycle, Equation 1,

[6] E. Rudzitis, Anal. Chem. 39, 1187 (1967).

[7] J. L. Settle, E. Greenberg, W. N. Hubbard, Rev. Sci. Instrum. 38, 1805 (1967).

$$\Delta Hf^{\circ}(MF_3,c) = \Delta H_L(MF_3,c) + \Delta Hf^{\circ}(M^{3+},g) + 3\Delta Hf^{\circ}(F^-,g) \quad (1)$$

In Eq. 1, M represents the rare earth metal, $\Delta H_L(MF_3,c)$ is the lattice enthalpy of its trifluoride, and the last two terms are the enthalpies of formation of the gaseous trivalent rare earth ion and the gaseous fluoride ion. Required for the calculation were the difficult-to-obtain values for $\Delta H_L(MF_3,c)$ and $\Delta E_i(M^{3+},g)$. The latter term, the energy of ionization of the gaseous metal atom to the trivalent ion, is related to $\Delta Hf(M^{3+},g)$ by the equation

$$\Delta Hf^{\circ}(M^{3+},g) = \Delta E_i(M^{3+},g) + \Delta H_s^{\circ}(M),$$

where $\Delta H_s^{\circ}(M)$ is the enthalpy of sublimation.

TABLE III-4. Measured and Estimated Enthalpies of Formation of Rare Earth Trifluorides[a] (Kcal mol^{-1})

Compound	$-\Delta Hf^{\circ}_{298}$	Compound	$-\Delta Hf^{\circ}_{298}$	Compound	$-\Delta Hf^{\circ}_{298}$
$ScF_3(c)$	389.3	$SmF_3(c)$	401	$HoF_3(c)$	407.7
$YF_3(c)$	410.7	$EuF_3(c)$	376	$ErF_3(c)$	409.3
$LaF_3(c)$	419.0	$GdF_3(c)$	406.5	$TmF_3(c)$	403
$CeF_3(c)$	420	$TbF_3(c)$	406.8	$YbF_3(c)$	383
$PrF_3(c)$	423	$DyF_3(c)$	407.5	$LuF_3(c)$	393
$NdF_3(c)$	395.8, 418[b]				
$PmF_3(c)$	417				

[a]Experimental values are underlined.
[b]See text.

The calculations were made as follows: The ionization energies and enthalpies of sublimation of yttrium and lanthanum and the enthalpies of formation of their trifluorides, trichlorides, and sesquioxides were inserted into Eq. 1 and its analogs to give the corresponding lattice enthalpies. Next, use was made of the Born-Landé equation to estimate the lattice enthalpies of the trifluorides, trichlorides, and sesquioxides of all of the remaining rare earths. According to the Born-Landé equation, the variation in lattice energy in an isostructural series is inversely proportional to the cube root of the molecular volume. The estimated lattice enthalpies were then inserted into Eq. 1 together with any known experimental values for the enthalpies of formation in order to calculate sets of values of $\Delta E_i(M^{3+},g)$. From the sets of values obtained, "best" values for each $\Delta E_i(M^{3+},g)$ were selected. Finally, these "best" values and the lattice enthalpies were again inserted into Eq. 1 to calculate the enthalpies of formation of the crystalline trifluorides. For the elements Gd, Ho, and Er, the values of ΔE_i deduced from the fluoride data and those from other compounds agreed to within a

couple of kcal mol^{-1}, lending confidence to the method. For Nd, such agreement was not obtained; the value of $-\Delta Hf^{\circ}_{298}(NdF_3)$ predicted by the "best" value (418) disagrees markedly with the experimental value (395.8). The cause of the discrepancy is unknown; at present we are inclined to regard the estimated value as the more reliable.

3. Extended Hückel Molecular Orbital Calculations for the Chalcogen Hexafluorides

Our experimental determination[8] of the enthalpies of formation of the hexafluorides of sulfur, selenium, and tellurium showed that the average bond energies in this series varied nonmonotonically, and qualitative rationalizations of this fact were advanced. It would be desirable to have these rationalizations put on a more quantitative basis. Extended Hückel molecular orbital (EHMO) calculations, which should yield theoretical information on the nature of the bonding, charge transfer between atoms, and bond energies, are therefore being made.

Valence-state ionization energies for the various possible electronic configurations of both the chalcogen and the fluorine atoms were deduced from atomic spectral data.[9] The atomic wave functions were approximated by Slater-type orbitals.[10] Screening parameters, which are a measure of the screening of the valence electrons from the nucleus by the inner electrons, were calculated by the method of Burns.[11] A computer program[12] was used to evaluate both chalcogen-fluorine and fluorine-fluorine overlap integrals, and resonance integrals were calculated for all 48 valence electrons (7 on each fluorine, and 6 on the chalcogen atom). A 48 x 48 secular determinant was solved to yield the orbital energy levels, the electronic configurations of the atoms, and the charge distributions within each molecule. The procedure was iterated until input and output charge distributions were in accord.

The following charge distributions have been obtained for the three hexafluoride molecules:

$$S^{+1.66}(F^{-0.28})_6$$

$$Se^{+1.70}(F^{-0.28})_6$$

$$Te^{+2.34}(F^{-0.39})_6$$

---

[8] P. A. G. O'Hare, J. L. Settle, W. N. Hubbard, Trans. Faraday Soc. 62, 558 (1966).

[9] C. E. Moore, "Atomic Energy Levels," Natl. Bur. Std. (U.S.), Circ. 467 (1964).

[10] J. C. Slater, Phys. Rev. 26, 57 (1930).

[11] G. Burns, J. Chem. Phys. 41, 1521 (1964).

[12] Dr. Audrey Companion of Illinois Institute of Technology very kindly made much of this program available to us and has assisted in many other ways.

These results indicate considerably more charge transfer in TeF_6 than in SF_6 or SeF_6; the Te-F bonds are more ionic than the S-F or Se-F bonds. This result is consistent with the original qualitative rationalizations and with other chemical evidence, such as the much greater ease of hydrolysis of TeF_6 in polar solvents.

No allowance for the effect of charge transfer on the valence-state ionization energies and the screening parameters was made in these calculations. Therefore, a new iteration is required before the results can be subjected to more detailed scrutiny of the energy levels, etc.

E. Chemistry of Liquid Metals

1. Ultrasonic Measurements in Liquid Metallic Solutions

The power of ultrasonic methods for the detection of complexes in nonmetallic solutions is well documented, and the formation of aqueous complexes has been unequivocally correlated with the appearance of anomalies in curves of sonic velocity vs. composition.[1-3] (The composition variable is most conveniently expressed in terms of the ratio of the constituents of possible complexes. This is known as Job's method.[4]) The concept that similar anomalies might be sought for the detection of complexes in liquid metal systems has not been previously examined. This study was undertaken to search for this kind of evidence of association in liquid metal solutions. The pulse-echo method, which involves the measurement of the time of transit of a short pulse of acoustic waves along a predetermined path in a specimen liquid, was selected for measuring ultrasonic velocity. The equipment (see Fig. III-14) and procedure have been described in previous reports.[5]

From conductivity[6] and other measurements it has been suspected that the stable, solid compound of magnesium and tin, Mg_2Sn, melts to form a stable liquid complex with the same composition. Accordingly, the interaction of magnesium and tin in solution in liquid cadmium was examined. Cadmium was chosen as a solvent because it was expected not to interact strongly with either constituent of the presumed complex. To verify this assumption, the concentration dependences of sonic velocity in Cd-Sn and Cd-Mg solutions were measured.

---

[1] S. Prakash, F. M. Ichhaporia, J. D. Panday, J. Phys. Chem. 68, 3078 (1964).
[2] T. Satyavate, P. J. Reddy, S. V. Subrahmanyam, J. Phys. Soc. Jap. 17, 1061 (1962).
[3] J. R. Saraf, P. N. Sharma, J. Sci. Res. Inst. (Tokyo) 49, 236 (1955).
[4] P. Job, Ann. Chem. (Paris) [10] 9, 113 (1928).
[5] ANL-7225, p. 159; ANL-7325, p. 131.
[6] J. R. Wilson, Phys. Letters 20, 571 (1966).

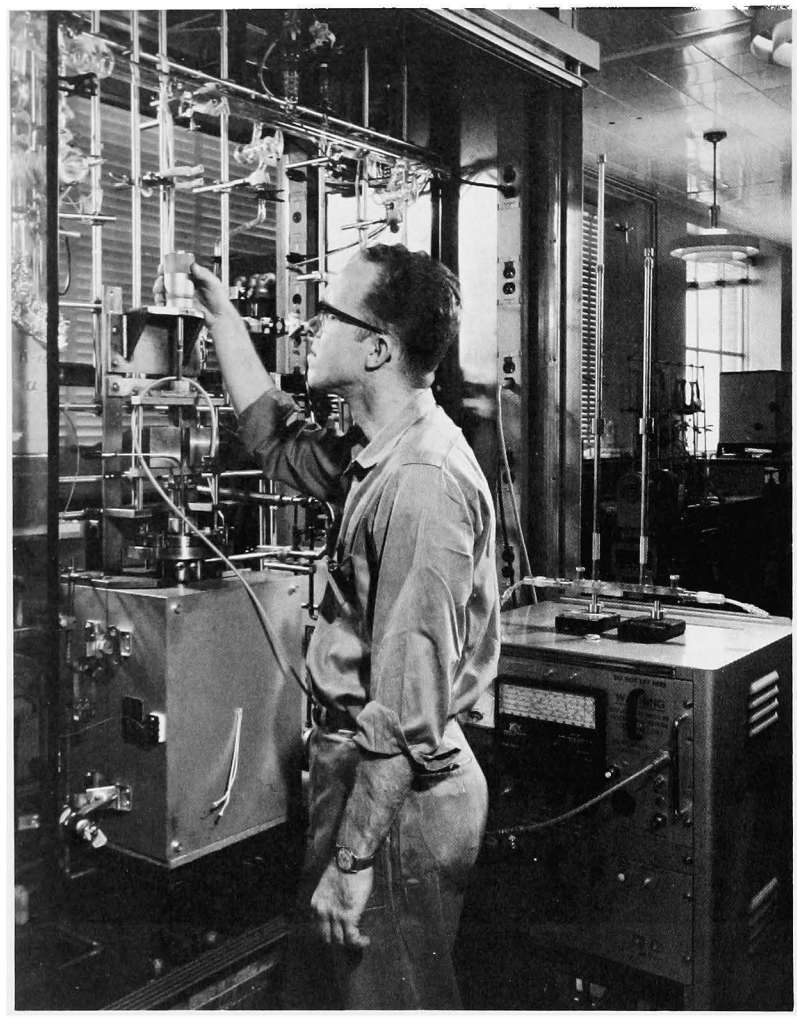

Fig. III-14. Apparatus for the Measurement of Velocity and Attenuation of Ultrasound in Liquid Metallic Systems.

At ~342°C, the velocity of sound in a Cd-Sn solution containing 0, 10, 25, 40, and 100 a/o Sn was 2237, 2257, 2292, 2328, and 2454 m/sec (all ±7 m/sec), respectively. The data are shown in Figure III-15. Within experimental uncertainty, the velocities vary linearly between the pure metals.[7] Therefore, it appears that for Cd-Sn solutions, sonic velocity is an additive property, in accord with expectations for weakly interacting substances.

Velocities of 2278 ± 7 and 2320 ± 7 m/sec were measured at ~340°C for Cd-Mg solutions with 5 and 10 a/o Mg, respectively, as shown in Figure III-15. Because sonic velocity data are not available for liquid magnesium, a test for additivity in the Cd-Mg system could not be made.[8]

[7] From a more limited study at a lower temperature, O. J. Kleppa [J. Chem. Phys. 18, 1331 (1950)] reached a similar conclusion.

[8] Magnesium melts at 651°C; measurements in the present apparatus are limited to a maximum temperature of ~360°C.

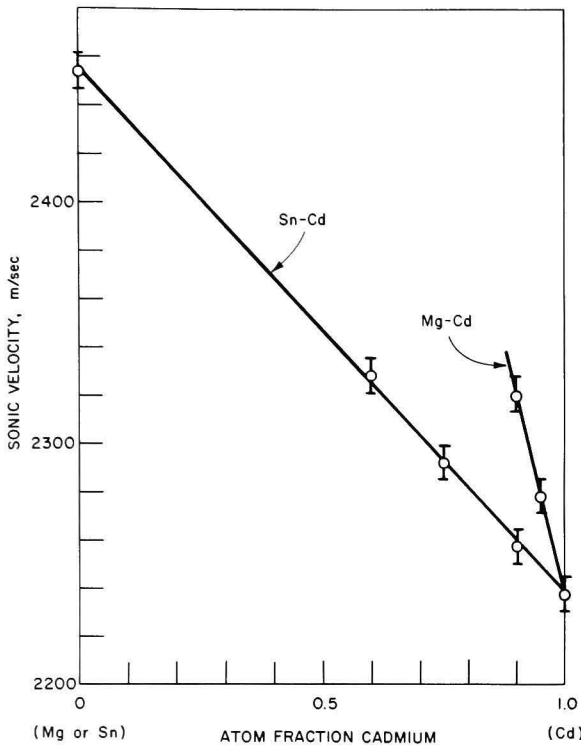

Fig. III-15. Sonic Velocity vs. Composition in Liquid Binary Cd-Sn and Cd-Mg Alloys at 342°C.

Over the short composition range studied, however, the variation of sonic velocity with concentration is linear within experimental uncertainty; the possibility of additivity, therefore, is not precluded.

On the basis of these preliminary measurements, cadmium was judged to be a suitable solvent for this study. The velocity of sound in several liquid Cd-Mg-Sn ternary alloys was measured at 342°C. In these alloys the ratio of Mg to Sn was varied, but the total concentration of Mg + Sn remained constant at 10 a/o. The variation of sonic velocity with composition is shown in Figure III-16.

Within experimental error, no anomaly in velocity was found at a ratio of Mg/Sn = 2; thus, no evidence was obtained to show that the complex Mg_2Sn exists in detectable concentrations. It is still possible, of course, that the complex exists in other media but dissociates in cadmium, i.e., the equilibrium constant for the formation of Mg_2Sn is so lowered in cadmium that its concentration in the ternary solution falls below detectable limits. To avoid the uncertainty introduced by a third component, in future studies binary rather than ternary liquid solutions will be examined. In addition, the possibility of using ultrasonic absorption measurements for the detection and study of complex formation in liquid alloys will be examined. Such measurements have led to valuable information concerning various structural relaxation processes in nonmetallic liquids, and recent studies have suggested that relaxation processes also occur in liquid metals.

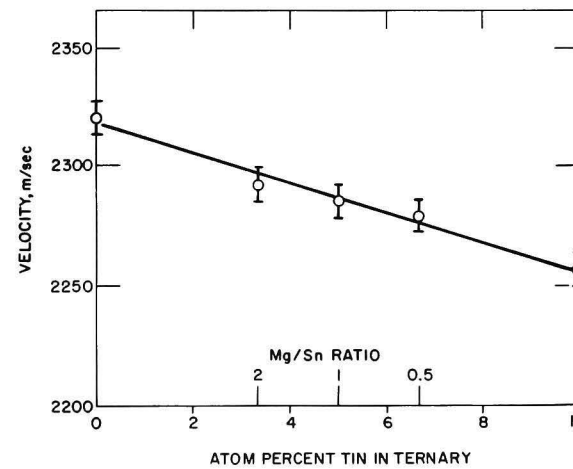

Fig. III-16. Variation of Ultrasonic Velocity with Composition in Liquid Cadmium Alloys Containing 10 a/o Magnesium + Tin at 342°C.

2. Carbon Transport Experiments in Liquid Sodium Systems

Carbon transport in sodium systems has been studied extensively in recent years. These studies have shown the following:

1) Carbon migrates through sodium from ferritic steels having a high activity of carbon to austenitic steels having a low activity of carbon.[9]

2) The diffusion of carbon in the solid structural materials is the rate-controlling factor in carbon transport.[10]

3) The total carbon content of sodium, within the limits of analytical variability, does not change during the transport of carbon. Therefore, differentiation of transported carbon-bearing species from pre-existing carbon has proved difficult.[11]

The mechanism of carbon transport is still unknown, and uncertainty about the nature of the carbon-bearing species that undergoes transport in sodium has hampered progress in understanding this mechanism. Therefore, an attempt is being made to detect, assay, and identify such species. Because the carbon transported must be differentiated from the carbon that pre-exists in sodium, beta-active carbon-14 ($t_{1/2}$ = 5770 y) is being used to trace the migration of carbon to and from structural materials exposed to liquid sodium.

In a preliminary experiment, the power and sensitivity of the carbon-14 tracer method was clearly demonstrated. A cyclindrical crucible (2.4-cm dia. by 3.5 cm) and matching lid were fabricated from an 18-mil-thick sheet of a ferritic Fe-C alloy prepared from carbon enriched with carbon-14. Enough molten, reactor-grade sodium (9 g) was added to the crucible to completely immerse an austenitic (type 304) stainless steel coupon (2 cm by 1.5 cm by 10 mils) suspended by a tantalum wire welded to the crucible lid. The crucible was welded shut, heated at 650°C for 150 hr, cooled to room temperature, and opened for analysis. The filling, welding, opening, and sampling were done in a helium-atmosphere glovebox.

The surface of the coupon, after being washed free of sodium with ethyl alcohol, was found to be highly beta active. Moreover, significant amounts of beta activity persisted after polishing off several mils of the surface, which indicates that the tagged carbon had diffused into the coupon. Autoradiographs of the coupon showed a fairly uniform distribution of

---

[9] W. C. Hayes, O. C. Shepard, "Corrosion and Decarburization of Ferritic Chromium-Molybdenum Steels in Sodium Coolant Systems," USAEC Report NAA-SR-2973 (December 1, 1958).

[10] W. J. Anderson, G. V. Sneesby, "Carburization of Austenitic Stainless Steel in Liquid Sodium," USAEC Report NAA-SR-5282 (September 1, 1960).

[11] R. W. Lockhart et al, "Sodium Mass Transfer: IX. The Effect of Carbon and Carbonate Additions in a Sodium Test Loop," USAEC Report GEAP-4436.

the carbon-14. The coupon and sections of the crucible that had been exposed to molten sodium were analyzed for total carbon content, with the following results:

	Crucible	Coupon
Initial C, %	0.0263	0.075
Final C, %	0.0020	0.53

Since the initial carbon contents of the coupon and sodium could account for, at most, 20% of the coupon's final carbon content, it was concluded that the carbon in the ferritic crucible had been transported to the austenitic coupon. This conclusion is consistent with the finding (noted above) that thermodynamic driving forces, i.e., activity gradients rather than concentration gradients, play a decisive role in the carburization of steels in sodium systems.

The final tagged-carbon content of the sodium, which represents carbon originating from the crucible, was determined to be 0.17 ppm. A filtration experiment on this sodium showed that the tagged carbon in it could not pass through a 5 μ-porosity filter. The observations naturally lead to the speculation that the transport of carbon in sodium systems may involve carbon-bearing particulates. This speculation, which is particularly plausible because a concentration of 0.17 ppm exceeds the measured solubility of carbon in sodium ($<$0.005 ppm[12] up to 450°C), will be tested in future experiments.

Identification of the migrating, tagged, carbon-bearing species will also be attempted. Because identification by direct methods is not possible for unisolable, low-concentration substances, an indirect approach will be used. Attempts will be made to deduce the nature of the migrating ^{14}C-bearing species from analyses of the labeled products in the off-gases, solutions, and residues resulting from aqueous dissolution of sodium samples taken during transport experiments. To interpret the findings from such experiments unambiguously, the extent of exchange between the tagged species and carbon-bearing species that pre-exist in sodium must be known. Accordingly, the exchange between carbonaceous contaminants of molten, reactor-grade sodium and various added ^{14}C-labeled compounds will be investigated.

3. The Nature of Nitrogen in Sodium

Information about the nature and concentration of nitrogen-bearing impurities in sodium is nearly completely lacking. The nitridation of structural materials in contact with sodium systems at elevated temperatures, however, is well documented. To begin to obtain basic

[12] C. Luner, A. Cosgarea, Jr., H. M. Feder, "Solubility of Carbon in Sodium," Alkali Metal Coolants, pp. 171-179, Int. Atomic Energy Agency, Vienna (1967).

information on nitrogen and its common compounds in sodium, the solubilities of sodium cyanide and of nitrogen gas are being measured.

a. Solubility of NaCN in Sodium

In most compounds containing it, the cyanide ion acts as a pseudohalide[13] ion; thus, the phase diagram of the Na-NaCN system was expected qualitatively to resemble those of other sodium-sodium halide systems.[14] A typical sodium-sodium halide phase diagram shows a monotectic at the salt-rich end and a miscibility loop that nearly spans the diagram.

A NaCN-rich monotectic at 566 ± 2°C was found earlier by thermal analysis. An attempt was made to measure the width of the miscibility loop by the equilibration-sampling method devised by Bredig et al[15] for sodium-sodium halide phase studies. Molten sodium cyanide and sodium were mixed in a tantalum container by means of a rocking furnace and then allowed to separate by settling. The upper (sodium) phase was poured into a sidearm of the container and assayed for cyanide. The cyanide content of the samples taken in this way, however, showed unusual scatter, for reasons that are not clear at this time. Any further work to define the miscibility loop will use either thermal analysis or some other sampling technique.

The solubility of cyanide in sodium below the monotectic is being measured by equilibration of a sodium melt with excess solid NaCN at a preselected temperature, sampling of the liquid with a tantalum pipette provided with a 5 μ-porosity stainless steel filter, and assay of the sample for cyanide. Preliminary measurements indicate the solubility to be 0.035 m/o NaCN at 550°C.

b. Solubility of Nitrogen in Liquid Sodium

Interest in the solubility of nitrogen in liquid sodium arises from the fact that its magnitude may be important to understanding certain corrosion phenomena in sodium systems. Scientifically, there is a further interest that arises from the observation that in all liquid metals in which the solubility of nitrogen has been previously examined the gas dissolves monatomically. But all these metals form fairly stable nitrides, whereas sodium does not. The question is then whether N_2 will dissolve in liquid sodium as atoms or dimers.

---

[13] F. A. Cotton, G. Wilkinson, Advanced Inorganic Chemistry, p. 560, Interscience Publishers, New York (1966).

[14] M. A. Bredig, in Molten Salt Chemistry, M. Blander (ed.), p. 367, Interscience Publishers, New York (1964).

[15] M. A. Bredig, J. W. Johnson, W. T. Smith, Jr., J. Amer. Chem. Soc. 77, 307 (1955).

An existing solubility apparatus was modified for this study (see Fig. III-17). The measurements were made by saturating liquid sodium at a preselected temperature with nitrogen at a known pressure, stripping the dissolved nitrogen with helium, trapping the stripped gas, and assaying it with a mass spectrometer. Because the solubility of nitrogen is quite small, it is necessary to differentiate the dissolved nitrogen from the minute amounts of atmospheric nitrogen that may contaminate the apparatus. For this purpose, nitrogen gas enriched in ^{15}N was used to saturate the sodium.

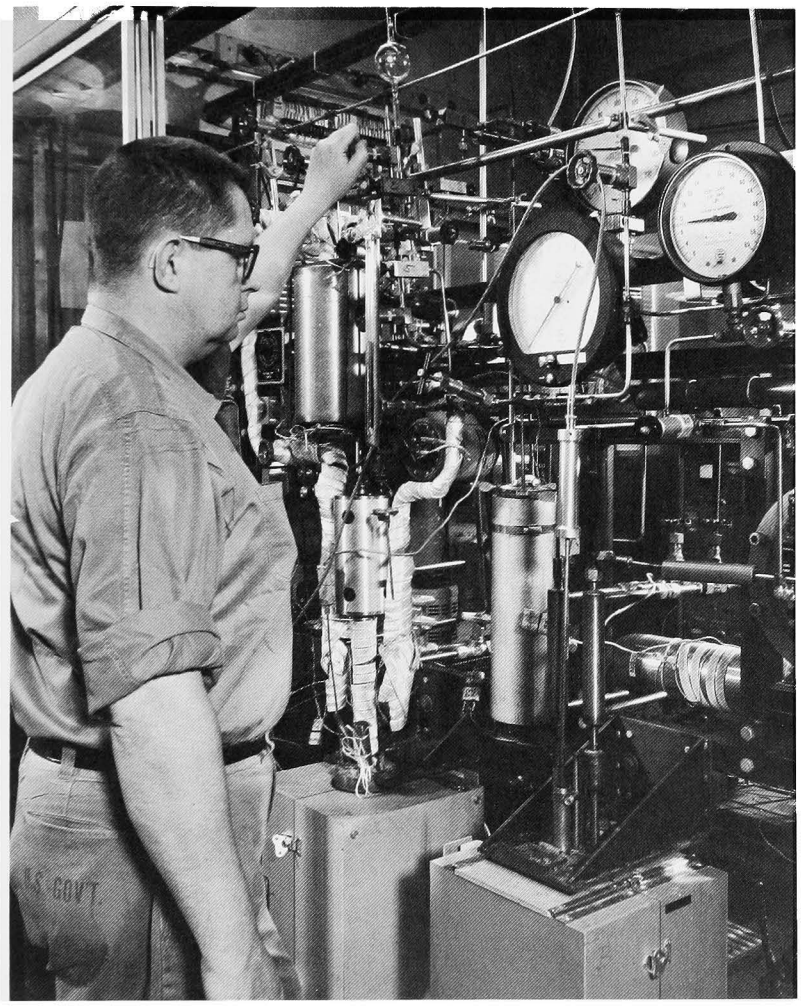

Fig. III-17. Equipment Used in Measuring the Solubilities of Gases in Liquid Sodium.

The question of whether nitrogen dissolves in sodium atomically or molecularly was first examined. Nitrogen of known isotopic composition (20.4 m/o $^{15}N_2$, 77.9 m/o $^{14}N_2$, 1.6 m/o $^{14}N^{15}N$, 0.1 m/o impurities) was circulated through two liters of sodium at 345°C. Samples of the equilibrated gas were taken intermittently over 96 hr. Mass

spectrometric analysis of these samples revealed that the isotopic composition of the gas after equilibration with sodium had not been altered significantly. If nitrogen had dissolved monatomically and the atoms recombined randomly on exsolution, a significant change in the isotopic constitution of the starting mixture toward equilibrium (4.5 m/o $^{15}N_2$, 62.1 m/o $^{14}N_2$, 33.4 m/o $^{14}N^{15}N$) might have resulted. Within experimental error, isotopic exchange did not occur, and it is probable that nitrogen dissolved diatomically. Future experiments on the pressure dependence of nitrogen solubility should confirm the manner in which nitrogen dissolves: a linear dependence of the solubility on pressure would indicate diatomic dissolution, whereas a square root dependence would indicate monatomic dissolution.

The reliability of the solubility apparatus for recovering spiked amounts of tracer nitrogen was tested prior to beginning the solubility experiments. In six experiments, 99 ± 2% of the spiked nitrogen was recovered. Having established the effectiveness of the apparatus and method, solubility measurements were started. From preliminary measurements at 500°C, the solubility, expressed in terms of the Ostwald coefficient, i.e., the volume of nitrogen dissolved per unit volume of sodium, was $1.4 \pm 0.6 \times 10^{-7}$.

IV. REACTOR SAFETY

The program on reactor safety comprises studies that fall into two major areas of research: (1) studies relating to thermal (water-cooled) reactors and (2) studies relating to fast (sodium-cooled) reactors.

A. Thermal Reactor Safety Studies

In water-cooled nuclear reactors, a loss of coolant or a severe nuclear excursion could cause the reactor fuel materials to melt and disperse rapidly in the water. Exothermic chemical reactions between metals present, such as the Zircaloy cladding in a power reactor, and water could result in the release of large amounts of energy which can approach or even exceed the energy released by the fission process during a nuclear excursion. The dispersion of molten materials in the water coolant can also cause an explosive energy release. Such an occurrence is believed to have resulted in the destruction observed in the SPERT ID destructive test. Studies of these chemical reactions and physical interactions are being carried out so that realistic estimates can be made of the rates and extents of reactions and interactions occurring during hypothetical reactor accidents. Both nuclear-excursion and loss-of-coolant accident simulation experiments are also being carried out, as well as calculational studies in which experimental results are used to develop methods of accident analysis.

1. Analysis of Loss-of-Coolant Accidents

The loss-of-coolant accident resulting from a break in the primary-system water pipe is considered the "maximum credible accident" for power reactors built to date. Upon release of the coolant, the reactor core is exposed to a steam environment. In the absence of auxiliary cooling, decay of fission products in the core releases sufficient energy to cause the cladding to be heated to temperatures at which metal-steam reactions can occur.

A computer program (CHEMLOC-II) has been developed to describe the course of a loss-of-coolant accident through the period of core meltdown. This program is an extension of CHEMLOC-I (ANL-7350, p. 69), which described the accident (core heating and chemical reaction) up to the time of core melting. The CHEMLOC-II program incorporates a core-slumping model which follows the behavior of the core successively through melting, slumping, movement, and finally heating of the bottom grid support plate. The extended program also considers: 1) the effects of heat transfer by axial radiation, 2) the effects of heat transfer from the core to the top and bottom grid support plates and to the wall surrounding the core, 3) the effects of core movement due to slumping, and 4) the effects of other reactive materials, such as fuel element shrouds and spacers (referred to as can material).

The principal input parameters required for the program include slump (melting or collapse) temperature of the fuel-cladding material and the quantity of slumping required to stop steam flow in a given zone within the core.

Calculations have been performed to describe core behavior throughout a loss-of-coolant accident at three assumed slump temperatures (1750, 2200, and 2800°C). The axial variation in fuel temperatures over incremental lengths of fuel rods in the center zone of the core are shown in Fig. IV-1 at different times after blowdown. The fuel temperature profiles are nearly identical in each of the three cases of specified slump temperature. Each case showed a thermal arrest at the assumed slumping temperature.

Additional calculations indicate the following major effects of changing the slumping temperature:

1) The quantity of hydrogen released is less at the lower slumping temperature (about one-half of that released at the highest slumping temperature). This is due, in part, to the fact that at low slumping temperatures steam flow to portions of the core is blocked by slumping of the core at an earlier time in the event, thereby reducing metal-steam reaction in those portions of the core.

2) The temperature of the bottom grid support plate increases more rapidly and reaches a failure temperature earlier in the case of an assumed low slumping temperature (about 20% earlier than in the high slumping temperature case). The rapid increase in grid plate temperature is due to hot molten material falling onto the grid plate from slumped fuel.

2. Pressure Generation due to Particle Coolant Energy Transfer

In order to analyze adequately the consequences of an accident in a water-cooled thermal reactor in which hot fuel materials are injected and dispersed into the water coolant, knowledge of the manner in which large amounts of energy are transferred from these particles to the coolant is needed. Laboratory-scale experiments are being made, using two different techniques, to obtain heat transfer and energy transfer data. The first technique involves determination of boiling heat transfer between a moving sphere and water. The second technique employs a pressure transducer to measure the forces generated owing to void formation when hot particles are immersed in a water column.

a. Boiling Heat Transfer from Spheres to Water: Swinging Arm Method

A series of experiments have been performed to study the forced-convection heat transfer from spheres in water. In the experiments, a heated silver metal sphere is propelled through the water by means of a

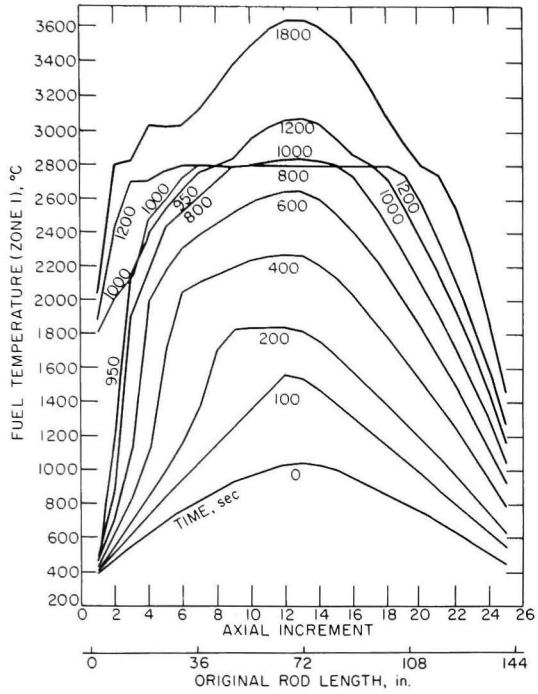

Slumping Temperature, 2800°C

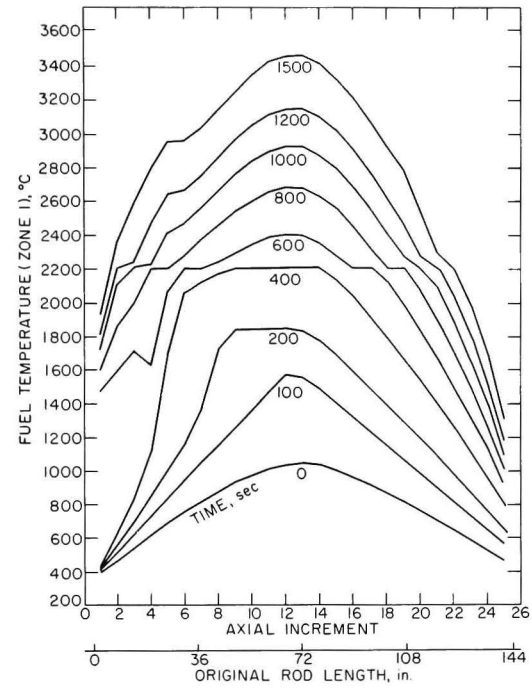

Slumping Temperature, 2200°C

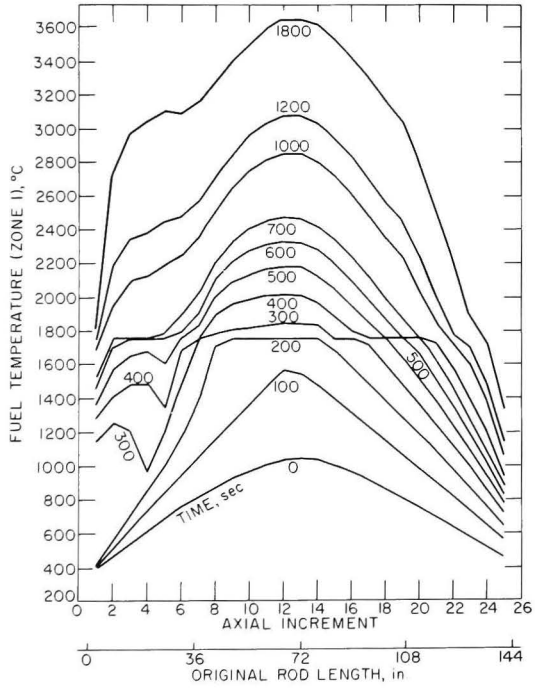

Slumping Temperature, 1750°C

Fig. IV-1

Calculational Results of Axial Variation of Zone 1 Fuel Temperatures for a 3300 MW(t) Boiling Water Reactor.

motor-driven swinging arm. The temperature of the sphere is continuously monitored by a thermocouple attached to the sphere through the arm. The rate of heat transfer from the sphere to water is calculated using the time-averaged bulk temperature of the sphere (the arithmetic average temperature before entering and after leaving the water). Heat transfer rates from recent experiments using a 1/4-in. dia. sphere are plotted in Fig. IV-2 as a function of the average bulk sphere temperature. The heat transfer rate curves are of the classic shape for boiling liquids[1,2] and show two regimes of boiling: nucleate boiling and film boiling. Nucleate boiling was observed (with water initially at 24°C) at average sphere temperatures from about 100°C up to 350°C, with increased rates of heat transfer at the higher temperatures. At average sphere temperatures above 350°C, transition to film boiling occurs, manifested by a decrease in heat transfer rate.

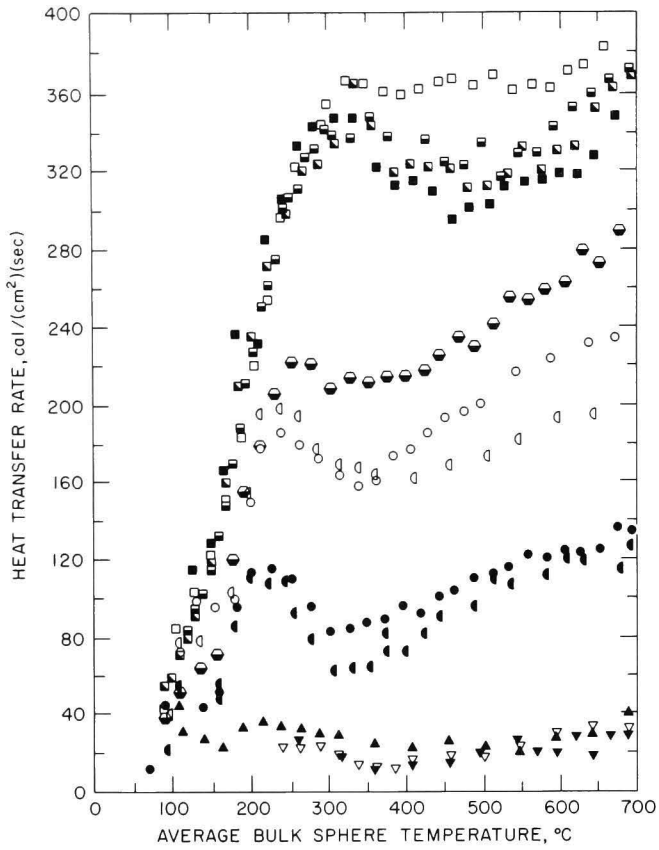

Fig. IV-2. Heat Flux from Swinging Arm Experiment with 1/4-in. dia. Silver Sphere Moving through Water at 13.9 ft/sec.

Water Boiled Prior to Experiment	Water Not Boiled Prior to Experiment
□ 24.0°C water	■ 24.4°C water
	⬓ 23.8°C water
	◪ 20.8°C water
	⬢ 43.5°C water
○ 59.0°C water	● 65.0°C water
◖ 60.0°C water	◖ 62.0°C water
▽ 90.0°C water	▼ 88.5°C water
	▲ 88.4°C water

The results shown in Fig. IV-2 indicate that the effect of heating the water is to lower the temperature at which the transition to film boiling occurs. Dissolved air in the water also tends to initiate the transition to film boiling at lower temperatures. This effect was less marked at water temperatures of 24 and 90°C than at intermediate temperatures. Heat transfer rates in the film boiling region were 75% greater for runs with boiled water at 60°C.

The theoretical equation for heat transfer from a sphere (previously given as Equation 2 in ANL-7350, p. 74) for correlating sodium

[1] S. Nukiyama, "Maximum and Minimum Values of Heat Transmission from Metal to Boiling Water under Atmospheric Pressure," Journal of the Society of Mechanical Engineers (Japan) 36, 367 (1934).

[2] E. A. Farber, R. L. Scorah, "Heat Transfer to Water Boiling under Pressure," Trans. ASME 70, 369 (1948).

heat transfer data has been used to correlate all experimental data obtained with boiled water:

$$q/A = K\left(\frac{U_\infty \rho_\ell C_{p\ell} k_\ell}{D}\right)^{1/2} (T_\ell - T_B). \qquad (1)$$

Since Equation 1 can be expressed in terms of dimensionless numbers, experimental data were correlated by plotting $Nu\Delta T/(Re\ Pr)^{0.5}$ vs ΔT (Fig. IV-3), where Nu, Re, and Pr are the Nusselt, Reynolds, and Prandtl numbers, respectively. It is apparent from the figure that, within the nucleate boiling regime, the experimental data obtained at several sphere velocities correlate well.

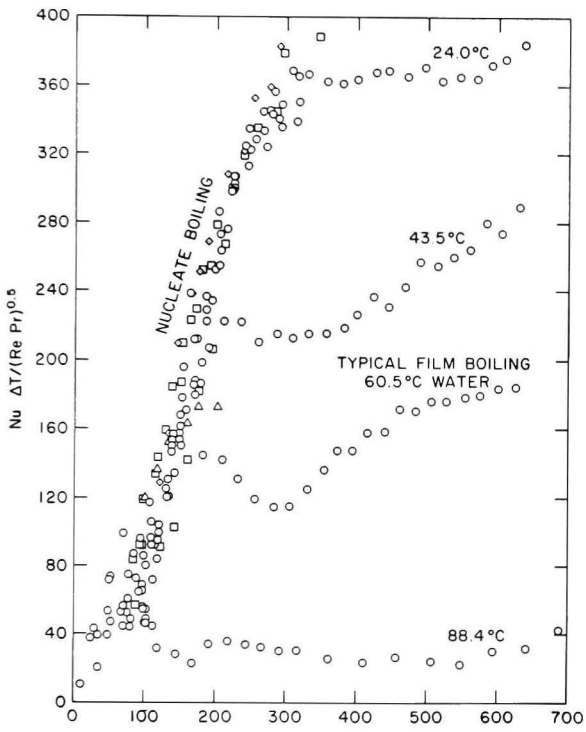

Fig. IV-3. Heat Flux from Swinging Arm Experiments with 1/4-in. dia. Silver Sphere in Water. (ΔT = difference between average bulk sphere temperature and water temperature.)

Experimental Data	
Symbol	Sphere Velocity (ft/sec)
◇	3.4
□	7.2
○	13.9
△	25.5

Since Equation 1 is based on the assumption of forced convection (negligible vapor formation) with superheating of the liquid near the sphere-liquid interface, the equation does not accurately predict the observed heat transfer rates at large values of ΔT. Apparently vapor formation contributes to the higher rates, although superheating of the liquid is nevertheless significant. Future experiments will be directed toward determining the conditions related to water superheating and vapor formation, and toward defining more clearly the contribution of each to heat transfer.

b. Reaction Force Column Study of Vapor Void Formation

A series of experiments were performed to measure the forces generated during heat transfer from hot spheres falling through a column of water, thereby simulating the ejection of hot reactor fuel particles into the water coolant. The apparatus used is shown in Fig. IV-4. Upon production of steam bubbles within the liquid, a momentum change is induced in the water column, the magnitude of which can be dynamically measured by a quartz pressure transducer. In addition to

measurements of the dynamics of void formation, high-speed motion pictures of falling spheres were obtained to establish the nature of the boiling regime (film, transition, or nucleate).

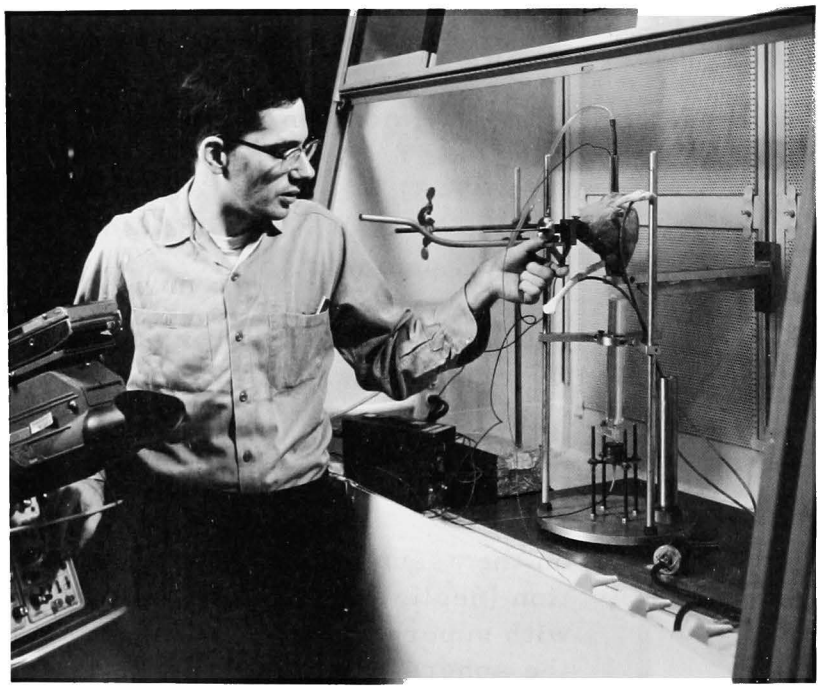

Fig. IV-4

Apparatus to Measure Forces Generated when High-Temperature Fuel Materials Contact Water.

As shown in Fig. IV-5, the magnitude of the forces generated by void formation is markedly affected by both sphere temperature and water temperature. With water near the boiling point, forces up to only 0.2 lb were recorded, while at lower water temperatures much larger forces were generated. In all cases, the maximum force was observed with sphere temperatures less than 500°C; at higher temperatures essentially no disturbances

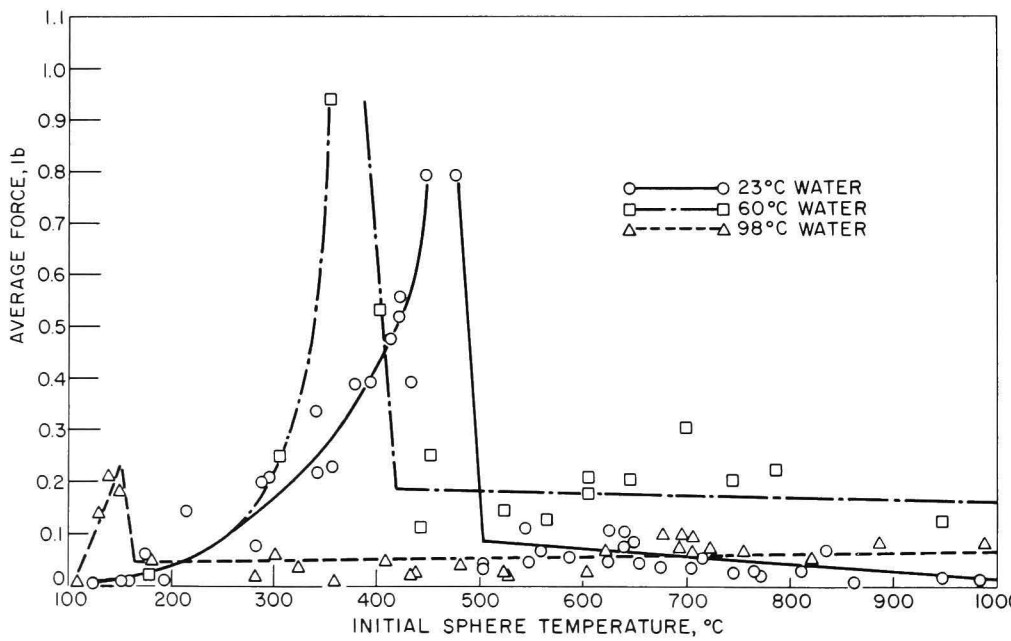

Fig. IV-5. Forces Generated by 1/4-in. dia. Heated Platinum Sphere Falling through Water.

were recorded. Photographs of heated spheres falling through water indicated that the mode of water vapor formation varied with sphere temperature (Fig. IV-6). With a sphere at 500°C, the vapor is formed irregularly on the sphere surface and appears as discrete bubbles with short lifetimes. This behavior is characteristic of the transition from film to nucleate boiling and corresponds to rather large measured forces. An extended wake, characteristic of film boiling, is produced by spheres at 820°C falling through 95°C water. During film boiling the vapor occupies a constant volume; the rate of evaporation near the sphere surface equals the rate of condensation in the wake, and no disturbances are generated in the water column.

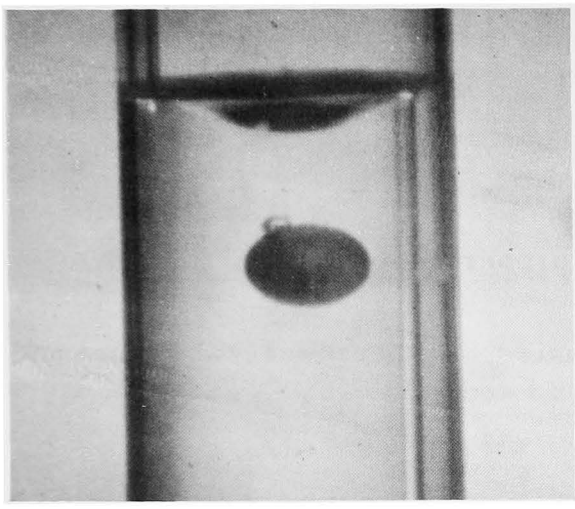

a. Sphere temperature = 25°C
Water temperature = 25°C

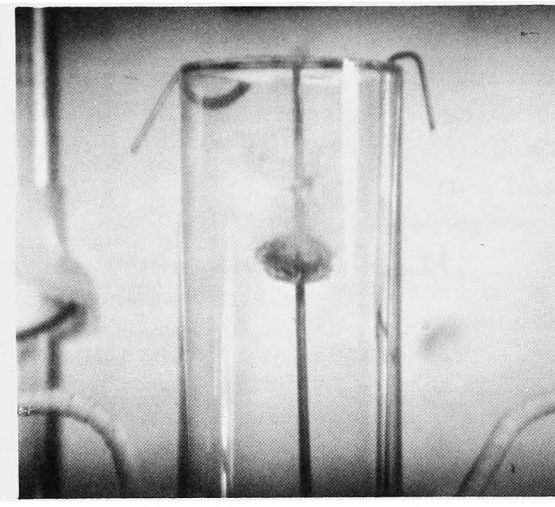

b. Sphere temperature = 500°C
Water temperature = 25°C

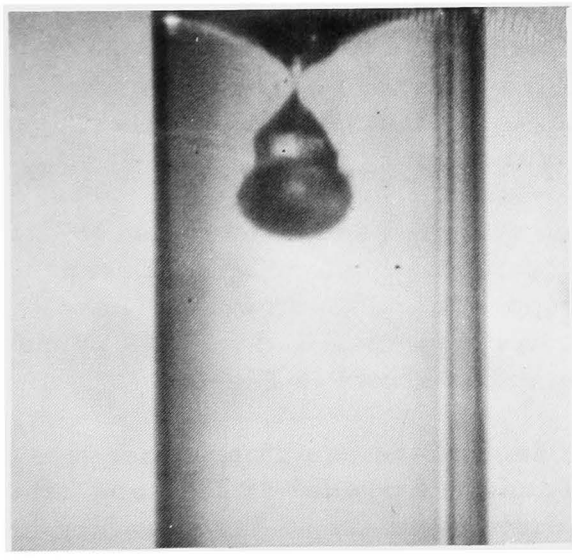

c. Sphere temperature = 820°C
Water temperature = 25°C

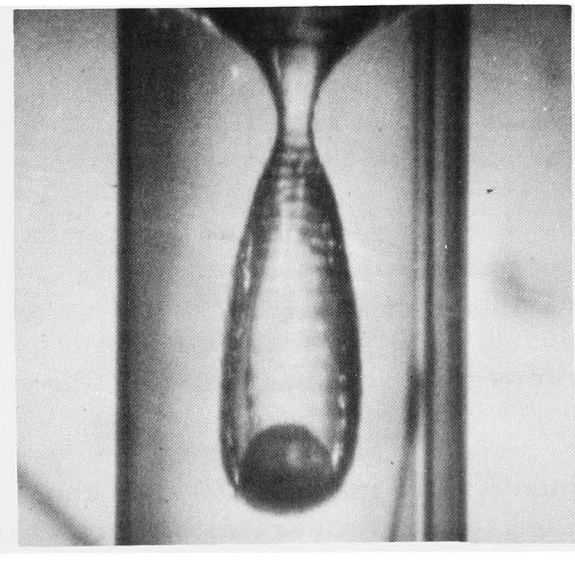

d. Sphere temperature = 820°C
Water temperature = 95°C

Fig. IV-6. One-Quarter-in. dia. Platinum Spheres Falling through Water. (Sphere velocity = 3.40 ft/sec.)

A simplified calculational model has also been developed that should allow correlation of the measured forces with void (bubble) growth.

B. Fast Reactor Safety Studies

In sodium-cooled fast reactors, coolant failure or a nuclear excursion could cause fuel failure, fuel melting, and dispersion of hot reactor material in the sodium. This dispersion of fuel materials can cause explosive pressure rises due to vapor formation resulting from extremely fast energy transfer from the fuel materials to the sodium coolant. A breach in the primary system could allow the sodium coolant to come into contact with air in the containment vessel, resulting in an exothermic chemical reaction. To assess these and other potential problem areas, the following studies relating to the safety of fast reactors are being carried out:

1) high temperature physical properties of fast reactor materials (liquid and vapor state),
2) pressure generation associated with the dispersal of fuel and cladding materials into liquid sodium,
3) reaction of sodium sprays in air, and
4) fuel migration and segregation in mixed uranium-plutonium compounds.

1. High Temperature Physical Properties

Current experimental work on high temperature physical properties of fast reactor materials has been directed toward the measurement of the heat content of uranium dioxide. It is intended to find the heat of fusion and the specific heat of the liquid, important quantities in fast reactor safety calculations, from these measurements.

A drop calorimeter has been designed and constructed to carry out heat content measurements to temperatures above 3200°C. Encapsulated samples are heated by induction and dropped into a commercial (Parr, series 1230) adiabatic calorimeter that has been modified for this purpose. An overall schematic view of the equipment is shown in Fig. IV-7.

In order to test the performance of the equipment, measurements were made of the heat content of tungsten powder at 2550 and 2850°C. Tungsten containers with 30-mil thick walls were used. Temperature measurements were made using a tube (with a length-to-diameter ratio of about ten) extending into the container. The results shown below were found by subtracting the heat content of an empty container from that of a filled one.

Temperature (°K)	$H_T - H_O$ °K (cal/mole), Experimental	$H_T - H_O$ °K (cal/mole), Literature[3]	Difference (%)
2825	19,778	19,475	1.6
3125	22,504	22,125	1.7

The agreement of these results with the literature values[3] is considered satisfactory.

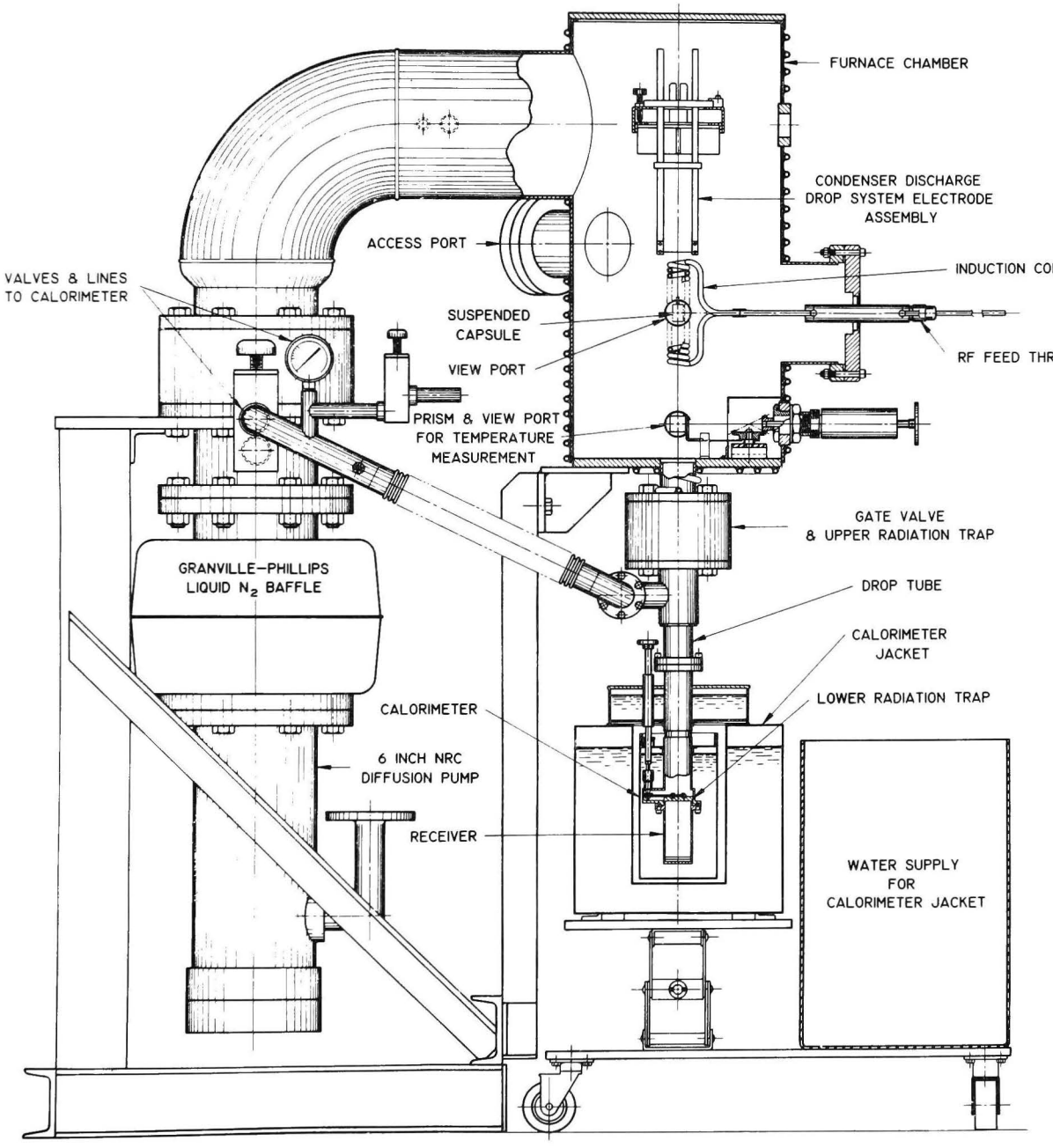

Fig. IV-7. High Temperature Calorimetric System for Measurement of the Heat Capacity of Liquid Uranium Dioxide.

[3] V. A. Kirillin, A. E. Sheindlin, V. Ya Chekhovskoi, V. A. Petrov, Russ. J. Phys. Chem. 37, 1212 (1963).

Heat content measurements have been initiated with uranium dioxide. The possible use of double-walled tungsten capsules, to reduce heat losses during the higher temperature drops, is being explored.

2. Pressure Generation due to Particle Coolant Energy Transfer

a. Heat Transfer from a Hot Sphere Moving in Liquid Sodium

Experimental studies of heat transfer between small metal spheres and sodium have continued using the swinging-arm method described in ANL-7350, p. 71. Forced convection heat transfer data have been obtained for tantalum spheres at temperatures both above and below the boiling point of sodium. Several methods for correlating the heat transfer data for both conditions were investigated and a correlation involving two empirical equations (depending on whether the sphere temperature was above or below the boiling point of sodium) was found satisfactory. Although a generalized correlation to relate all data by a single expression has not yet been achieved, the acquisition of additional experimental data over a wider range of variables is expected to allow the formulation of such a general correlation for forced convection heat transfer.

b. In-Pile Study of Violent Fuel Failure in Sodium

In an effort to provide information necessary for the evaluation of potential fuel failure problems encountered in the operation of sodium-cooled fast reactors, an experimental autoclave has been designed and constructed that will allow measurement of pressures generated within a sodium environment during fuel meltdown at high energy inputs. The autoclave assembly consists principally of a fuel-cluster container and a piston coupled to a linear-motion transducer to measure the rate of expulsion of sodium from the fuel-cluster container during an energy transient. Variable-impedance transducers will measure the pressure generated during the transient.

A calibration test has been made in TREAT, without sodium in the autoclave, to correlate reactor-integrated power with fission energy generated in the fuel rods. Minor modifications of some of the components of the autoclave are now being made in preparation for the sodium expulsion experiments.

3. Reaction of Violently Sprayed Sodium with Air

An experimental study is under way to investigate the reaction of liquid sodium aerosol with air. Of particular interest in this investigation is the accumulation of data on the rate of pressure generation and peak pressures and temperatures achieved in the oxidation reaction. The apparatus used in this work (Fig. IV-8) consists of a reaction chamber of known

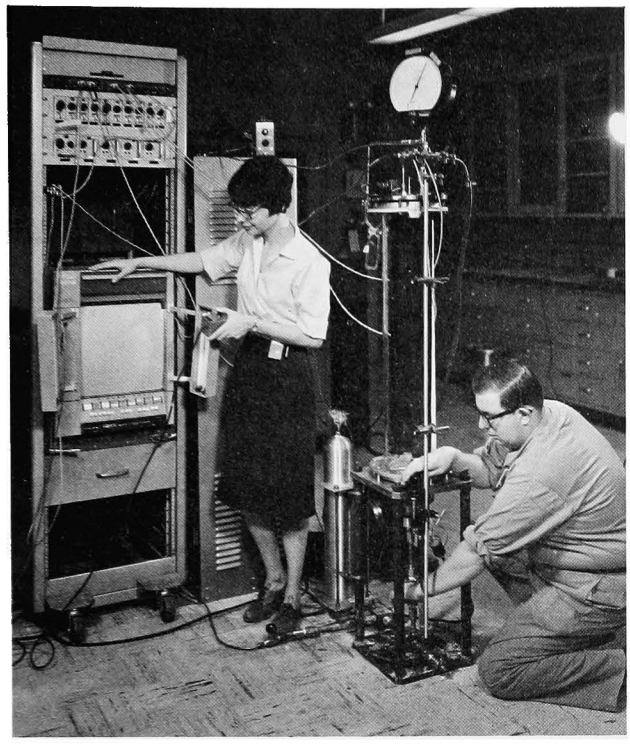

Fig. IV-8. Apparatus for the Study of the Reaction of Sprayed Sodium with Air.

volume and a pneumatically operated piston spray injector capable of discharging 11 g of molten sodium into the chamber.

The particle-size distribution of the sodium spray, produced by injecting the sodium with a piston under pressure of 1000 psig, has been determined by spraying sodium into a refrigerated Dewar and sieving the solid particles. The results indicate a rather uniform particle-size distribution over the range 0 to 840 μ. Visual observation of particles larger than 840 μ revealed that they were mostly agglomerates of smaller particles.

High-speed motion pictures of molten sodium at 400°C injected vertically into air indicated that the oxidation reaction proceeds vigorously, and, as the spray impinges upon a baffle at the top of the chamber, the intensity of the reaction increases owing to dispersion and diminution of the particles.

Temperature and pressure measurements from a typical burning test are shown in Fig. IV-9. Further experiments are being performed to establish the effects of changes in the piston driving pressure and the oxygen concentration on the pressure and temperature generated in the reaction.

On the basis of a mathematical model (proposed by Mouradian and Baker),[4] an attempt is being made to predict the rate of pressure rise in a closed volume due to the sodium-air reaction. If it is assumed that the sodium burning rate is controlled by diffusion of oxygen to the combustion zone, the usual heat transfer and diffusion correlations can be used to determine steady-state reaction rates for single spherical particles of sodium at any given set of conditions. A quasi-steady-state approach and averaging technique can then be used to correlate the reaction rates of individual particles with the burning rate of the spray and the rate of pressure rise within the reaction chamber.

[4] E. M. Mouradian, L. Baker, Jr., "Burning Temperatures of Uranium and Zirconium in Air," Nucl. Sci. Eng. 15, 288 (1963).

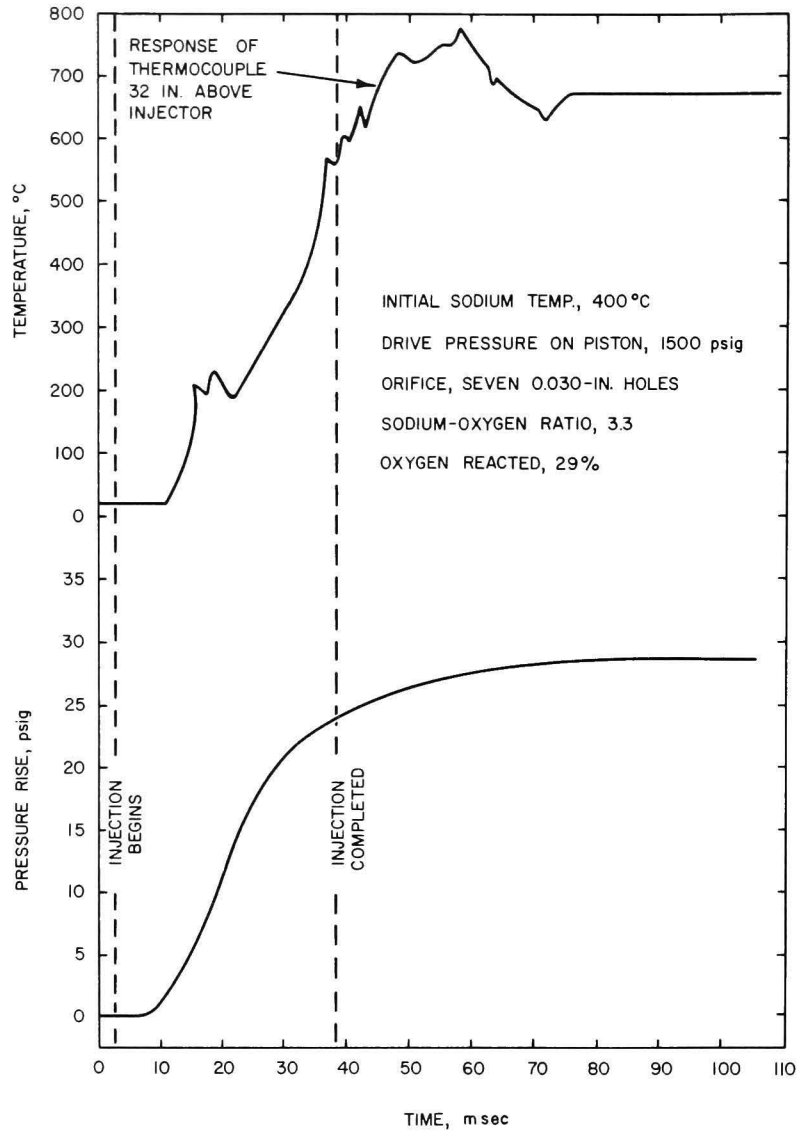

Fig. IV-9. Temperature and Pressure Traces from Typical Sodium Injection Experiment into Dry Air.

4. Migration of Fuel Components under a Thermal Gradient

Migration and segregation of fissile and fertile material within a fast reactor fuel during its operational lifetime could have significant effects on the operational safety of the fuel. Redistribution of plutonium in $(U,Pu)O_2$ fuels might change the chemical and physical properties of the affected regions enough to vary the neutronics of the system, effect fuel-cladding compatibility, and change the resultant fission product distribution. Investigation of the migration of plutonium and fission products in a thermal gradient is under way for mixed-oxide fuels. These experiments are being performed to evaluate the extent of migration that can occur and to help in understanding the mechanisms involved in the migration processes.

An apparatus to produce an axial thermal gradient of about 1000°C/cm in a fuel pellet has been developed and tested. Figure IV-10 shows a schematic drawing of the furnace in which the pellet's top surface is maintained at about 2000°C by thermal radiation from an electrically heated tungsten foil. The apparatus utilizes ion and sublimation pumps and is virtually vibration-free. Figure IV-11 shows the complete apparatus in position within a plutonium glovebox.

Initial experiments with mixed-oxide fuels are being performed on cylindrical pellets 1/2 in. high by 1/2 in. in diameter. These pellets are nominally 20 m/o PuO_2 and were prepared from coprecipitated PuO_2 and UO_2. Photomicrographs indicate the pellets are of single phase with relatively fine grain size.

The experiments are performed by heating the sample in the apparatus for the desired time period. The specimens are then longitudinally sectioned and examined ceramographically; α-track autoradiographs are made and the specimens analyzed for uranium and plutonium by means of an electron probe microanalyzer.

Some of the experiments were performed with the specimens contained in an inverted tungsten crucible that served as a barrier to loss of material by evaporation. Because of heat conduction down the metal walls of the crucible, somewhat smaller gradients were obtained in these experiments.

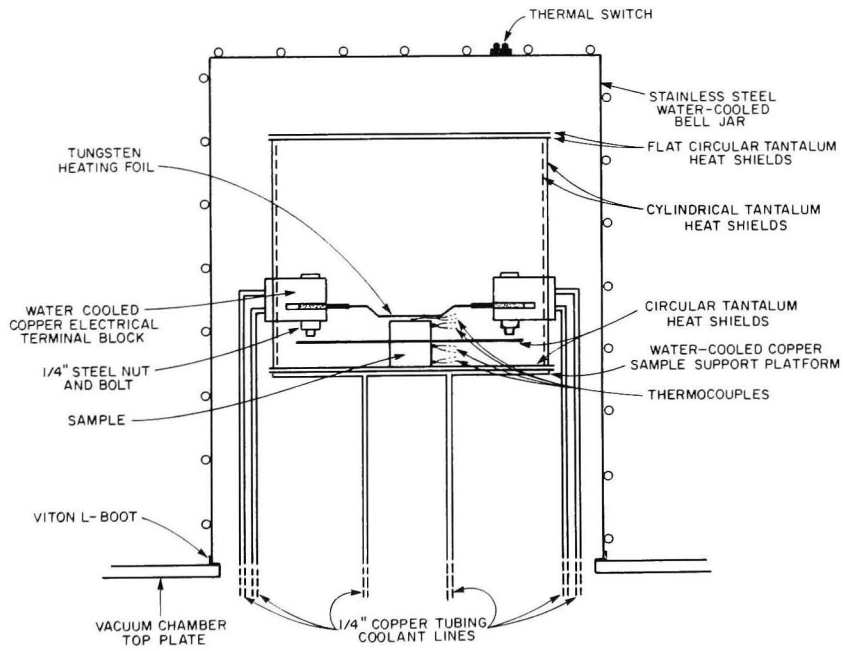

Fig. IV-10. Schematic Drawing of Thermal Gradient Furnace in Position inside the Vacuum Chamber.

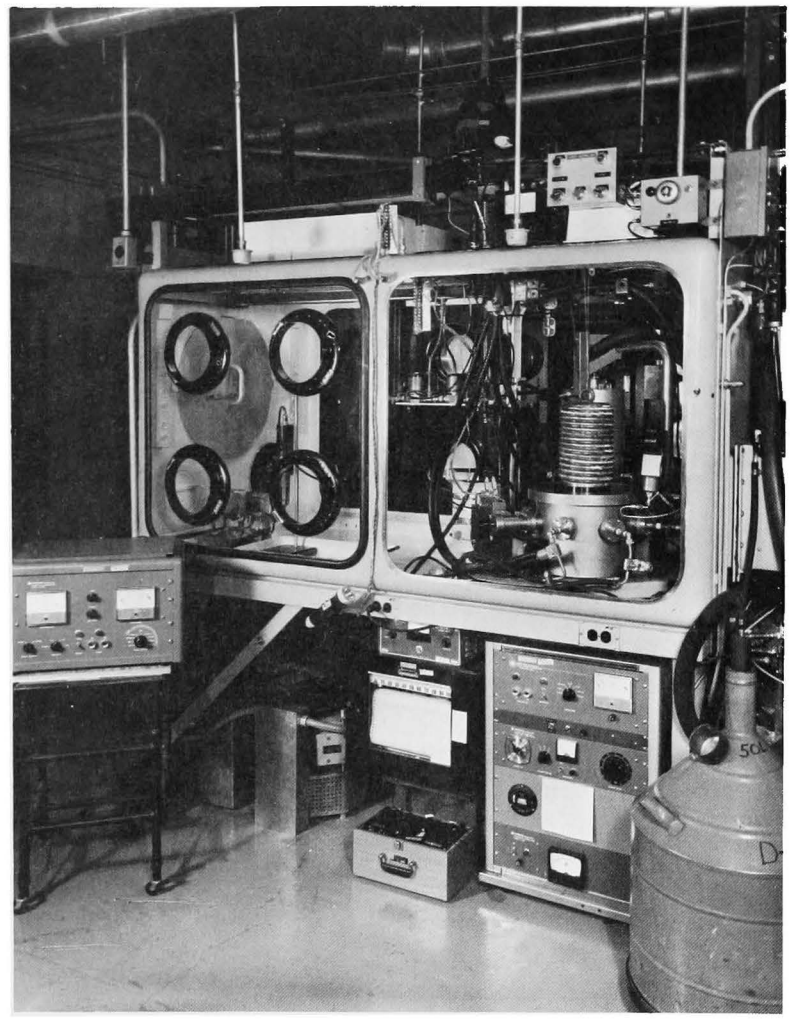

Fig. IV-11. Thermal Gradient Apparatus in Position in Glovebox with Power Supplies and Controls Located outside the Glovebox.

Table IV-1 gives the experimental conditions under which the various samples were heated. Figure IV-12 presents the data for plutonium distribution along the axis of the pellets. There appears to have been no

TABLE IV-1. Experimental Conditions for Thermal Gradient Experiments Using $(U_{0.8}Pu_{0.2})O_2$ Pellets

Run	Vapor Barrier[a]	Time at Temp. (hr)	Top Temperature (°C)	Bottom Temperature (°C)
P-1	Yes	100	1980	1280
P-2	No	100	2070	975
P-3	Yes	509	1980	1250
P-4	No	504	2040	960

[a]Inverted tungsten crucible.

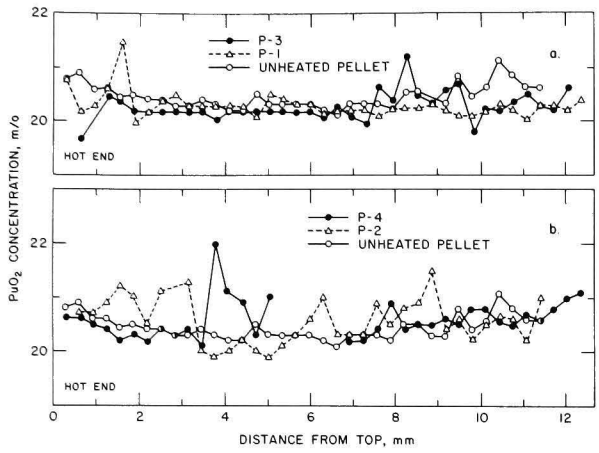

Fig. IV-12

PuO_2 Distribution in $(U_{0.8}Pu_{0.2})O_2$ Pellets Heated in a Thermal Gradient; (a) with vapor barrier, (b) without vapor barrier.

significant migration in the case of the samples heated in the inverted crucibles. Some migration toward the hotter end is evidenced in the pellets heated without an evaporation barrier. In general, however, these changes are not large; the apparent migration may well be a result of stoichiometry changes due to loss of oxygen from the hottest regions.

Longer anneals and higher temperatures are planned for future experiments. It is hoped to systematically investigate the effects of stoichiometry and pellet density on migration of plutonium in oxide fuels subjected to a thermal gradient.

V. ENERGY CONVERSION

A. Research on High-Specific-Energy, High-Specific-Power Secondary Cells

1. Emf Studies of the Lithium-Tellurium System

One of the chief requirements of our rapidly developing technology is a versatile array of electrical power sources, energy converters, and energy-storage devices. Research on new high-specific-power, high-specific-energy cells and batteries is a part of the Chemical Engineering Division's energy conversion program. This program is concerned with the development of systems in which thermal energy can be converted into electrical energy by means of an electrochemical reaction. As a guide in selecting the most promising systems for engineering development, electromotive force (emf) or voltage studies are being carried out on candidate systems. The emf studies of the lithium-tellurium system have identified it as particularly promising for use in secondary (electrically rechargeable) cells.

Tellurium is known to have a high energy of interaction with lithium. The strength of this interaction between the elements is qualitatively related to the high melting point of Li_2Te, the most stable compound in the system. Quantitatively, the high energy of interaction is related to the large potential (1.7-1.8 volt) for the concentration cell:

$$Li(\ell) \,//\, Li^+ (\ell) \,//\, Li \text{ in } Te(\ell)$$

A previous study[1] has indicated that the free energy of formation of $Li_2Te(s)$ is -77.9 kcal/mole at 798°K.

Measurements of emf were made for cells in which the liquid lithium anode and the liquid lithium-tellurium alloy cathode were contained in separate porous BeO crucibles, both of which were immersed in a common bath of electrolyte. The electrolyte consisted of the molten eutectic mixture of LiF-LiCl-LiI. The cathode alloy was formed *in situ* by placing a weighed quantity of tellurium in the porous BeO cup, adding a layer of molten electrolyte, and floating a weighed quantity of lithium on the electrolyte. A tungsten rod was lowered into the cup so that a shorted electrochemical cell was formed, and all of the lithium was thereby electrochemically transferred into the tellurium. The alloy was thus formed without the danger of a violent reaction, as is often encountered when liquid lithium is directly added to liquid tellurium.

[1]This study was alluded to in ANL-7175, p. 185 and reported in more detail by M. S. Foster, and C. C. Liu in J. Phys. Chem. 70, 950 (1966).

The open-circuit voltage of the cell was measured potentiometrically at various temperatures between 660 and 840°K, with cathode compositions of 0.174, 0.263, 0.303, and 0.332 atom fraction Li in tellurium. The temperature changes were made in random order to avoid possible systematic errors. Under conditions corresponding to the formation of a solid phase in the cathode alloy, difficulties with supercooling were overcome by vibrating the cathode alloy.

The emf's as a function of temperature for cells with the indicated cathode alloy compositions are shown in Fig. V-1. Two solids evidently precipitate at the lower temperatures as indicated by the abrupt changes in the slopes of the curves. For the cell with a cathode alloy containing 0.174 atom fraction Li, the precipitation starts at about 728°K. The solid precipitating is $LiTe_3$, which was identified by X-ray diffraction analysis. At higher concentrations of lithium in the cathode alloy, e.g., 0.332 atom fraction, precipitation of Li_2Te begins when the temperature is lowered to about 725°K.

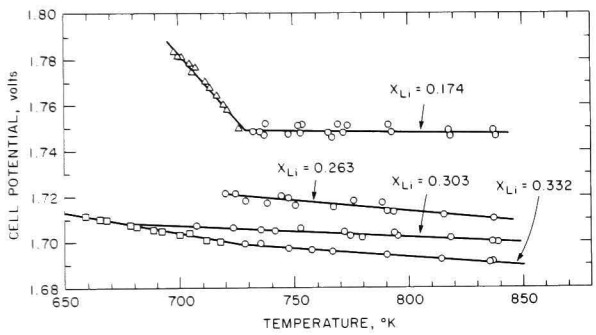

Fig. V-1. Temperature Characteristics of Li/Te Cell Potential.

The activity coefficient of lithium, γ_{Li}, was calculated from the cell potentials using the relationship

$$-FE = RT \ln X_{Li} + RT \ln \gamma_{Li}$$

where F is the value of the faraday, E the cell potential, R the universal gas constant, T the absolute temperature, and X_{Li} the atom fraction of lithium in the cathode alloy. The activity coefficient of lithium as a function of composition is shown in Fig. V-2 for three temperatures. Further treatment of the data should yield the standard Gibbs free energy of formation of $LiTe_3$ and Li_2Te as a function of temperature.

Fig. V-2

Activity Coefficient of Lithium in Tellurium.

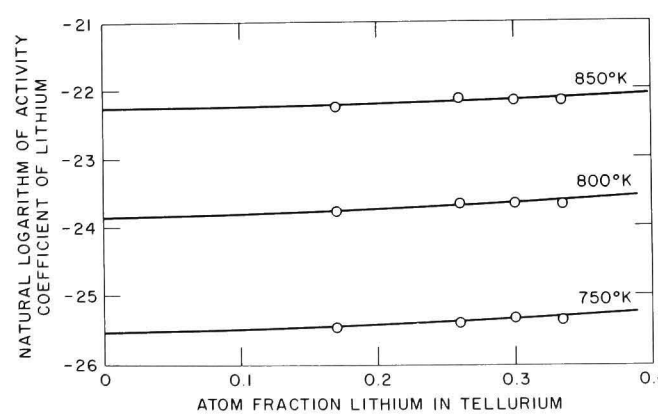

2. Secondary Cell Experiments

a. Secondary Cells with Liquid Electrolytes

The recent increase of emphasis on high-specific-energy (watt-hr/lb), high-specific-power (watt/lb) sources of electricity has resulted in a great deal of research and development work devoted to new secondary cells which show promise of power and energy characteristics superior to those of currently available cells.

Previous studies at Argonne on the sodium/bismuth cell (see ANL-7350, p. 81) indicated that when a suitable cathode material is used with a sodium anode and a fused alkali halide electrolyte, bimetallic galvanic cells can achieve the current density-voltage characteristics required for high-specific-energy, high-specific-power secondary cells. Subsequent studies have been concerned with the development of secondary cells having higher cell voltages and lower cell weights.

The voltage of a bimetallic cell can be made greater than that of the sodium/bismuth cell by selecting a more electropositive anode material such as lithium, and a more electronegative cathode material such as tellurium. In addition, the equivalent weights of lithium and tellurium are much lower than those of sodium and bismuth, yielding a cell of higher energy density. The emf-composition characteristics for the lithium/tellurium cell, reported in section VA1 above, indicate that the open-circuit terminal voltages are relatively insensitive to cathode alloy composition, and that values of 1.7 to 1.8 volts are to be expected.

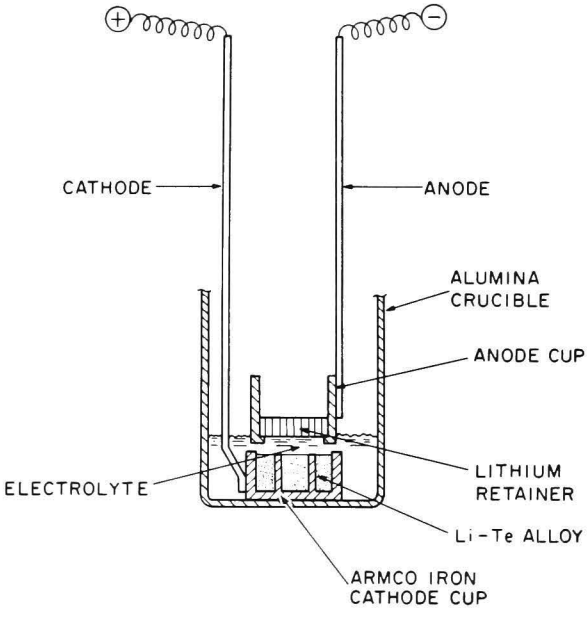

Fig. V-3. Lithium/Tellurium Cell.

A simple experimental lithium/tellurium secondary cell was constructed as shown schematically in Fig. V-3. The Armco iron cathode cup provided an active cathode area of 10 cm^2. An annular fin was included in the cathode cup to aid in current collection. Two stainless steel anode current collectors of different geometric area, which also served as lithium retainers, were used in these experiments: a) 3.9 cm^2 and b) 10 cm^2. The 10-cm^2 anode cell was somewhat modified in design to reduce internal resistance. The LiF-LiCl-LiI eutectic (m.p. = 340.9°C) was utilized as the electrolyte.

The amounts of lithium and tellurium in the cell were varied, but the maximum ratio of lithium to tellurium corresponded to 30 a/o Li in tellurium in the cathode alloy at complete discharge. The maximum capacity of the cell was 9.55 amp-hr. The melting point of tellurium (449.80°C) determined the minimum operating temperature of the cell; the range of temperatures most frequently used was 467 to 500°C. All of the experiments were performed in a high-purity helium atmosphere.

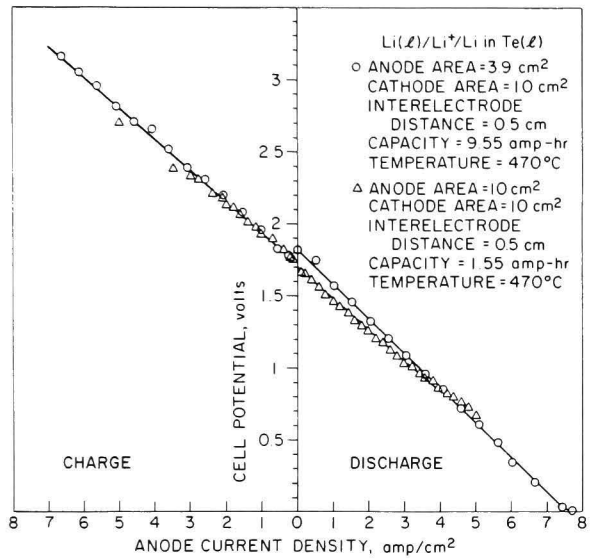

Fig. V-4. Steady-State Voltage-Current Density Curves for Lithium/Tellurium Cell.

Typical "steady-state" current density-voltage curves for lithium/tellurium cells operating at 470°C are shown in Fig. V-4. It it noteworthy that current densities in excess of 7 amp/cm^2 were obtained on discharge, and because similar current densities can be accommodated on charge, practical cells based on this system could be charged in 15 minutes or less for a cell capacity of 1.75 amp-hr/cm^2. Similar results were obtained with both anodes (3.9 cm^2 and 10 cm^2), and hence the behavior at the cathode was not significantly different in the two runs. Since both the charge and discharge curves are straight lines, it is expected that only negligible concentration and activation overvoltages were present; the largest losses were resistive in nature. All of the data in Fig. V-4 correspond to "steady-state" curves at the cathode alloy composition of 20 a/o lithium in tellurium.

A typical short-term discharge curve for the 10-cm^2 anode cell is shown in Fig. V-5. This cell was charged between readings and the data were taken within several seconds after discharge was initiated. Because of this procedure, the lithium content of the cathode was kept low--about 5 a/o Li in tellurium. Note that a current density of 7 amp/cm^2 was obtained at 0.7 volt (resistance losses included), corresponding to a power density of 4.9 watt/cm^2. The maximum current density observed was 12.7 amp/cm^2. The maximum temperature rise observed during the high current density discharges was 30°C.

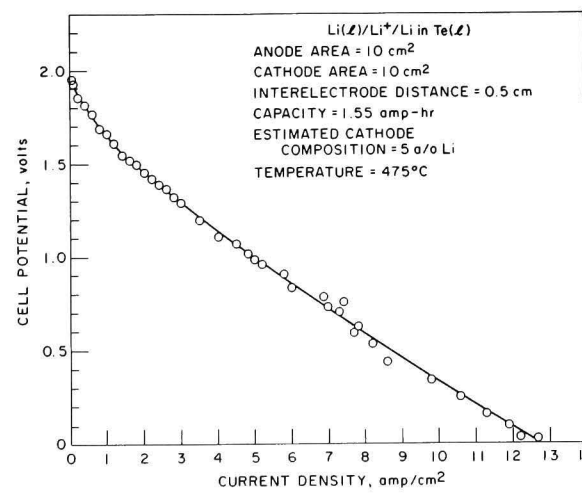

Fig. V-5. Short-Time Voltage-Current Density Curve for Lithium/Tellurium Cell.

The voltage-capacity curves for the constant-current charge and discharge of the cell with the 10-cm^2 anode at 480°C are shown in Fig. V-6. The curve marked "0 amp" shows the open-circuit voltage as a function of time (upper abscissa), while the other curves show the terminal voltage of the cell as a function of charge accepted or delivered at various constant charge and discharge rates. The plateau voltages of Fig. V-6 correspond to some of the points on the curve shown in Fig. V-4 while the initial voltages at the ordinate of Fig. V-6 correspond approximately to the voltages shown in Fig. V-5.

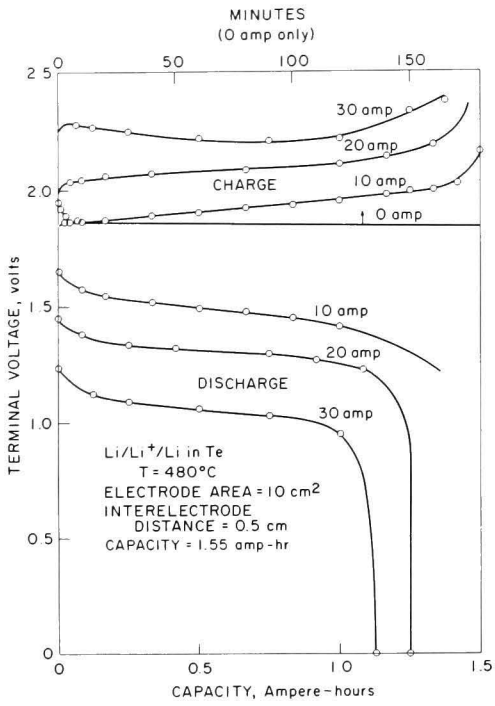

Fig. V-6. Constants-Current Voltage-Capacity Curves for Lithium/Tellurium Cell).

The constancy of the voltages in Fig. V-6 is a unique characteristic of the lithium/tellurium cell, and was expected on the basis of the work of Foster and Liu.[1] This behavior contrasts with that of the sodium/bismuth cell, in which a more distinct decrease of cell voltage with extent of discharge was observed, particularly at high current densities.

When selenium is used in place of tellurium as the cathode material, the cell has a lower weight because of the lower atomic weight of selenium (78.96 vs. 127.6 for tellurium) and has a lower operating temperature because of the lower melting point of selenium (217 vs. 450°C for tellurium). Experiments were performed with lithium/selenium cells to determine whether or not these advantages could be realized while retaining high cell performance.

An experimental lithium/selenium cell, similar in design to the lithium/tellurium cell described above was constructed and operated in the temperature range 350 to 400°C. The cell was tested using 3.9-cm^2 and 10-cm^2 anodes and 10-cm^2 cathodes of various configurations. The capacity of the cell was determined by the amount of lithium in the anode, and varied from 4 amp-hr to 8.9 amp-hr; selenium was always present in excess. The maximum ratio of lithium to selenium corresponded to 60 a/o Li in selenium at complete discharge. Because of the relatively high resistivity of selenium, it was expected that the configuration of the cathode current collector would have a significant effect on the internal resistance of the cell, and hence on its performance. To maximize cell performance, a number of cathode current collectors were tested. Various forms of iron were used to facilitate current collection.

It was found that the cell performance was directly related to the current-collector configuration of both electrodes, the selenium electrode current collector being the more critical. Figure V-7 shows voltage-current density curves for several cells which were identical except for the cathode current collector. The lowest performance (1.0 amp/cm^2 at 1 volt) was obtained from a cell which had a simple iron cup with a single annular fin as the cathode current collector. The addition of 60 w/o iron filings to the selenium improved the performance somewhat (1.8 amp/cm^2 at 1 volt), with further improvements being achieved by the addition of iron turnings (2.3 amp/cm^2 at 1 volt). The best performance was obtained by using a stack of five expanded iron meshes welded to the cathode cup (6.2 amp/cm^2 at 1 volt). The optimum current-collector designs were found to be a spiral (of type 18-8 stainless steel) for the lithium electrode and the expanded metal meshes (pure iron) for the selenium electrode.

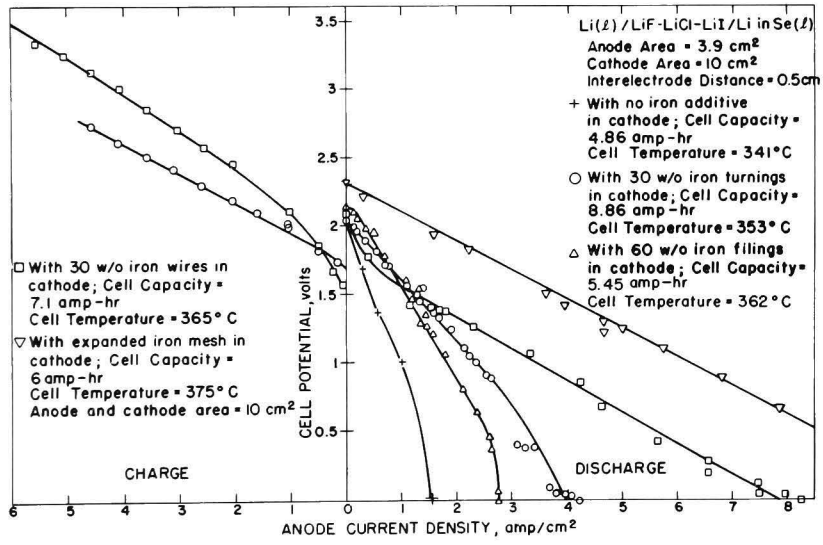

Fig. V-7. "Steady-State" Voltage-Current Density Curves for Lithium/Selenium Cells with Various Cathode Current Collectors.

The performance of the cell with the iron-mesh cathode current collector on discharge was measured in two ways: 1) short-term performance measured from the fully charged condition for each data point, corresponding to about 5 a/o Li in selenium and 2) "steady-state" performance measured on the voltage plateau, corresponding to a cathode composition of about 25 a/o Li in selenium. These performance curves are shown in Fig. V-8. The behavior on charging is representative of that of a fully discharged cell, hence the steeper slope of the voltage-current density curves for charging.

The voltage-current density curves for discharge in Fig. V-8 show that a potential of 2.3 to 2.4 volts is available at open circuit, and short-circuit densities of 11 to 13 amp/cm^2 can be achieved. The

maximum power density for short-term operation is 7.8 watts/cm^2 (at 1.2 volts) and at "steady state" is 6.3 watts/cm^2 (at 1.1 volts). Measurements of the overvoltage by current interruption techniques indicate that, in the range 1 to 4 amp/cm^2, the overvoltage was 90% resistive (mostly due to the electrolyte), the remainder being associated with the diffusion of lithium into the cathode alloy.

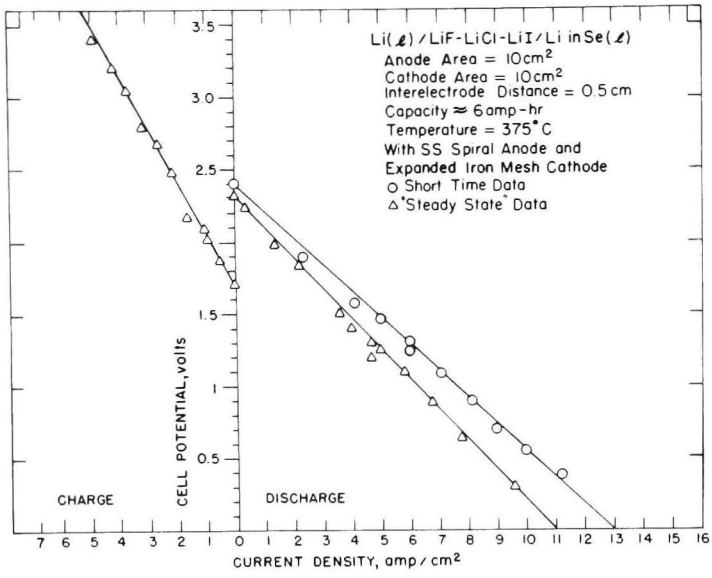

Fig. V-8

Voltage-Current Curves for a Lithium/Selenium Cell with an Iron Mesh Cathode Current Collector.

Constant-current charge and discharge voltage-capacity curves for the 10-cm^2, 6.4-amp-hr cell (1.66 g Li) with the iron-mesh cathode current collector (3.5 g Fe, 12.8 g Se) are shown in Fig. V-9. The cathode alloy composition at complete discharge was 59.6 a/o Li in selenium, corresponding to the presence of solid Li_2Se during the latter part of the discharge curve. The accumulation of solid Li_2Se caused the second plateau in the discharge curves (3 to 5 amp-hr). The first plateau (0.5 to 2 amp-hr) corresponds to an all-liquid cathode, in which the lithium probably forms soluble Li_2Se. The voltage differences between the various charge and discharge curves are primarily due to resistive losses in the cell, largely electrolytic in nature. It can be seen from the capacity curves that this cell can be completely charged (6 amp-hr) in less than 15 min, an important feature. The open-circuit voltage is quite stable, and thus indicates a low rate of self-discharge.

b. Secondary Cells with Immobilized Fused-Salt Electrolytes

In connection with the many possible applications of galvanic cells with fused-salt electrolytes, the use of an electrolyte in the form of an immobile "semi-solid" paste would have many advantages over the use of a liquid electrolyte. One of these advantages, the versatility in cell design, is such an important consideration that the development of an immobilized electrolyte is considered essential to both the regenerative

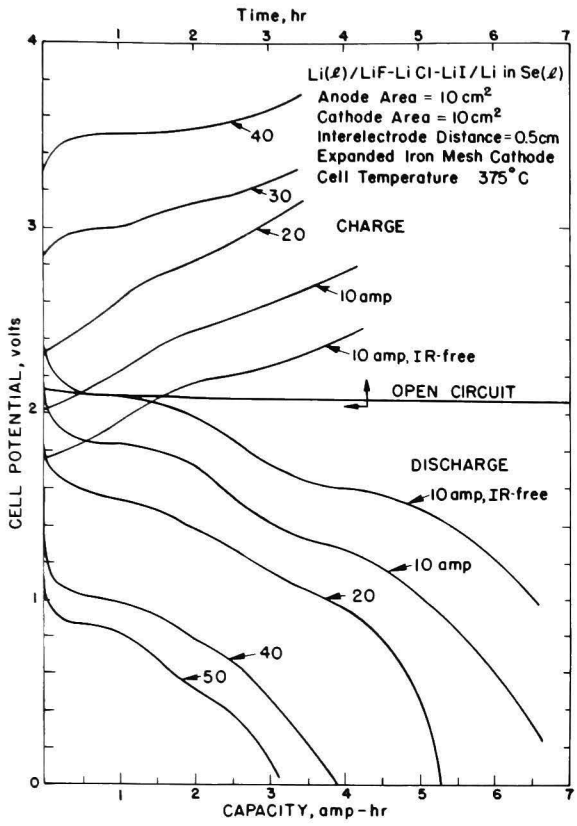

Fig. V-9. Constant-Current Voltage-Capacity Curves for Lithium/Selenium Cell.

cell and secondary cell programs being pursued in this Division. Consequently, secondary cells having liquid lithium anodes, liquid bismuth or tellurium cathodes, and fused lithium-halide electrolytes immobilized as a rigid paste have been designed and tested.

The lithium/tellurium cell, made of pure iron, had current collectors consisting of sheets of sintered porous stainless steel in the anode compartment, and a network of pure iron wires in the cathode compartment. Figure V-10 shows this cell with meshes in the cathode compartment rather than the iron-wire network. The exposed electrolyte area was 3.25 cm^2; the electrolyte thickness was 0.32 cm. The cell compartments were loaded with 0.75 g of lithium and 5.45 g of tellurium, corresponding to 71.6 a/o Li in tellurium at complete discharge.

The paste electrolyte was based on the ternary LiF-LiCl-LiI eutectic which melts at 340.9°C and has a specific conductance of 2.3 ohm^{-1} cm^{-1} at 475°C. The electrolyte components were melted together to form the eutectic, the electrolyte was solidified, pulverized to -300 mesh size, and mixed (50 w/o) with an inert filler material. The electrolyte-filler powder mixture was then molded into discs. All operations except for the hot-pressing were carried out in a pure helium atmosphere. Discs 2.5 cm in dia. were pressed at room temperature and then sintered at 400°C, eliminating all exposure to air.

The paste electrolyte has a continuous phase of fused lithium halide eutectic at the cell operating temperature. The relative amounts of finely divided inert filler and lithium halide are chosen such that the electrolyte fills the interstitial spaces among the very small filler particles, and holds the paste firmly by means of its high surface tension, low contact angle with the filler, and the small pore size of the compact. Similar paste electrolytes have been used with success in molten-carbonate fuel cells.

The voltage-current density curves of the lithium/tellurium cell with a paste electrolyte operating at 475°C are shown in Fig. V-11.

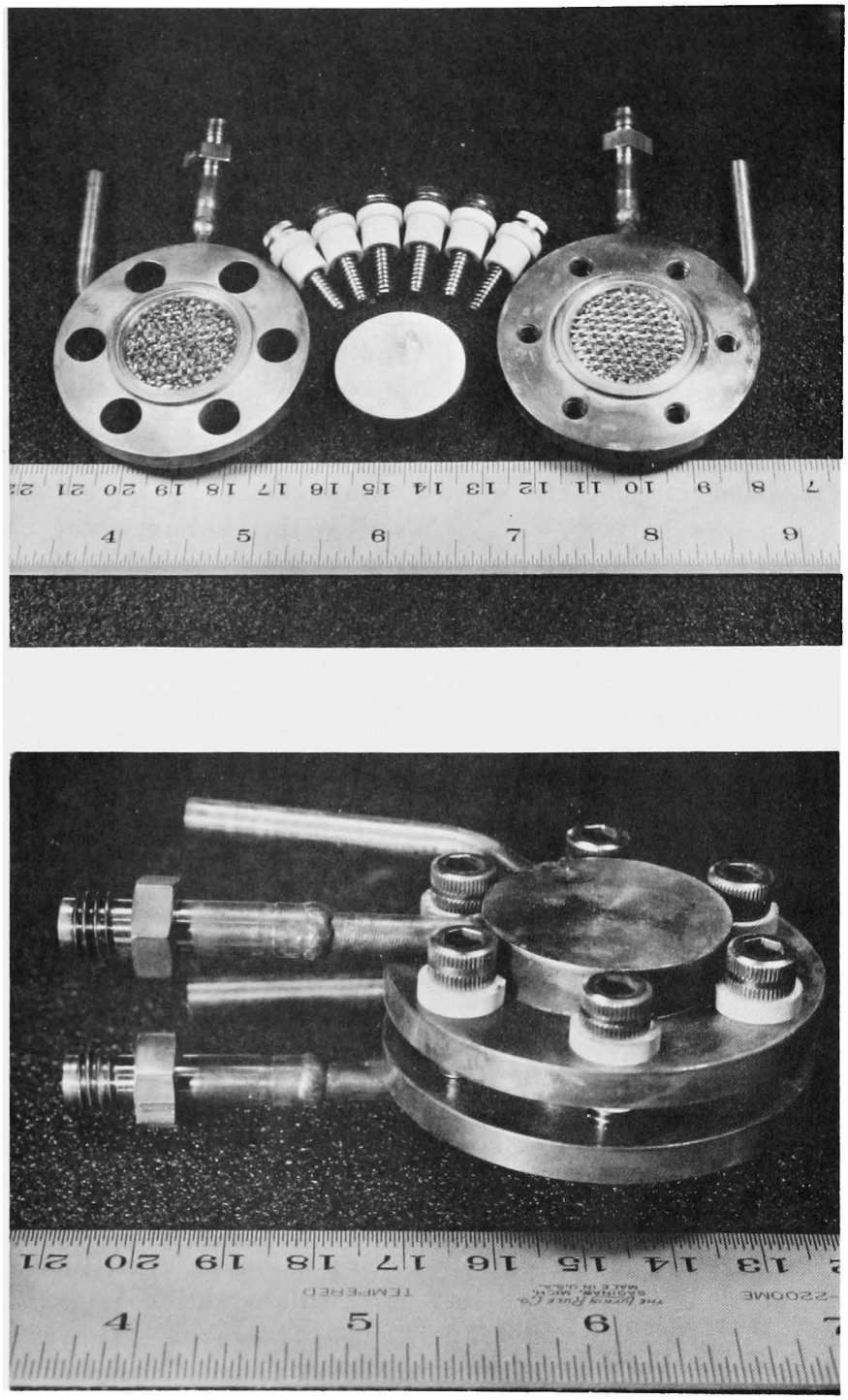

Fig. V-10. Lithium/Tellurium Cell Utilizing Paste Electrolyte.

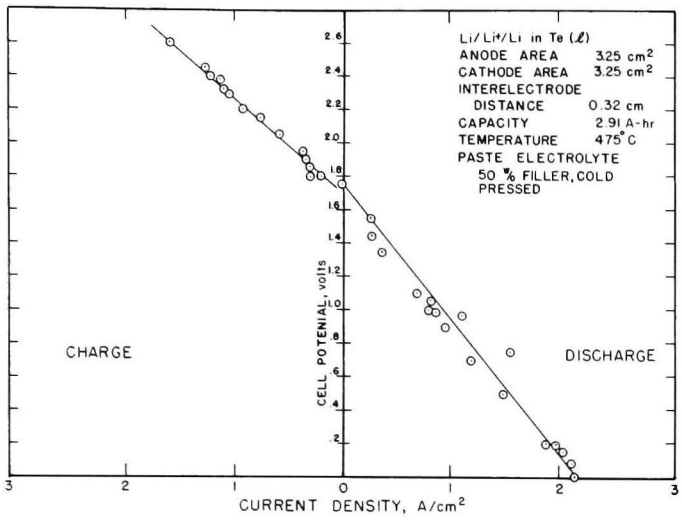

Fig. V-11. Voltage-Current Density Curves for a Lithium/Tellurium Cell with Paste Electrolyte.

As expected, the open circuit voltage was 1.7 to 1.8 volts, and the voltage-current density curves were straight lines, indicating the absence of any significant concentration or activation overvoltages. The short-circuit current density was 2.2 amp/cm^2, and the maximum power density was 1 watt/cm^2 at 0.9 volt.

The internal resistance of the lithium/tellurium cell during discharge was 0.24 ohm, compared to 0.065 ohm calculated from the electrolyte conductivity and a paste-to-pure electrolyte resistivity ratio of 2.

The lithium/tellurium cell, with a total capacity of 2.91 amp-hr, could be fully charged from complete discharge in less than half an hour corresponding to a capacity per unit area of 1 amp-hr/cm^2. This is a much higher charge rate than can be used with secondary cells having aqueous electrolytes or cells with nonaqueous organic solvent electrolytes.

Extensive investigations of constant-current charge and discharge characteristics, charge retention, and cycle life still remain to be done.

In summary, estimated performances of lithium/tellurium and lithium/selenium batteries with either liquid or paste lithium-halide eutectic electrolytes were derived from the experimental results and these are presented in Table V-1. The specific energy and specific power values are estimates based on a simple bipolar type of cell design. A detailed explanation of these calculations can be found elsewhere.[2] The cell temperature of the lithium/tellurium cell (470°C) is limited by the melting point of tellurium (450°C), while the temperature of the lithium/selenium cell (370°C) is limited by the melting point of the lithium halide eutectic (340.9°C). The specific power and specific energy of the lithium/selenium cell are about 60% higher than those of the lithium/tellurium cell because of the higher cell voltage and the lower equivalent weight of selenium. The specific power and energy values shown in Table V-1 compare with a specific power of 10 watt/lb and a specific energy of 10 watt-hr/lb for a

[2]H. Shimotake, E. J. Cairns, in "Advances in Energy Conversion Engineering," p. 951, Am. Soc. Mech. Engrs., New York (1967).

lead-acid battery.[3] These performance analyses and design calculations indicate the lithium/tellurium and lithium/selenium cells allow many new applications to be considered, including military and special vehicular applications.

TABLE V-1. Estimated Performances of Li/Te and Li/Se Batteries

Cell System	Electrolyte	Cell Temperature (°C)	Specific Energy[a] (watt-hr/lb)	Specific Power[a] (watt/lb)
Lithium/Tellurium	liquid	470	90	300
Lithium/Selenium	liquid	370	140	500
Lithium/Tellurium	paste	470	80	150
Lithium/Selenium	paste	370	110	300

[a]Specific energy and specific power are defined as follows:

$$\text{Specific energy} = \frac{\int E\ I\ dt}{Wc}$$

$$\text{Specific power} = \frac{E\ I}{Wc}$$

where E is a cell terminal voltage at a cell current I, Wc is the cell weight including terminals and housings, and t is time.

B. Spectroscopic Investigations of Intermetallic Systems

A number of spectroscopic techniques are currently being applied to the task of characterizing the species present in intermetallic systems. Infrared, visible, and ultraviolet absorption spectroscopy and the Raman spectrophotometric method described previously (ANL-7350, p. 84) have been investigated as means for studying intermetallic compounds in the solid state and as solutes in fused salt media.

A number of intermetallic compounds of direct interest to the energy conversion program form red-colored solutions in fused salts. The success of our Raman investigations on these colored melts will depend on their ability to scatter the 6328 Å helium-neon laser exciting line. In preparation for handling red solutions, a sample of the HgI_2-KI eutectic, which forms a bright red melt is being used to develop experimental techniques. Figure V-12 shows the Raman spectrum of a melt containing 60 m/o HgI_2 in KI at 130°C. A single band is observed at +138 cm^{-1} in the Stokes region (-137 cm^{-1} in the anti-Stokes region) which can be attributed to the symmetric stretching motion of the linear triatomic species, HgI_2. The observation of a clear, unambiguous spectrum from this highly colored fused-salt sample is encouraging in connection with Raman studies of red solutions of intermetallic compounds in fused salts.

[3] U.S. Department of Commerce, Panel on Electrically Powered Vehicles, "The Automobile and Air Pollution," Part I and Part II, Wash. D.C. (1967).

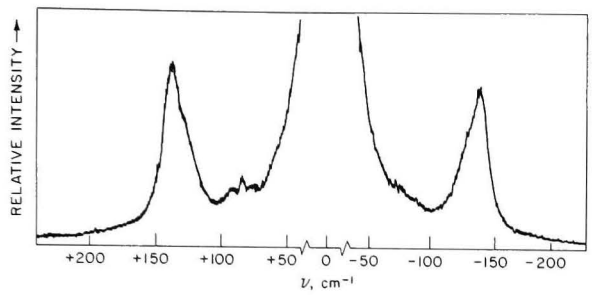

Fig. V-12. The Raman Spectrum of 60 m/o HgI_2 in KI at 130°C.

Preliminary studies have been conducted to investigate the possibility of gaining structural information about fused salt solutions of actinide metal oxides in $MgCl_2$-containing fused salts by Raman spectroscopy.[4] Figure V-13 shows a Raman spectrum of fused $MgCl_2$-2KCl. The analysis of these data indicate the presence of at least two magnesium (II) chloride complexes of composition $MgCl_n^{+(2-n)}$. Experiments are in progress to determine the value of n for each complex.

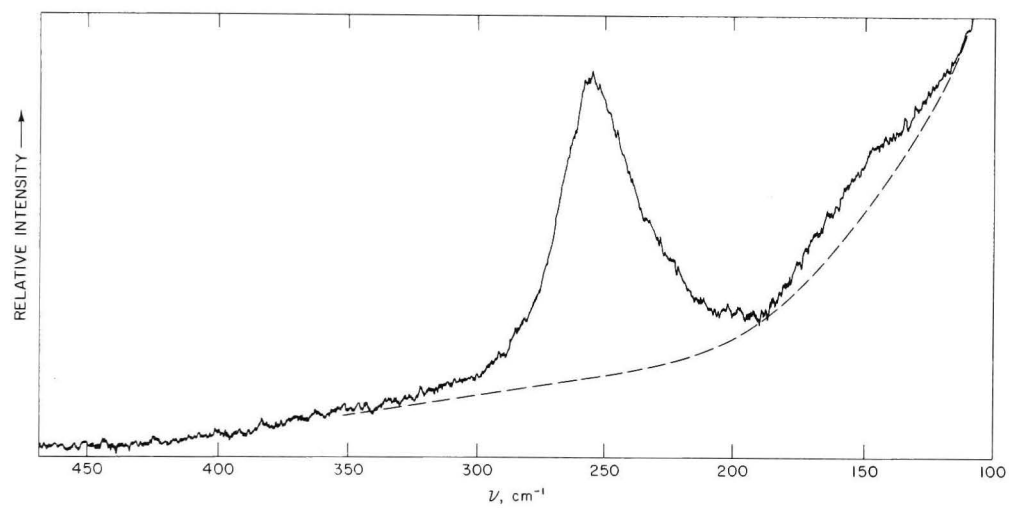

Fig. V-13. The Raman Spectrum of Fused $MgCl_2$-2KCl at 480°C.

Future studies will examine the structure of UO_2^{++} complexes in fused salts composed of $MgCl_2$ with various other alkali and alkaline earth chlorides and fluorides.

A novel approach has been taken in the study of Raman-active lattice vibrations in solid samples of intermetallic compounds as a function of pressure.[5] The sample is introduced between two diamond windows set in a specially designed holder which allows a known pressure to be applied across the faces of the diamonds. The laser beam is passed through the diamond windows and the light scattered at 180° to the incident beam is focused into the monochromator. Figure V-14 shows the well-characterized longitudinal (249 cm^{-1}) and transverse (215 cm^{-1}) optical lattice modes of ZnSe obtained with this cell at a pressure of 15,000 atmospheres.

[4]This portion of the work was performed in cooperation with the CEN Pyrochemical Research Group.

[5]This portion of the work is being performed in cooperation with J. R. Ferraro and C. Postmus, Jr. of the ANL Chemistry Division, who supplied the diamond cell, the ZnSe, and the infrared instrument.

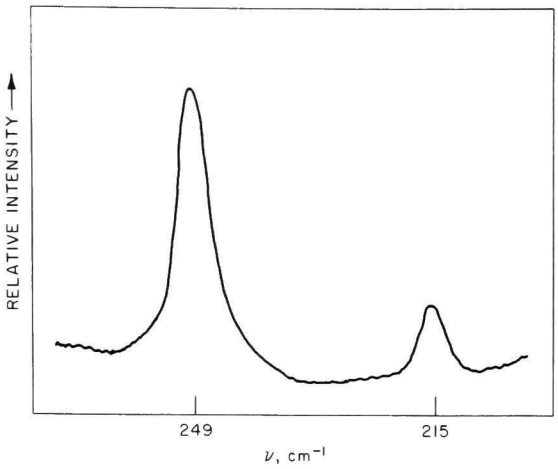

Fig. V-14. The Raman Spectrum of Crystalline ZnSe at 15,000 atm.

Part of the current effort to perform spectroscopic measurements on intermetallic systems has been directed toward the synthesis and characterization of the pure compounds. Lithium selenide has been prepared by vapor-phase transfer of selenium into molten lithium. The lithium and selenium react stoichiometrically in the ratio of 2:1 to produce high purity Li_2Se, which has been shown by X-ray diffraction to have the CaF_2 structure.

The infrared absorption spectrum of crystalline Li_2Se has been investigated as a function of pressure using the same diamond cell described above. One strong band is observed with a maximum at 276 cm^{-1} at atmospheric pressure. The dependency of the energy of the band maximum on pressure is illustrated in Fig. V-15. From the large shift of the maximum to higher wave numbers (cm^{-1}) with increasing pressure, it can be concluded that this band is the infrared active lattice vibration expected for a crystal having the CaF_2 structure. The absence of any other bands which could be attributed to molecular vibrations indicated that Li_2Se is an ionic solid.

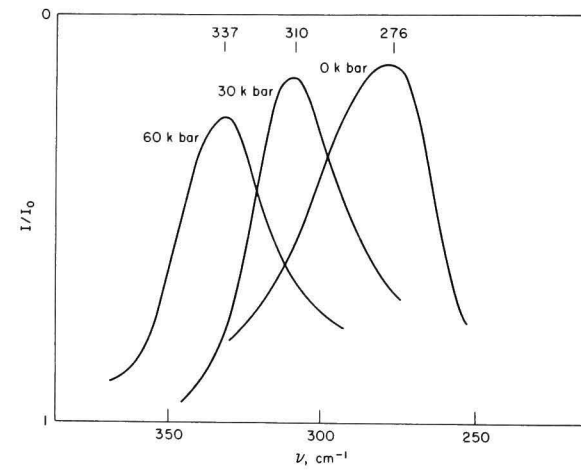

Fig. V-15. The Infrared Spectrum of the Li_2Se Lattice Vibration as a Function of Pressure. (1 kbar ≈ 1,000 atmospheres.)

Solutions of Li_2Se in the LiF-LiCl eutectic have no absorption maxima in the visible region, but their long wavelength edge is at lower energy than that of the pure fused eutectic. Experiments to obtain Raman spectra of intermetallics dissolved in fused salts are progressing with the investigation of the system Li_2Se in LiF-LiCl eutectic. Plans for the near future include more quantitative infrared and Raman studies of intermetallic compounds, both as solutes in fused salts and as crystalline solids under pressure.

C. Thermodynamics of the Sodium-Lead System by Vapor-Liquid Equilibrium Techniques

The sodium-lead system is the basis for one of the sodium-anode, thermally regenerative bimetallic cells that have been studied. The design

of such a cell entails the considerations of vapor-liquid equilibrium. Thus measurements were performed in order to supply data on such equilibria.

The vapor pressure data were obtained by a combination of total vapor pressure measurements (by the quasi-static method) and vapor density and composition determinations (by the transpiration method). Both the transpiration and the total pressure data were used to obtain values for the activity of sodium in liquid sodium-lead alloys at 853°C and across the entire composition range. In the calculation of sodium activities, the equilibrium constant for the gas-phase reaction, $Na_2 \leftrightarrows 2Na$, had to be introduced in order to determine the partial pressure of monatomic sodium. The activity coefficients of lead were obtained from the sodium data by means of a graphical Gibbs-Duhem integration.

In the interpretation of the thermodynamic data for the sodium-lead system, the quasi-ideal solution model was used. This model, which successfully correlated the activity data for the sodium-bismuth system in an earlier study (see ANL-7350, p. 78), applies to the liquid phase and is based on the assumption that all species in the molten system, including certain compound species that are presumed to be present, form ideal solutions with one another. For the sodium-lead system, five compounds are known to exist in the solid phase: $NaPb_3$, NaPb, Na_9Pb_4, Na_5Pb_2, and $Na_{15}Pb_4$. The melting points of the last three compounds fall in a narrow range (14°C) so that their stabilities are judged to be similar. Also, their average composition is $Na_{2.9}Pb$, which is close to the stoichiometry 75 a/o Na-25 a/o Pb. The average contribution of these three compounds to the thermodynamic properties was approximated by assuming the existence of a single, hypothetical, representative compound, Na_3Pb. Three compound species, then, Na_3Pb, NaPb, and $NaPb_3$, together with the component species, Na and Pb, served as the basis for the quasi-ideal solution treatment.

The necessary mathematical expressions were developed in a way closely parallel to Högfeldt's[6] treatment of the quasi-ideal systems (though Högfeldt did not use the term "quasi-ideal"). The expressions that were derived for the activity coefficient, γ, of the components (Na = A, Pb = B) are

$$\gamma_A = \frac{x_A}{X_A} = \frac{1 + K_1 x_A x_B + 3K_2 x_A^3 x_B + 3K_3 x_A x_B^3}{1 + K_1 x_B + 3K_2 x_A^2 x_B + K_3 x_B^3}$$

and

$$\gamma_B = \frac{x_B}{X_B} = \frac{1 + K_1 x_A x_B + 3K_2 x_A^3 x_B + 3K_3 x_A x_B^3}{1 + K_1 x_A + K_2 x_A^3 + 3K_3 x_A x_B^2}$$

[6] E. Högfeldt, Arkiv für Kemi 7, 315 (1954).

where X's are mole fractions of the components, x's are mole fractions of species, and the K's are the equilibrium constants of the formation reactions for the three compound species (K_1 for AB, K_2 for A_3B, and K_3 for AB_3). It is possible to obtain tentative values for these K's from a plot of experimental values of γ_A and γ_B as a function of composition; the necessary information is contained in the values of the activity coefficients at both extremes of infinite dilution and at the intersection point of the two curves.

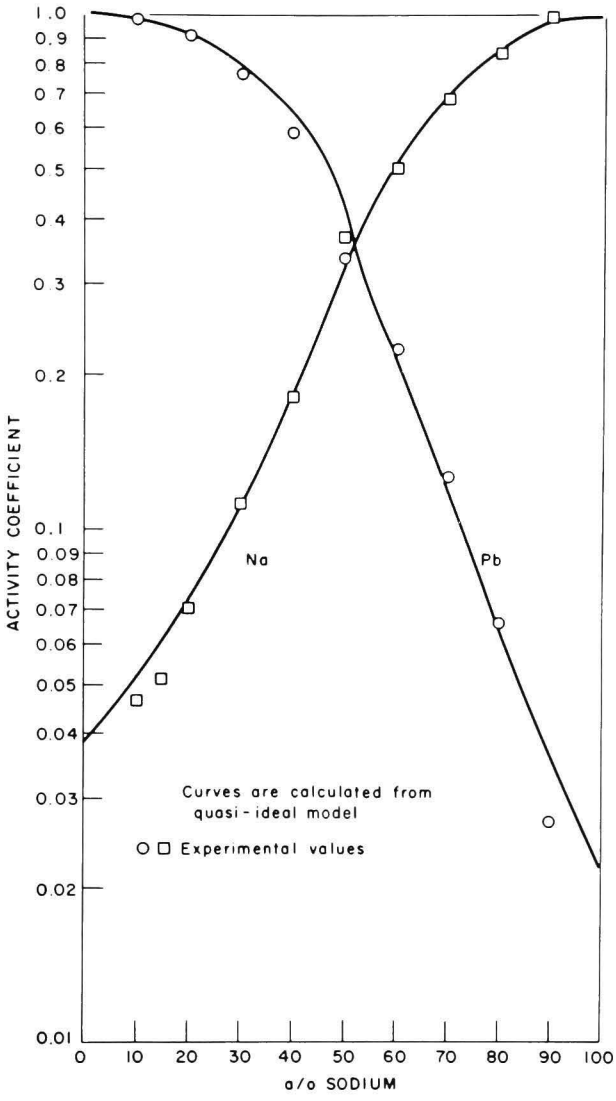

Fig. V-16. Calculated and Observed Activity Coefficients for the Sodium-Lead System at 853°C.

An equation can be derived that expresses x_B as a cubic function of x_A and the K's. By using this equation, a succession of points to generate the γ curves is obtained from a series of values of x_A. The calculations yield, in succession, x_B, γ_B, X_B, X_A, and γ_A for each value of x_A. The fit between the computed curves and the experimental points serves as a basis for adjusting the K's in order to compute a "best-fitting" pair of curves.

The final result is shown in Fig. V-16, in which the curves are based on the values $K_1(NaPb) = 20.3$, $K_2(Na_3Pb) = 24.0$, and $K_3(NaPb_3) = 4.8$. Experimental points and calculated curves agree well. A noteworthy aspect is the correlation between the melting points of the compounds and the stability of the presumed compound species in the melt. Often, a ranking of the stability of intermetallic compounds may be obtained by ranking their melting points. In the present case, the melting point of "Na_3Pb" is taken to be around 390°C, which is about the average of the melting points of $Na_{15}Pb_4$, Na_5Pb_2, and Na_9Pb_4. The melting points of NaPb and $NaPb_3$ are 368 and 320°C, respectively. If the K's are converted to standard free energies of formation, the $\Delta G°$ values are -7.1, -6.7, and -3.5 kcal/mole for Na_3Pb, NaPb, and $NaPb_3$, respectively. Thus, the melting point trend parallels the stability trend.

The quasi-ideal model has certain limitations and can not be applied to all systems. Other physical tools are needed to firmly establish the molecular phenomena suggested by the model.

VI. NUCLEAR CONSTANTS

A. Neutron Reaction Cross Sections

Neutron interactions with reactor structural, control, and fuel materials are of considerable importance to the design and performance of fast breeder reactors. Neutron cross sections of reactor components are necessary for calculations of breeding gain, fuel burnup, and neutron efficiency. These data are also valuable for developing and testing theories of nuclear reactions so that unknown neutron cross sections can be predicted from theoretical considerations.

Measurements of neutron capture cross sections are being made as a function of neutron energy between about 100 keV and 2 MeV and also as a function of the neutron energy distribution of EBR-II. Experimentally, this is achieved by the activation technique, in which a sample is irradiated in a neutron beam and the radioactive reaction products are measured by counting in an X-ray counter, beta counter, or, more often, a gamma-ray spectrometer. Monoenergetic neutrons are produced by bombarding lithium targets with protons from a Van de Graaff accelerator and measuring the neutron intensity by gold monitor foils and a fission chamber. Integral (reactor spectrum) neutron energy distributions are obtained by placing samples in various core or blanket positions in EBR-II.

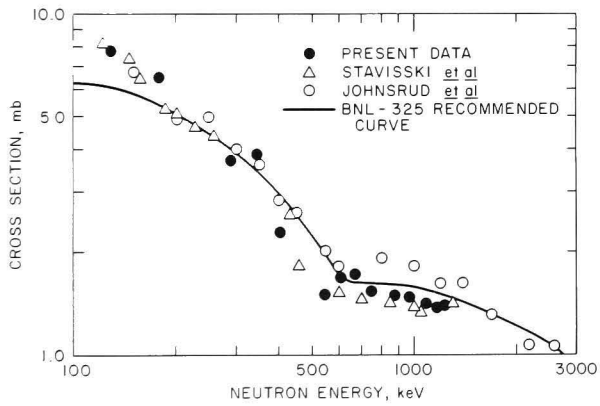

Fig. VI-1. Capture Cross Section of ^{51}V.

Experimental measurements of capture cross sections for three isotopes irradiated with monoenergetic neutrons have been completed. These data are presented in Figs. VI-1, -2, and -3, for the reactions $^{51}V(n,\gamma)^{52}V$, $^{85}Rb(n,\gamma)^{86m}Rb$, and $^{89}Y(n,\gamma)^{90m}Y$, respectively. Data

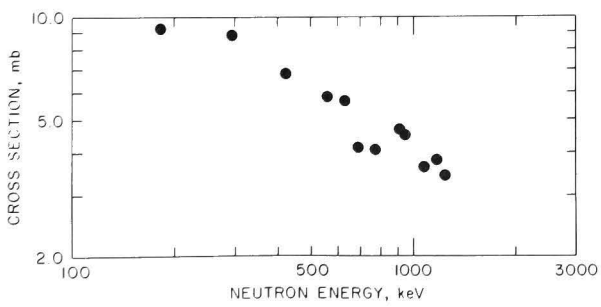

Fig. VI-2. Capture Cross Section of ^{85}Rb for the Production of ^{86m}Rb.

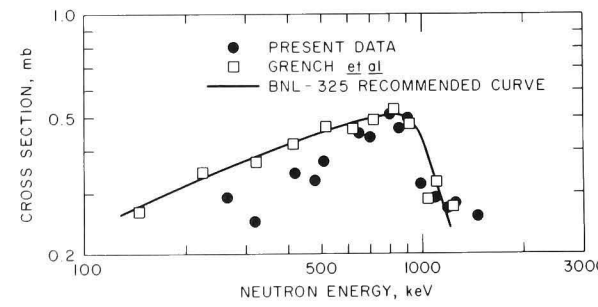

Fig. VI-3. Capture Cross Section of ^{89}Y for the Production of ^{90m}Y.

of other investigators[1-4] are also given when available. Cross sections for the reactions $^{89}Y(n,\gamma)^{90}Y$ and $^{85}Rb(n,\gamma)^{86}Rb$ were reported previously (ANL-7125, p. 214 and ANL-7350, p. 89).

As a part of the irradiation studies of structural materials, type 304 stainless steel spacers in EBR-II subassemblies are being examined. Analytical schemes have been devised for the separation of long-lived (n,p) and (n,α) reaction products of the stainless steel constituents, and analyses are in progress. Calculations of the yields of hydrogen and helium from (n,p) and (n,α) reactions in stainless steel have been completed (see Section VIB, below) and will be compared with experimental results.

A comparison of integral and monoenergetic cross sections can provide information about the energy distribution and the neutron intensity as a function of position in EBR-II.

B. Low-Mass Fission Yield Studies

Low-mass fission products such as tritium, hydrogen, and helium are of concern to fast reactor technology because of their practical importance in the development of fast reactor fuel-processing systems and because of the effects of their interactions with cladding material. Studies of low-mass fission product yields can also be expected to contribute information necessary for the theoretical understanding of the fission process.

A review of experimental and theoretical information on low-mass particle yields from fission has been completed, and semi-empirical calculations of hydrogen, tritium, and helium yields from fast-neutron fission of potential fast reactor fuels have been made. Table VI-1 presents a summary of calculated tritium yields per fission event for several fissionable nuclei at several neutron bombarding energies. The following

TABLE VI-1. Calculated Yields of Tritium from Neutron-Induced Fission

Fissionable Material	Neutron Energy	Calculated Yield (atoms/fission)	Fissionable Material	Neutron Energy	Calculated Yield (atoms/fission)
^{233}U	Thermal	1.1×10^{-4}	^{238}U	Thermal	2.6×10^{-4}
^{235}U	Thermal	1.3×10^{-4}		2.5 MeV	1.4×10^{-4}
	1.0 MeV	1.2×10^{-4}	^{239}Pu	Thermal	2.3×10^{-4}
	2.5 MeV	1.1×10^{-4}		1.0 MeV	2.5×10^{-4}
	3.0 MeV	8.2×10^{-5}	^{241}Pu	Thermal	2.6×10^{-5}

[1] Yu Ya Stavisski, V. A. Tolstikov, At. Energ. (USSR) 9, 401 (1960).
[2] A. E. Johnsrud, M. G. Silbert, H. H. Barschall, Phys. Rev. 116, 927 (1959).
[3] H. A. Grench, K. L. Coop, H. O. Menlove, F. J. Vaughn, Bull. Amer. Phys. Soc. 10, 498 (1965).
[4] Brookhaven National Laboratory, BNL-325, 2nd ed., Supp. 2, February 1966.

estimates were made of tritium production in EBR-II assuming full operating power: 340 Ci of tritium per year from ^{235}U fuel, 710 Ci per year from ^{239}Pu fuel, and 280 Ci per year from 28,000 kg of ^{238}U (the amount specified in the reactor design) in the blanket. Calculations of the production of hydrogen and helium from all neutron-reaction sources in EBR-II have been performed and are summarized in Table VI-2. The calculated rates of hydrogen and helium production in stainless steel will be compared with results of experiments described in the preceding section.

TABLE VI-2. Calculated Production of Hydrogen and Helium in EBR-II

Source	H Atoms / MW(t)-day	% of Total Hydrogen	He Atoms / MW(t)-day	% of Total Helium
Fission	4.3×10^{17}	2.5	55.0×10^{17}	82.5
Na	10.5×10^{17}	6.1	3.2×10^{17}	4.8
Stainless Steel				
Fe	53×10^{17}	30.8	1.7×10^{17}	2.6
Ni	101×10^{17}	58.5	0.4×10^{17}	0.6
Cr	1.1×10^{17}	0.6	4.8×10^{17}	7.2
Other	2.6×10^{17}	1.5	1.5×10^{17}	2.3
Total	172.5×10^{17}		66.6×10^{17}	

Experimental measurements of low-mass yields from fast fission will also be carried out and will be compared with the calculated yields given in Table VI-1. The method for the determination of fast fission yields of the low-mass particles will involve bombardment of fissionable targets with monoenergetic neutrons from the Argonne 4-MeV Van de Graaff accelerator. The energy distributions of the emitted particles will be measured, and the mass and charge determined by means of an electronic particle identification technique employing a two-detector telescope and associated electronics. The yield of each particle, X, will be determined by requiring a coincidence between particle X and a fission fragment. Spontaneously fissioning ^{252}Cf will be used as the reference and calibration standard.

VII. DETERMINATION OF BURNUP IN FAST REACTOR FUELS

The program for the development of methods for measuring burnup in fast reactor fuels is continuing. To achieve the program's objective it is necessary not only to develop accurate analytical methods of determining the concentration of fission products that can be used as burnup monitors, but also to establish accurate fast fission yield values for these fission products.

A. Methods for the Determination of Fission Products

During the past year, two methods of determining fission product concentration in irradiated fuels have been under investigation. The status of each of these methods is discussed below.

1. Spectrophotometric Titration of Total Rare Earths

A method that employs a spectrophotometric titration of the rare earths as a group is being developed to monitor burnup. Earlier work on this method and some of its advantages were reported previously (see ANL-7175, p. 223 and ANL-7350, p. 93).

Several changes in the method were made during the past year. The separation procedure was modified to achieve a better separation of rare earths from other fission products, and the titration procedure was changed to overcome incomplete reaction of the rare earths with ethylenediaminetetraacetic acid (EDTA).

The procedure as presently conceived involves the following steps: (1) evaporation of the fuel solution to dryness with perchloric acid to volatilize ruthenium, (2) anion exchange in concentrated hydrochloric acid to separate the rare earths from uranium and/or plutonium and most fission products, (3) anion exchange in 10% 5 N nitric acid-90% methanol to separate the rare earths from the remaining fission products including yttrium, (4) addition of excess EDTA and a spectrophotometric back titration of the excess EDTA with a standard lanthanum solution.

Conditions have been established that provide optimum separation of the rare earths from yttrium. Under the same conditions it has been established that (1) the fission products zirconium, molybdenum, ruthenium, palladium, and cadmium do not interfere, and (2) the constituents of stainless steel (a commonly used cladding material) do not interfere when the weight ratio of stainless steel constituents to rare earths is 15 to 1 (the ratio expected in a typical sample of UO_2 fuel discharged from a fast power reactor).

The method was applied to a sample of an oxide fuel that had been irradiated to approximately 6 a/o burnup. Gamma spectrometry of the separated rare earths showed that only rare earth activities were present. The titration of the separated rare earths proceeded normally and gave no indication of the presence of interfering ions. Evaluation of the accuracy of the results cannot be made until an accurate value of the burnup is obtained by an established procedure, namely, the mass-spectrometric determination of lanthanum-139. However, the results are within 6% of the value predicted on the basis of the estimated burnup and the existing fission yield data for the rare earths. The agreement between the experimental results and the predicted value is very promising.

2. X-Ray Spectrometric Determination of Rare Earth Fission Products

The feasibility of measuring burnup by using X-ray spectrometry for the determination of fission products in fast reactor fuels is under consideration. X-ray spectrometry has a very important advantage when compared with radiochemistry, mass spectrometry, and spectrophotometry in that the separation procedure does not have to provide a fission product of high chemical purity. The procedure must only provide (1) a separation from active fission products that is sufficient to protect the analyst from overexposure and (2) a separation from gross amounts of uranium, plutonium, and the other fission products.

The initial application of X-ray spectrometry to fission product analysis is directed toward the rare earths. The rare earths were chosen because they do not diffuse out of oxide fuels, which are of major importance to the fast reactor fuel program. The following general procedure is being considered:

1) Addition of an internal standard, i.e., a known amount of a rare earth that is not a fission product.

2) Isolation of the rare earths from uranium, plutonium and fission products such as zirconium, niobium, ruthenium, and cesium, which have high specific gamma activities. Since the internal standard and the fission product rare earths will behave identically in the separation scheme, the rare earth recovery does not have to be quantitative.

3) Transfer of all or a portion of the solution of separated rare earths onto a plate and evaporation to dryness.

4) Assay of the plated sample in the X-ray spectrometer for one or more of the principal rare earth fission products (lanthanum, cerium, praseodymium, or neodymium) and the internal standard.

5) Determination of the atom ratio of the fission product (F.P.) to the internal standard (I.S.) from a calibration curve in which $\text{concentration}_{F.P.}/\text{concentration}_{I.S.}$ has been plotted against the X-ray intensity ratio, $I_{F.P.}/I_{I.S.}$

Both the K-spectra and L-spectra are available for use in rare earth X-ray spectrometry. The most attractive feature of the K-spectra is simplicity; only two principal emission lines per element are present. On the other hand, the K-spectra exhibit several disadvantages. High potentials are necessary to excite the K-spectra and adequate spectral dispersion is difficult to attain. Line-to-background ratios are poor; this in turn affects the ultimate sensitivity attainable.

The L-spectra, on the other hand, exhibit a much more attractive line-to-background ratio, and much greater sensitivity can, therefore, be obtained. A typical L-spectra X-ray spectrogram is displayed in Figure VII-1. The quantities of the rare earths on this plate were 13, 24, 18 and 42 μg of lanthanum, cerium, praseodymium and neodymium, respectively. These amounts, which produce adequate X-ray intensities, would be present in one gram of fuel when the burnup is 0.03 a/o.

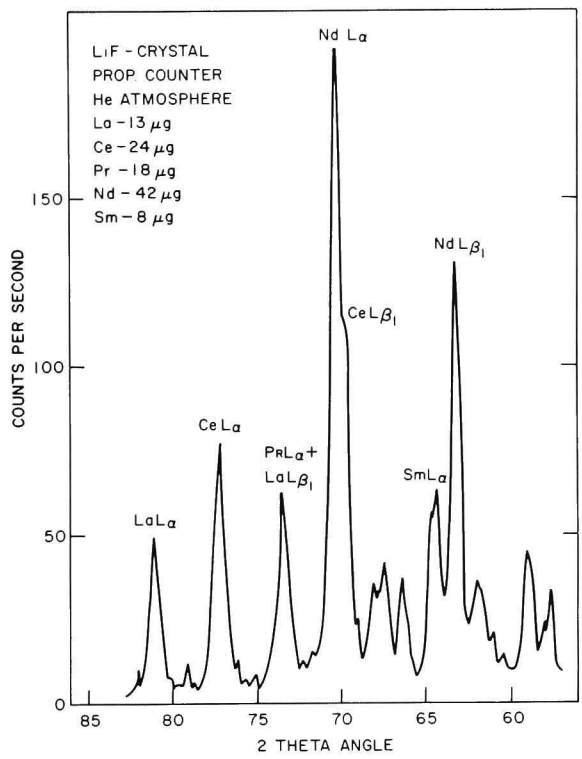

Fig. VII-1. X-ray Spectrogram of Simulated Rare Earth Fission Product Mixture.

Now that both the sensitivity and selectivity of the method for the individual rare earths have been established, efforts are being directed to the problems of making the method quantitative, i.e., establishing an accurate relationship between the intensity of a particular X-ray and the amount of rare earth on the mount. A series of six plates, each containing 58 μg of rare earths and 8 μg of terbium as an internal standard, were prepared to demonstrate the precision obtainable with the use of intensity ratios. Although the individual X-ray intensities varied considerably from plate to plate, the intensity ratio, $I_{F.P.}/I_{I.S.}$, was constant to within 3% for all major emission lines. A calibration curve will next be prepared and its application to unknowns studied.

B. Evaluation of Burnup Monitors for Oxide Fuels

A necessary part of the development of burnup methods is a demonstration that a monitor is applicable to a particular type of fuel

(e.g., oxide, carbide). Migration of a fission product or a precursor out of the fuel is the chief cause of a monitor's nonapplicability.

Two burnup monitors, technetium and molybdenum, were evaluated for oxide fuels. These fission products had previously been used successfully to monitor burnup of metal fuel samples. Moreover, the analytical procedures could be carried out more easily than the analyses (described above) for total rare earths. The evaluations showed that both molybdenum and technetium migrated out of oxide fuels and were therefore unsuitable as burnup monitors for this type of fuel. This information is of particular significance because both of these elements have been used, or have been considered for use, in other programs for determining burnup of oxide fuels.

C. Irradiation in EBR-II

An irradiation is being carried out in EBR-II to provide materials for establishing fission yield values to ±1% accuracy. A discussion of the basic philosophy behind this irradiation and a description of the materials being irradiated were reported previously (ANL-7350, p. 94). This irradiation is progressing much more slowly than was anticipated (1 to 2% burnup per year rather than 4 to 6% per year). It is evident that the time necessary to achieve the desired 25% burnup would be inordinately long, and a "short-term" irradiation is therefore being considered.

The "short-term" irradiation would be carried out in a driver subassembly for one full fuel cycle. For the isotopes of interest (^{233}U, ^{235}U, ^{239}Pu, and ^{241}Pu) this would result in a burnup of 2 to 3 a/o. The number of fissions which have occurred in each material will be determined by summing the number of atoms of heavy-element fission products produced. This involves four determinations (total rare earth, cesium, barium, and xenon) and an estimation of the concentrations of two of the minor heavy-element fission products (iodine and tellurium) by extrapolation of the other data. This approach was not feasible when the long-term irradiation was initiated since suitable analytical techniques were not available. The development of the total rare earth and the X-ray spectrometric rare earth methods has provided a means for determining 50% of the heavy fission products with the requisite accuracy.

The "short-term" irradiation experiment will provide data that are less accurate by about a factor of two than those that will be derived from the long-term irradiation experiment. However, the short-term data will be available several years before any data are forthcoming from the long-term irradiation.

ADDENDUM

Publications
by
Chemical Engineering Division
Personnel

(From Jan. 1, 1967 to April 30, 1968)

A. Open Literature

J. J. Barghusen
Volatility Processes
Power Reactor Technol. and Reactor Fuel Process. 10(1), 70-78 (Winter 1966-1967).

J. J. Barghusen
Volatility Processes
Power Reactor Technol. and Reactor Fuel Process. 10(2), 160-164 (Spring 1967).

J. J. Barghusen
Volatility Processes
Reactor and Fuel Process. Technol. 10(3), 226-233 (Summer 1967).

J. J. Barghusen, A. A. Jonke
Safety Considerations in the Processing of Plutonium and Radioactive Materials
Power Reactor Technol. and Reactor Fuel Process. 10(2), 170-172 (Spring 1967).

G. J. Bernstein
Equipment for Disposal of High-Level Solid Wastes from the EBR-II Fuel Cycle Facility
Proc. Conf. Remote Syst. Technol., 15th, Amer. Nucl. Soc., Chicago, 1967, 85-92 (1967).
Also published in Trans. Amer. Nucl. Soc. 10(2), 673 (1967).

F. A. Cafasso, V. N. Khanna, H. M. Feder
Thermodynamic Properties and Ordering in Liquid NaK Alloys
Advan. Phys. 16(63), 535-543 (1967).

E. J. Cairns, H. Shimotake
Recent Advances in Fuel Cells and Their Application to New Hybrid Systems Preprints of Papers Presented at the Biennial Fuel Cell Symposium, 154th Natl. ACS Mtg., Chicago, Sept. 10-15, 1967. Vol. 11, No. 3, pp. 321-350, Am. Chem. Soc., Div. Fuel Chem., Washington, D. C. (1967).

M. G. Chasanov
Compatibility of Type-304 Stainless Steel with Sodium Paste Reactor Fuels
Nucl. Sci. Eng. 30(2), 310 (1967). Note.

N. R. Chellew, R. K. Steunenberg
Extraction of Plutonium from Uranium-Plutonium Alloy with Uranium Trichloride*
Nucl. Appl. 3(3), 142-146 (1967).

A. A. Chilenskas
Fission-Product and Actinide Distribution during Reprocessing of Irradiated UO_2 by the Fluid-Bed Fluoride Volatility Method
Trans. Amer. Nucl. Soc. 10(1), 157 (1967).

A. A. Chilenskas, K. S. Turner
Engineering Development of a Fluidized-Bed Fluoride Volatility Process. III. Bench-Scale Studies with Irradiated Uranium Alloy Fuels
Nucl. Appl. 4, 6-16 (January 1968).

C. E. Crouthamel, H. L. Recht
Regenerative EMF Cells
Advan. Chem. Ser. 64, Am. Chem. Soc., Washington, D. C. (1967).

J. J. Dutton, D. H. Lennox, K. K. Brown, J. Royal, R. Gold, B. A. Schmeh, eds.
Power Reactor Technol. and Reactor Fuel Process.
Division of Technical Information, U. S. Atomic Energy Commission, Vol. 10(1) (Winter 1966-1967).

J. J. Dutton, D. H. Lennox, K. K. Brown, J. Royal, R. Gold, B. A. Schmeh, eds.
Power Reactor Technol. and Reactor Fuel Process.
Division of Technical Information, U. S. Atomic Energy Commission, Vol. 10(2) (Spring 1967).

J. J. Dutton, D. H. Lennox, K. K. Brown, J. Royal, R. Gold, P. H. Gregory, eds.
Reactor and Fuel Process. Technol.
Division of Technical Information, U. S. Atomic Energy Commission, Vol. 10(3) (Summer 1967).

A. K. Fischer
Phase Diagram Considerations for the Regenerative Bimetallic Cell Chapter in Regenerative EMF Cells, Advan. Chem. Ser. 64, 121-135 (1967).

A. K. Fischer, S. A. Johnson, S. E. Wood
Liquid-Vapor Phase Diagram and Thermodynamics of the Sodium-Bismuth System
J. Phys. Chem. 71(5), 1465-1472 (1967).

D. F. Fischer, M. G. Chasanov
Thermal Gradient Apparatus for Use in a Glovebox
Rev. Sci. Instr. 38(11), 1574 (1967).

*Also listed in ANL-7350.

M. S. Foster
Laboratory Studies of Intermetallic Cells
Chapter in Regenerative EMF Cells, Advan. Chem. Ser. 64, 136-148 (1967).

J. D. Gabor
Wall Effects on Fluidized Particle Movement in a Two-Dimensional Bed
Proc. Int. Symp. Fluidization, Eindhoven, 1967, p. 230, Netherlands Univ. Press, Amsterdam, 1967.

E. L. Gasner, H. H. Claassen
Raman Spectrum of Xenon Hexafluoride
Inorg. Chem. 6, 1937-1938 (October 1967). Note.

E. Greenberg, W. N. Hubbard
Fluorine Bomb Calorimetry. XXIII. The Enthalpy of Formation of Carbon Tetrafluoride
J. Phys. Chem. 72(1), 222-227 (1968).

L. J. Harrison, R. C. Liimatainen, F. J. Testa
Photographic Studies of UO_2 Pellet Fuel Rods in Water Subjected to Nuclear Transients in TREAT
Trans. Amer. Nucl. Soc. 10(1), 127 (1967).

P. S. Harris, B. A. Phillips, M. H. Rand, M. Tetenbaum
The Volatility of Plutonium Carbides. Part I
UKAEA Report AERE-R 5353 (March 1967).

J. C. Hesson, M. S. Foster, H. Shimotake
Self-Discharge in Alkali Metal-Containing Bimetallic Cells
Electrochem. Soc. Fall Mtg., Chicago, Ill., October 15-20, 1967. Extended Abstracts of Battery Division, J-1, Vol. 12, pp. 46-47.

J. C. Hesson, R. O. Ivins, L. Baker, Jr.
Calculation of the Extent of Metal-Water Reaction and Core Heating during a Loss-of-Coolant Accident (CHEMLOC Program)
Trans. Amer. Nucl. Soc. 10(2), 705 (1967).

J. C. Hesson, H. Shimotake
Thermodynamic and Thermal Efficiencies of Thermally Regenerative Bimetallic and Hydride EMF Cell Systems
Chapter in Regenerative EMF Cells, Advan. Chem. Ser. 64, 82-104 (1967).

J. C. Hesson, H. Shimotake, J. M. Tralmer
Densities of Molten Sodium-Lead and Sodium-Bismuth Alloys
J. Metals 20, 6-7 (February 1968).

J. T. Holmes, L. B. Koppel, A. A. Jonke
Fluidized-Bed Disposal of Fluorine
Ind. Eng. Chem. Process Design Develop. 6(4), 408-413 (1967).

W. N. Hubbard
Thermochemistry*
Encyclopedia Britanica 21, 1010-1015 (1967).

R. L. Jarry, M. J. Steindler
The Reaction of Gaseous Bromine Pentafluoride with Uranium Compounds - I. The Kinetics of the Reactions with UF_4 and UO_2F_2
J. Inorg. Nucl. Chem. 29(7), 1591-1597 (1967).

C. E. Johnson, M. S. Foster, M. L. Kyle
Purification of Inert Atmospheres
Nucl. Appl. 3, 563-567 (September 1967).

C. E. Johnson, R. R. Heinrich
Thermodynamics of the Lithium Hydride Cell
Chapter in Regenerative EMF Cells, Advan. Chem. Ser. 64, 105-120 (1967).

C. E. Johnson, S. E. Wood, E. J. Cairns
Reply to the Comments of Bredig (on Lithium Hydride-Alkali Halide Systems)
J. Chem. Phys. 46(10), 4168 (1967).

G. K. Johnson, E. Greenberg, J. L. Margrave, W. N. Hubbard
Fluorine Bomb Calorimetry. Enthalpies of Formation of the Diborides of Zirconium and Hafnium*
J. Chem. Eng. Data 12(1), 137-141 (1967).

G. K. Johnson, E. Greenberg, J. L. Margrave, W. N. Hubbard
Fluorine Bomb Calorimetry. Enthalpies of Formation of the Diborides of Niobium and Tantalum
J. Chem. Eng. Data 12(4), 597-600 (1967).

I. Johnson
Partition of Metals between Liquid Metal Solutions and Fused Salts
Applications of Fundamental Thermodynamics to Metallurgical Processes, pp. 153-177, G. R. Fitterer (ed.), Gordon and Breach, Science Publishers, N. Y. (1967).

T. R. Johnson
Compact Pyrochemical Processes
Power Reactor Technol. and Reactor Fuel Process. 10(1), 79-84 (Winter 1966-1967).

T. R. Johnson
Compact Pyrochemical Processes
Power Reactor Technol. and Reactor Fuel Process. 10(2), 165-169 (Spring 1967).

*Also listed in ANL-7350.

T. R. Johnson
Compact Pyrochemical Processes
Reactor and Fuel Process. Technol. 10(3), 234-240 (Summer 1967).

T. R. Johnson
Tables for the Calculation of Operating Parameters for Compound Solvent-Extraction Columns
A.I.Ch.E. (Amer. Inst. Chem. Engrs.) J. 13(3), 607 (1967).
Communication.

T. R. Johnson, F. G. Teats, R. D. Pierce
An Induction Probe for Measuring Levels in Liquid Metals
Nucl. Appl. 4(1), 47 (1968).

A. A. Jonke, M. Levenson, N. M. Levitz, M. J. Steindler, R. C. Vogel
Fluoride Volatility: Candidate for Second-Generation Fuel-Reprocessing Plants
Nucleonics 25(5), 58-63 (1967).

A. A. Jonke, D. Ramaswami
Basic Fluidization Studies at Argonne
Argonne National Laboratory Reviews 4, 76 (July-October 1967).

A. A. Jonke, M. J. Steindler, N. M. Levitz
Development of Fluoride Volatility Reprocessing Methods for Plutonium-Containing Fuels
Chem. Eng. Progr. Symp. Ser. 63(80), 130-141 (1967).

A. A. Jonke, M. Levenson, R. K. Steunenberg, R. C. Vogel
Reprocessing of Reactor Fuels by Fluoride Volatility and Pyrochemical Techniques
Plutonium as a Reactor Fuel, pp. 537-547, Int. Atomic Energy Agency, Vienna (1967).

L. R. Kelman, H. V. Rhude, J. G. Schnizlein, H. Savage
Metallic Plutonium Alloys for Fast Critical Experiments
Plutonium 1965, pp. 510-524, A. E. Kay and M. B. Waldron (eds.), Chapman and Hall, London (1967).

R. W. Kessie
Removal of Plutonium Hexafluoride from Cell Exhaust Air by Hydrolysis and Filtration
in Proceedings of the Ninth AEC Air Cleaning Conference, Boston, Massachusetts, 13-16 September 1966, Vol. 2, pp. 741-762, J. M. Morgan, Jr. and M. W. First (eds.), USAEC Report CONF-660904 (January 1967).

R. W. Kessie
Plutonium and Uranium Hexafluoride Hydrolysis Kinetics*
Ind. Eng. Chem. Process Design Develop. 6(1), 105-111 (1967).

*Also listed in ANL-7350.

I. E. Knudsen, W. F. Olsen
Direct Indication of Particle Size in Fluidized Beds
Chem. Eng. 74(8), 244-246 (1967).
Republished in Chem. Eng. 75(2), 190 (1968) in recognition of an award.

M. L. Kyle, L. F. Coleman, R. D. Pierce, J. D. Arntzen
Removal of Nitrogen from Argon with Titanium-Metal Sponge
Abstracts of Papers Presented at Am. Chem. Soc. Meeting, Chicago, Sept. 10-15, 1967, N-46. Abstract.

L. Leibowitz, L. Mishler
Study of Aluminum-Water Reactions by Laser Heating
J. Nucl. Mater. 23(2), 173-182 (1967).

L. Leibowitz
Thermodynamic Equilibria in Sodium-Air Systems
J. Nucl. Mater. 23(2), 233-235 (1967).

J. O. Ludlow, T. W. Eckels, J. E. A. Graae, P. A. Nelson, M. A. Slawecki
Shielded Fuel Evaluation Facility (SFEF)
Proc. Conf. Remote Syst. Technol., 15th, Amer. Nucl. Soc., Chicago, 1967, 197-205 (1967).
Also published in Trans. Amer. Nucl. Soc. 10(2), 682 (1967).

C. Luner, A. Cosgarea, Jr., H. M. Feder
Solubility of Carbon in Sodium
Alkali Metal Coolants, pp. 171-179, Int. Atomic Energy Agency, Vienna (1967).

W. E. Miller, G. J. Bernstein, R. M. Fryer, R. F. Malecha, R. C. Paul, M. A. Slawecki
EBR-II Plant Equipment for Oxidation of Melt Refining Skulls
Proc. Conf. Remote Syst. Technol., 15th, Amer. Nucl. Soc., Chicago, 1967, 43-51 (1967).
Also published in Trans. Amer. Nucl. Soc. 10(2), 670 (1967).

P. A. Nelson, D. K. Butler, M. G. Chasanov, D. Meneghetti
Fuel Properties and Nuclear Performance of Fast Reactors Fueled with Molten Chlorides
Nucl. Appl. 3, 540-547 (September 1967).

E. J. Petkus, P. A. Nelson, S. Vogler, P. W. Krause
Fluidized-Bed Technique for Preparation of Uranium-Plutonium Monocarbide
Chem. Eng. Progr. Symp. Ser. 63(80), 111-120 (1967).

E. Rudzitis, E. H. Van Deventer, W. N. Hubbard
Fluorine Bomb Calorimetry. Enthalpy of Formation of Nickel Difluoride*
J. Chem. Eng. Data 12(1), 133-135 (1967).

*Also listed in ANL-7350.

E. Rudzitis
Separation of Volatile Fluorides by a Combination of Transpiration and Gas Chromatographic Techniques
Anal. Chem. 39, 1187-1188 (1967). Note.

E. Rudzitis, H. M. Feder, W. N. Hubbard
Fluorine Bomb Calorimetry. XXII. The Enthalpy of Formation of Aluminum Trifluoride
Inorg. Chem. 6, 1716-1717 (1967).

J. G. Schnizlein, D. F. Fischer
The Kinetics of Oxidation of Plutonium Metal and a Plutonium-3.4 a/o Aluminum Alloy at Temperatures from 140° to 550°C*
J. Electrochem. Soc. 114(1), 23-29 (1967).

D. W. Scott, W. T. Berg, I. A. Hossenlopp, W. N. Hubbard, J. F. Messerly, S. S. Todd, D. R. Douslin, J. P. McCullough, G. Waddington
Pyrrole: Chemical Thermodynamic Properties
J. Phys. Chem. 71(7), 2263-2270 (1967).

J. L. Settle, E. Greenberg, W. N. Hubbard
Two-Compartment Bomb for Calorimetric Combustions
Rev. Sci. Instr. 38(12), 1805-1806 (1967).

H. Shimotake, E. J. Cairns
Performance Characteristics of a Sodium-Bismuth Cell
Electrochemical Soc. Spring Mtg., Dallas, May 7-12, 1967. Extended Abstracts of Ind. Electrolytic Div., I-5, Vol. 3, pp. 4-8.

H. Shimotake, J. C. Hesson
Corrosion by Fused Salts and Heavy Liquid Metals--A Survey
Chapter in Regenerative EMF Cells, Advan. Chem. Ser. 64, 149-185 (1967).

H. Shimotake, E. J. Cairns
Bimetallic Galvanic Cells with Fused-Salt Electrolytes
Advances in Energy Conversion Engineering, Papers Presented at Miami Beach, August 13-17, 1967. Am. Soc. Mech. Eng., New York, 1967, p. 951.

H. Shimotake, J. C. Hesson
A Sodium-Bismuth Bimetallic Galvanic Cell
Denki Kagaku 35(8), 583-586 (1967).

H. Shimotake, N. R. Stalica, J. C. Hesson
Corrosion of Refractory Metals by Liquid Bismuth, Tin, and Lead at 1000°C
Trans. Amer. Nucl. Soc. 10(1), 141 (1967).

*Also listed in ANL-7350.

H. Shimotake, G. L. Rogers, E. J. Cairns
Performance Characteristics of a Lithium-Tellurium Cell
Electrochem. Soc. Fall Mtg., Chicago, Ill., October 15-20, 1967.
Extended Abstracts of Battery Division, J-1, Vol. 12, pp. 42-45.

M. J. Steindler, N. M. Levitz, A. A. Jonke
Development of Fluoride Volatility Methods for Reprocessing Reactor Fuels
Compt. Rend. Congr. Intern. Chim. Ind. 36 Brussels, 1966, 1, 730-733 (1967).

D. C. Stupegia, M. Schmidt, C. R. Keedy
Capture Cross Sections of Neptunium-237
Nucl. Sci. Eng. 29, 218 (1967).

A. D. Tevebaugh, D. L. Keller (eds.)
Preparation of Nuclear Fuels, Nuclear Engineering
Part XVIII.
Chem. Eng. Prog. Symp. Ser. 63(80), 1967.

L. E. Trevorrow, M. J. Steindler, D. V. Steidl, J. T. Savage
The Melting-Point Diagram for the System Uranium Hexafluoride-Plutonium Hexafluoride
Inorg. Chem. 6(5), 1060-1061 (1967). Note.

L. E. Trevorrow, M. J. Steindler, D. V. Steidl, J. T. Savage
Condensed Phase Equilibria in the System Molybdenum Hexafluoride-Uranium Hexafluoride
Paper in Lanthanide/Actinide Chemistry, Advan. Chem. Ser. 71, 308-319 (1967).

E. Veleckis, R. V. Schablaske, I. Johnson, H. M. Feder
Intermetallic Phases in the Systems of Zinc with Lanthanum, Cerium, Praseodymium, Neodymium, and Yttrium*
Trans. Met. Soc. AIME, 239, 58-63 (1967).

I. O. Winsch, M. L. Kyle, R. D. Pierce, L. Burris, Jr.
Tungsten Crucibles in Pyrochemical Processing of Nuclear Fuels
Nucl. Appl. 3, 245-251 (April 1967).

L. C. Witte, L. Baker, Jr., D. R. Haworth
Heat Transfer from High-Temperature Spheres to Liquid Sodium
Trans. Amer. Nucl. Soc. 10(1), 351 (1967).

L. C. Witte
An Experimental Study of Forced-Convection Heat Transfer from a Sphere to Liquid Sodium
J. Heat Transfer, 90, 9 (February 1968).

*Also listed in ANL-7350.

T. F. Young
Contributions to Proc. Conf. Biol. Hard Tissue, 1st, Princeton, N. J., 1965, pp. 42-44, 97-99, 255-264, New York Academy Sciences (1967).

B. Papers Accepted for Publication in the Open Literature

L. J. Anastasia, P. G. Alfredson, M. J. Steindler
Fluid-Bed Fluorination of UO_2-PuO_2-Fission Product Fuel Pellets with Fluorine
Accepted for publication in Nucl. Appl.

L. Baker, Jr., R. C. Liimatainen
Chemical Reactions*
Accepted for publication as Chapter 17, Vol. 2, of The Technology of Nuclear Reactor Safety, MIT Press.

J. J. Barghusen, A. A. Jonke, N. M. Levitz, M. J. Steindler, R. C. Vogel
Fluid-Bed Fluoride Volatility Processing of Reactor Fuel Materials
Accepted for publication as a chapter in Progr. Nucl. Energy, Ser. III, Process Chemistry, Vol. 4.

J. C. Hesson, H. Shimotake, J. M. Tralmer
Density, Surface Tension, and Viscosity of NaF-NaCl-NaI Eutectic
Accepted for publication in J. Chem. Eng. Data.

R. L. Jarry, M. J. Steindler
The Reaction of Gaseous Bromine Pentafluoride with Uranium Compounds - II. The Reactions with U_3O_8, UO_2, and UO_3
Accepted for publication in J. Inorg. Nucl. Chem.

L. Koppel
Dynamics and Control of a Batch Reactor
Accepted for publication in Ind. Eng. Chem. Process Design Develop.

M. Krumpelt, J. Fischer, I. Johnson
The Reaction of Magnesium Metal with Magnesium Chloride
Accepted for publication in J. Phys. Chem.

M. L. Kyle, R. D. Pierce, L. F. Coleman, J. D. Arntzen
Removal of Nitrogen from Argon with Titanium-Metal Sponge
Accepted for publication in Ind. Eng. Chem. Process Design Develop.

J. G. Schnizlein, D. F. Fischer
Ignition Behavior of Plutonium Metal and Certain Binary Alloys
Accepted for publication in J. Electrochem. Soc.

R. K. Steunenberg, R. D. Pierce, L. Burris, Jr.
Pyrometallurgical and Pyrochemical Fuel Processing Methods
Accepted for publication as a chapter in Progr. Nucl. Energy, Ser. III, Process Chemistry, Vol. 4.

*Also listed in ANL-7350.

D. C. Stupegia, M. Schmidt, C. R. Keedy, A. A. Madson
Neutron Capture between 5 keV and 3 MeV
Accepted for publication in J. Nucl. Energy.

A. D. Tevebaugh, L. Baker, D. Swift
Explosive Heat Transfer at Liquid-Liquid Interfaces*
Accepted for publication in Symposium on Molecular Processes in Chemical Engineering, University of Rochester (publisher).

L. C. Witte
Film Boiling from a Sphere
Accepted for publication in Ind. Eng. Chem., Fundam.

L. C. Witte
An Apparatus for Obtaining Extremely Large Heat Flux Densities
Accepted for publication in J. Sci. Instrum.

C. ANL Reports

A. A. Chilenskas, K. S. Turner, J. E. Kincinas, G. L. Potts
Engineering Development of Fluid-Bed Fluoride Volatility Processes. Part 10. Bench-Scale Studies on Irradiated, Highly Enriched, Uranium-Alloy Fuels
ANL-6994.

T. W. Eckels, A. Smaardyk
Design, Performance, and Evaluation of Shielding Window for FARET Containment Cell*
ANL-7157.

J. D. Gabor, D. Ramaswami
Engineering Development of Fluid-Bed Fluoride Volatility Process Part 12. Exploratory Tests on Fluorination of Uranium Oxide with BrF_5 in a Bench-Scale Fluid-Bed Reactor System
ANL-7362.

W. H. Gunther, M. J. Steindler
Laboratory Investigations in Support of Fluid-Bed Fluoride Volatility Processes. Part XIV. The Corrosion of Nickel and Nickel Alloys by Fluorine, Uranium Hexafluoride, and Selected Volatile Fission Product Fluorides at 500°C
ANL-7241.

M. L. Kyle, L. F. Coleman, R. D. Pierce, J. D. Arntzen
Kinetics of the Titanium-Nitrogen Reaction with Application to the Design of Gettering Systems
ANL-7167.

*Also listed in ANL-7350.

W. E. Miller, G. J. Bernstein, R. M. Fryer, R. F. Malecha, M. A. Slawecki, R. C. Paul
The EBR-II Skull Reclamation Process. Part III. Skull Oxidation Equipment
ANL-7338.

E. J. Petkus, T. R. Johnson, R. K. Steunenberg
The Preparation of Uranium Monocarbide by Reaction in a Liquid Metal Medium
ANL-7301.

M. A. Slawecki, G. J. Bernstein, L. F. Coleman
Tests of Commutating Brushes for Use in D.C. Motors Operating in a Dry Argon Atmosphere
ANL-7262.

L. E. Trevorrow, M. J. Steindler, D. V. Steidl, J. T. Savage
Laboratory Investigations in Support of Fluid-Bed Fluoride Volatility Processes. Part XII. The Melting Point Diagram for the System Uranium Hexafluoride-Plutonium Hexafluoride*
ANL-7234.

L. E. Trevorrow, M. J. Steindler
Laboratory Investigations in Support of Fluid-Bed Fluoride Volatility Processes. Part XV. Estimation of Rates of Thermal Decomposition of Plutonium Hexafluoride
ANL-7347.

R. C. Vogel, M. Levenson, J. H. Schraidt, J. Royal
Chemical Engineering Division Semiannual Report, January-June 1966
ANL-7225.

R. C. Vogel, M. Levenson, E. R. Proud, J. Royal
Chemical Engineering Division Semiannual Report, July-December 1966
ANL-7325.

R. C. Vogel, M. Levenson, E. R. Proud, J. Royal
Chemical Engineering Division Research Highlights May 1966-April 1967
ANL-7350.

L. C. Witte
Heat Transfer from a Sphere to Liquid Sodium during Forced Convection
ANL-7296.

*Also listed in ANL-7350.

D. Papers Presented at Scientific Meetings

L. Baker, Jr., D. T. Eggen, R. O. Ivins, S. A. Szawlewicz
The United States Liquid Metal Fast Breeder Reactor Safety Program
Presented at International Conference on the Safety of Fast Breeder Reactors, Aix-en-Provence, France, Sept. 19-22, 1967.

M. H. Barsky
Application of Gas Chromatography in Inorganic Analysis
Presented at Mid-America Spectroscopy Symposium, Chicago, Ill., May 16, 1967.

E. J. Cairns
Electrochemical Devices
Plenary lecture presented at 2nd Intersociety Energy Conversion Engineering Conference, Miami Beach, Fla., Aug. 13-17, 1967.

E. J. Cairns
Bimetallic Galvanic Cells with Fused Alkali Halide Electrolytes
Presented at Gordon Conference, Meridan, N. H., Aug. 28-Sept. 1, 1967.

P. M. Danielson, J. S. Hetherington
Ultrahigh Vacuum Equipment for Materials Studies above 2000°C
Presented at the 1967 International Vacuum Metallurgy Conference, New York, June 12-16, 1967.

P. M. Danielson, J. S. Hetherington
The Application of Ultrahigh Vacuum Techniques to High Temperature Materials Research
Presented at Annual Meeting of Midwest Section American Vacuum Society, Boulder, Colo., May 11-12, 1967.

R. K. Edwards
Report on Completed Program of Studies in the Uranium-Urania System and Current Plans in the Ternary Pu-U-O and Pu-U-C Systems
Presented at International Symposium on High Temperature Chemistry, Argonne, Ill., May 8-10, 1967.

R. K. Edwards
High Temperature Materials Program of Research
Presented at Oklahoma State University, Stillwater, Okla., June 15-17, 1967.

H. M. Feder
1) High Temperature Investigations of the Uranium-Oxygen System
2) Thermochemistry of Some Uranium and Plutonium Compounds
Presented at the U.S.-Japan Information Exchange Meeting on Ceramic Fuels, Richland, Wash., Sept. 25-27, 1967.

A. K. Fischer, S. A. Johnson, E. J. Cairns
Liquid-Vapor Equilibria and Thermodynamics of the Sodium-Lead System
Presented at Am. Chem. Soc. Mtg., Miami Beach, Fla., April 9-14, 1967.

M. S. Foster, G. H. McCloud, E. J. Cairns
Electrochemical Studies of the Sodium-Bismuth System
Presented at Am. Chem. Soc. Mtg., Miami Beach, Fla., April 9-14, 1967.

E. Greenberg, W. N. Hubbard
The Enthalpy of Formation of CF_4 by Fluorination of Graphite: Use of a Two-Compartment Bomb and Quartz Thermometer
Presented at the 22nd Annual Calorimetry Conference, Thousand Oaks, Calif., June 22-24, 1967.

R. L. Gulley, M. D. Freshley, R. C. Liimatainen, D. Armstrong
Transient Irradiation Testing of Oxide Fuels
Presented at the U.S.-Japan Information Exchange Meeting on Ceramic Nuclear Fuels, Richland, Wash., Sept. 25-29, 1967.

J. C. Hesson
Development of the CHEMLOC Code for Calculation of Fuel and Clad Heating, Metal-Water Reaction, and Core Meltdown Following a Loss-of-Coolant Accident
Presented at meeting on High Temperature Properties of Light Water-Cooled Reactor Materials under Accident Conditions, Washington, D. C., Feb. 28-Mar. 1, 1967.

J. T. Holmes
Advantages and Disadvantages of Factorial Experiments*
Presented at Oak Ridge National Laboratory, Oak Ridge, Tenn., Jan. 10, 1967.

W. N. Hubbard
Fluorine Bomb Calorimetry
Presented at Oklahoma State University, Stillwater, Okla., Oct. 25, 1967.

R. O. Ivins
Photographic Experiments with UO_2-Core Fuel Rods in TREAT
Presented at meeting on High Temperature Properties of Light Water-Cooled Reactor Materials under Accident Conditions, Washington, D. C., Feb. 28-Mar. 1, 1967.

R. O. Ivins
Research on Metal-Water Reactions and their Role in Reactor Accidents
Presented at AMU-ANL Student-Faculty Conference, Argonne, Ill., Aug. 24, 1967.

R. O. Ivins
Fuel Failure in Thermal Reactor Safety
Seminar given for Division of Regulation and Licensing, USAEC, Bethesda, Md., Oct. 23, 1967.

---

*Also listed in ANL-7350.

I. Johnson, J. B. Knighton, R. K. Steunenberg
Metal Purification by Oxidation-Reduction Transport between Liquid Metals
Presented at Met. Soc. AIME Meeting, Los Angeles, Calif., Feb. 22, 1967.

I. Johnson
Chemical Processing of Fast Breeder Nuclear Reactor Fuels
Presented at Monmouth College Seminar, Monmouth, Ill., May 3, 1967.

R. J. Meyer, R. D. Oldham, R. P. Larsen
A Complexiometric Titration of Rare Earths for Monitoring Burnup
Presented at Am. Chem. Soc. Mtg., Miami, Apr. 11, 1967.

P. A. G. O'Hare, W. N. Hubbard, H. M. Feder
Bond Energies in Chalcogen Fluorides
Presented at International Union of Pure and Applied Chemistry Symposium on Thermodynamics, Heidelberg, Sept. 12-14, 1967.

P. A. G. O'Hare, J. L. Settle, H. M. Feder, W. N. Hubbard
The Thermochemistry of Some Uranium Compounds
Presented at International Atomic Energy Agency Symposium on Thermodynamics of Nuclear Chemistry with Emphasis on Solution Systems, Vienna, Sept. 4-8, 1967.

K. K. S. Pillay, R. J. Meyer, R. P. Larsen
The Determination of Praseodymium-141 in Nuclear Fuels by Neutron Activation, Application to Burnup Analysis
Presented at Am. Chem. Soc. Mtg., Miami, Apr. 11, 1967.

L. E. Ross, R. P. Larsen, V. Drabek
Colorimetric Determination of Zirconium in Uranium
Presented at Analytical Chemistry Conference, Pittsburgh, Pennsylvania, Mar. 6, 1967.

E. Rudzitis, E. H. VanDeventer, W. N. Hubbard
The Enthalpy of Formation of Phosphorus Trifluoride by Fluorine Hypergolic Calorimetry
Presented at 22nd Annual Calorimetry Conference, Thousand Oaks, Calif., June 22-24, 1967.

H. Shimotake
Regenerative Galvanic Cells
Presented at Northwestern University, Evanston, Ill., Jan. 22, 1968.

H. Shimotake
Bimetallic Galvanic Cells
Presented at RESA Colloquium, Whirlpool Branch, St. Joseph, Michigan, Jan. 26, 1968.

N. R. Stalica
Experience at Argonne in Analyzing Radioactive Materials in an Unshielded ARL Microprobe
Presented at AEC Microprobe Conference, Boston, Mass., June 13, 1967.

N. R. Stalica
Preparation of Irradiated Material for Electron Probe Analysis
Presented at meeting of Midwest Electron Probe Users Group, The American Oil Co., Whiting, Indiana, June 29, 1967.

R. K. Steunenberg
1. Fast Breeder Reactor Fuel Cycles
2. Pyrometallurgical Processing of Fast Breeder Fuel
3. Salt Transport Processes for Ceramic Fast Breeder Fuels
Presented at Advanced Course in Fuel Reprocessing, Kjeller, Norway, Aug. 21-Sept. 1, 1967.

M. Tetenbaum
High Temperature Vaporization Measurements on Hypostoichiometric Urania
Presented at Atomic Energy Research Establishment, Harwell, UK, Jan. 23, 1967.

M. Tetenbaum
Recent Thermoelectric Parameter Measurements on Actinide Sulfides, Phosphides, and Their Solid Solutions
Presented at Atomic Energy Research Establishment, Harwell, UK, May 22, 1967.

M. Tetenbaum
Thermodynamic Properties of the Hypostoichiometric Urania Phase
Presented at Dounreay Experimental Reactor Establishment, Scotland, UK, June 29, 1967.

A. D. Tevebaugh
Review of AEC-Supported Work on Batteries
Presented at Electrochemical Working Group Meeting (PIC-BAT), Philadelphia, Pa., Apr. 11-12, 1967.

R. C. Vogel
Spent Fuel Recovery Problems
Presented at 8th Annual AMU-ANL Nucl. Engr. Conf., Argonne, Ill., Jan. 31, 1967.

R. C. Vogel
Program of the Chemical Engineering Division
Presented at First Naval Reserve Seminar on Nuclear Research in Life and Physical Sciences, Argonne, Ill., May 4, 1967.

R. C. Vogel
Salt Transport Processing of Fast Breeder Reactor Fuels
Presented at University of Minnesota, Minneapolis, Minn., Oct. 31, 1967.

R. E. Wilson
Experimental Studies of Metal-Water Reaction and Meltdown of Zircaloy-Clad UO_2 Fuel Rods under Loss-of-Coolant Accident Conditions
Presented at meeting on High Temperature Properties of Light Water-Cooled Reactor Materials under Accident Conditions, Washington, D. C., Feb. 28-Mar. 1, 1967.

L. C. Witte
An Experimental Study of Forced-Convection Heat Transfer from a Sphere to Liquid Sodium
Presented at ASME Winter Annual Meeting, Pittsburgh, Pa., Nov. 12-17, 1967.

L. C. Witte, L. Baker, Jr., D. R. Haworth
Heat Transfer from Spheres into Subcooled Liquid Sodium during Forced Convection
Presented at ASME Winter Annual Meeting, Pittsburgh, Pa., Nov. 12-17, 1967.

T. F. Young
Maxima, Minima, and Inflections in Thermal Variations of the Properties of Water
Presented at 18th Annual Mid-America Symposium on Spectroscopy, Society for Applied Spectroscopy, Chicago, Ill., May 15, 1967.

T. F. Young
Thermochemistry of Aqueous Sulfuric Acid Solutions
Presented at Gordon Conference, Meridan, N. H., Aug. 28-Sept. 1, 1967.

ARGONNE NATIONAL LAB WEST
3 4444 00011313 4